Morphology and Kinematics of Parsec-Scale Outflows from Young Stars

by

Fiona McGroarty
B. Sc.

A thesis submitted to
Dublin City University
for the degree of

Ph. D

Supervisor: *Prof. Tom Ray*
School of Cosmic Physics,
Dublin Institute for Advanced Studies
and
Supervisor: *Prof. Eugene Kennedy*
School of Physical Sciences,
Dublin City University

September, 2004

I hereby certify that this material, which I now submit for assessment on the programme of study leading to the award of Ph. D. is entirely my own work and has not been taken from the work of others save, and to the extent, that such work has been cited and acknowledged within the text of my work.

Signed: Fiona Mc Geaney

ID No.: 96542861

Date: September 9, 2004

Acknowledgements

There are many people that I would like to thank for their help, encouragement and support during my PhD

Firstly, Professor Tom Ray deserves much thanks for patiently explaining the many aspects of outflows, and not being in the least bit phased when asked to explain it again Also his extensive knowledge of the literature which can be used to backup any point cannot be understated! Thanks also to Professor Eugene Kennedy, my supervisor in DCU, for taking an active role in the supervision of this thesis with much enthusiasm despite it being a subject he is unfamiliar with I am grateful for a scholarship from DIAS, and also for the many opportunities afford to me by them to travel for observing, conferences and summer schools I would also like to acknowledge a scholarship from Enterprise Ireland

To all the people in DIAS who made it an interesting, if somewhat surreal, place to work, thanks! Especially Emma, Eileen and Patrica for all the tea breaks and non-work-related (gossip) chats and Agueda, our travel agent, for a great conference (!) trip to Budapest All the others in DIAS – Eimhear, Hilary, Deirdre, Dirk, Celine, Gareth, Cian, Brian, Luke, Ann, Matt, Justin, Anne, Stephane, David, Eric and Denis for contributing to a fantastic PhD experience in their own inimitable ways Hotel California – I'll be back!

My family and friends cannot be thanked enough for their support My parents, Nuala and Mick for their unwavering support and belief in me through university and my PhD My brother and sister, Michael and Catherine, and Celina, Joan and Ciara for many long distance chats and interesting holidays reminding me of the world outside of physics Ruth, Cormac, Barry and Simon for making the physics degree in DCU thoroughly enjoyable and the years since then equally cheerful Emma, who not only distracted me in work with tea breaks but ambushed me at home with bottles of wine and deep and meaningful discussions about work – your thesis is coming up, I'll get you back! And finally Simon, who now knows more than he ever wanted to about outflows, and kept me bordering on sanity for the last few months, possibly at the expense of his own

This thesis is dedicated to

Nuala and Mick

and

Simon

Summary

Numerous studies of young stellar objects (YSOs) have uncovered associated optical outflows, the majority of which are driven by low-mass, embedded, Class I sources Initially these outflows were thought to extend only a few thousand AU, however recent observations have shown that they can stretch for several parsecs In this thesis I examine the more massive intermediate-mass ($2M_\odot \lesssim M_* \lesssim 10M_\odot$) YSOs and the more evolved Class II low-mass YSOs (Classical T Tauri stars - CTTSs) for evidence of similar large-scale outflows

It is now well known that mass outflow accompanies the birth of stars Outflows occur early in the formation process when YSOs are optically obscured by large amounts of dust although the outflow itself may be optically visible They are an essential part of the star formation process and can remove significant amounts of excess angular momentum from a YSO as it forms On large scales outflows may generate turbulence in their parent cloud thus helping to support the cloud against gravitational collapse In this way outflows may even influence subsequent star formation Parsec-scale outflows, created over thousands of years, are also an important "fossil record" of the mass-ejection (and, to a lesser extent, of the accretion) history of their source

The intermediate-mass YSOs presented here were found to generate outflows of up to 8 parsecs in length Their morphology follows trends seen in large-scale outflows from embedded low-mass sources such as decreasing spatial frequency, increasing dimensions and increasing complexity of Herbig-Haro (HH) emission with distance from the source Extrapolating the decline in spatial frequency suggests that HH emission may exist on even greater scales than seen here i e tens of parsecs Remarkably, virtually all of the optical outflows from intermediate-mass YSOs have a high degree of collimation As very high mass YSOs are known to have poorly collimated outflows (e g the Orion Bullets), these observations therefore suggest that the transition from focused jet to poorly collimated wind must occur at higher masses than those studied here

The CTTSs observed were previously known only to drive "micro-jets" of several thousand AU in length The wide field observations presented here however

show that they also drive parsec-scale flows of the order of 0 5pc Their degree of collimation is again very high and comparable to what is observed in the case of more embedded sources of similar mass This implies that the collimation angle remains small even as the source evolves over 1 Myr timescales Again one observes the same decrease in spatial frequency of HH emission with increasing distance from the source as seen for the more embedded sources The apparent dynamical lifetimes of these large-scale outflows (around 10^{3-4} yrs) are comparable to the inferred time interval between major accretion events that give rise to FU Orionis outbursts This would suggest a link between major HH complexes and the FU Orioms phenomenon Finally my research would suggest that most optical outflows (both from intermediate mass YSOs and CTTSs) have blown out of their parent cloud and are much larger than inferred from their apparent size

A proper motion study was undertaken on the CTTS-driven outflows to determine tangential velocities, particularly for the more distant HH emission, as an aid to understanding outflow dynamics This study shows the more distant objects in the outflows to be moving with velocities of $\sim$ 200 kms^{-1} while the "micro-jets" themselves are slightly faster, suggesting that the velocities remain high with distance from the source

Publications

McGroarty, F , Ray, T P , & Bally, J 2004 **Parsec-scale outflows from intermediate-mass sources and Classical T Tauri stars** Baltic Astronomy, 13, 528

McGroarty, F & Ray, T P 2004 **Classical T Tauri stars as sources of parsec-scale optical outflows** A&A, 420, 975

McGroarty, F , Ray, T P , & Bally, J 2004 **Parsec-scale Herbig-Haro outflows from intermediate-mass stars** A&A, 415, 189

McGroarty, F & Ray, T P 2003 **Parsec-Scale Outflows from Intermediate-Mass Stars** Revista Mexicana de Astronomia y Astrofisica Conference Series, 15, 141

Contents

List of Figures

List of Tables

Glossary

YSO	Young Stellar Object
HH	Herbig Haro
GMC	Giant Molecular Cloud (*see page 1*)
ISM	Interstellar Medium
PMS	Pre-main-sequence
TTS	T Tauri Star (*see page 5*)
CTTS	Classical T Tauri Star (*see page 5*)
WTTS	Weak-line T Tauri Star (*see page 5*)
SED	Spectral Energy Distribution
HAeBe	Herbig Ae/Be (*see page 8*)
IRAS	Infrared Astronomical Satellite
PA	Position Angle (*see page 32*)
PSF	Point Spread Function
FUor	FU Orionis object (*see page 77*)

Chapter 1

Introduction

1.1 Initial Stages of Star Formation

Star formation takes place inside molecular clouds – dense clouds of predominantly molecular hydrogen (H_2) gas and dust The dominant process through which these clouds form from the interstellar medium (ISM) has not yet been identified Possible mechanisms include instabilities in the ambient ISM (Kim, Ostriker, & Stone, 2003, Elmegreen, 1993), "supershells" driven by multiple supernovae (McCray & Kafatos, 1987) and random coalescence of existing clouds (Elmegreen, 1993), however coalescence is no longer favoured as a method of forming the most massive clouds of $\sim 10^{5-6}M_\odot$ (Kim, Ostriker, & Stone, 2003)

Most of the mass of the molecular ISM is in the form of these Giant Molecular Clouds (GMCs) with masses of $\sim 10^{5-6}M_\odot$, diameters of $\sim$ 50 pc[1] (Blitz, 1993), temperatures of about 10K (Pratap et al , 1997) and lifetimes of about $\sim 10^7$ years (Williams, Blitz, & McKee, 2000) The majority of stars in the galaxy are formed in GMCs, while smaller molecular clouds with masses of several orders of magnitudes smaller than GMCs (called dark clouds or globules) are the locations of isolated, low-mass ($\leq 2M_\odot$) star formation GMCs are inhomogeneous and contain numerous regions of enhanced density called *clumps* (Blitz, 1993) Within these clumps are *cores*, the individual sites of star formation This terminology of cloud $\rightarrow$ clump $\rightarrow$ core is widely used to describe these structures of decreasing size Massive clumps with masses of $10^3M_\odot$ may form entire clusters of stars while

[1] 1 parsec = 3 08568 $\times$ 10^{16} m = 206265 AU = 3 26 light years

small dense cores form individual stars or small multiple systems (Larson, 2003) Clumps and cores, like the molecular clouds in which they form, are predominantly H_2 The nature of the interclump medium remains unclear, however recent observations suggest it is predominately atomic hydrogen and may form envelopes around the clumps (Blitz, 1993, Williams, Blitz, & Stark, 1995) Williams, Blitz, & Stark (1995) estimate a density contrast of ~ 40 between the dense clump and less dense interclump medium from their observations of the Rosette Molecular Cloud

The gravitational force in a molecular clouds is opposed by a number of forces which prevent the collapse of the cloud (and its substructures) under self-gravity While thermal pressure within the cloud will provide some support against gravity, low average temperatures of $\sim$ 10K suggests it is not the only force A number of arguments point to the necessity of turbulence within clouds Observationally, the CO line widths of clouds and clumps tend to be considerably larger than the thermal linewidths implied by the excitation temperature These wider linewidths are generally attributed to turbulent motions within the cloud/clump (Falgarone & Phillips, 1990) Magnetic fields are also essential to the structure, and evolution, of molecular clouds (McKee et al , 1993) However if there is insufficient magnetic flux clumps/cores become magnetically supercritical (Williams, Blitz, & McKee, 2000) and magnetic fields cannot prevent their rapid gravitational collapse This collapse ends in the formation of a cluster or a small multiple system/single star

The initial stages of star formation have been detailed above Here I give a brief overview of the star formation process for the most simple case of a core forming a single star Fig 1 1 also illustrates this process

- A high density core forms in a molecular cloud by some mechanism (instabilities in the ISM, supernovae driven shells and/or random coalescence of existing clouds)

- Part of the core becomes sufficiently massive and thus the gravitational force becomes greater than the turbulent pressure and magnetic fields that are supporting the cloud The core starts to collapse The timescale on which this collapse occurs

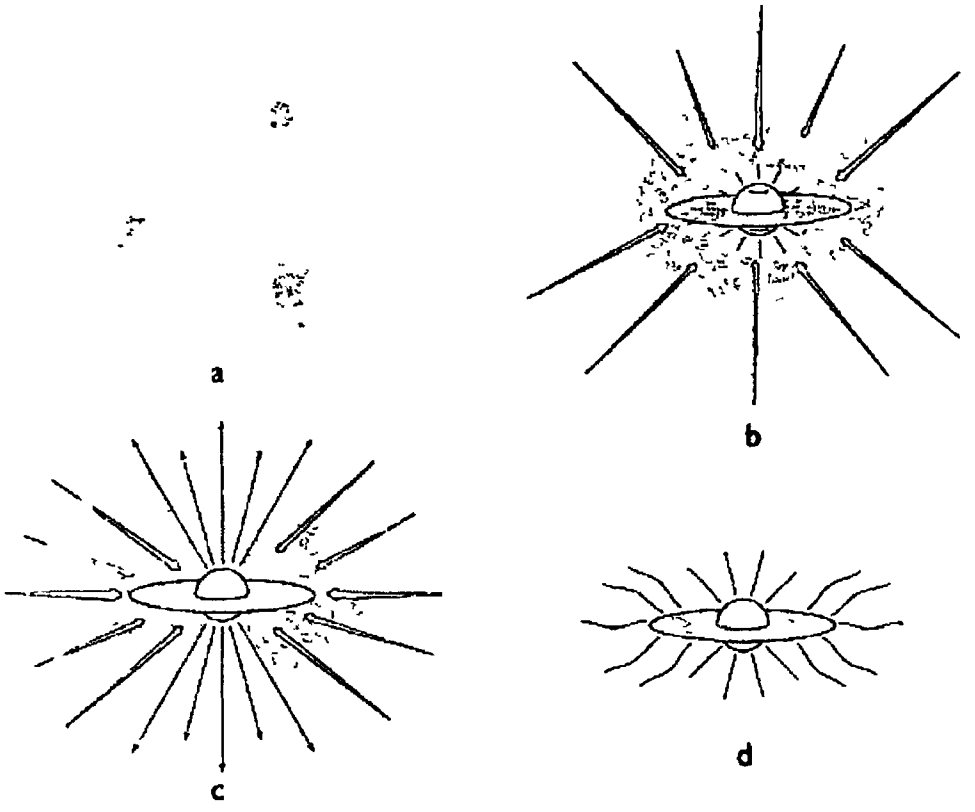

Figure 1 1 Stages of star formation (a) Cores form within molecular clouds and collapse as magnetic and turbulent support is lost due to self-gravity (b) A protostar with a surrounding disk forms at the centre of a cloud core collapsing from inside-out (c) A bipolar outflow breaks out along the rotational axis of the system (d) The infall terminates, revealing a newly formed star with a circumstellar disk (taken from Shu, Adams, & Lizano, 1987)

is governed by the timescale for gravitational collapse, called the free-fall time, τ_{ff}

$$\tau_{ff} = \sqrt{\frac{1}{G\rho}} \tag{1.1}$$

For a clump or core with n=10^4 cm^{-3}, τ_{ff} is of the order of 1×10^6 years

• As the density is greatest at the centre of the core, the free-fall time is shorter here than at the edges of the core so the interior collapses fastest (Shu, Adams, & Lizano, 1987) A protostar[2] forms at the centre and infalling material from the more slowly collapsing outer edges is accreted onto the stellar surface, mostly through a circumstellar disk which is formed around the protostar

• The circumstellar disk disperses (if planets are to be formed it will be from this remnant circumstellar disk) When the protostar has sufficient mass fusion commences in the core and it becomes a main sequence star

1.2 Stellar Classification

Protostars and stars of different mass undergo different evolutionary processes and/or have different evolutionary timescales and so mass can be used as a simple classification parameter Although there is a continuous range of masses stars can be divided into low-, intermediate- and high-mass In this thesis I consider low-mass stars to have $M_* \lesssim 2M_\odot$, intermediate-mass stars to be in the range $2M_\odot \lesssim M_* \lesssim 10M_\odot$ and high-mass stars to have $M_* \gtrsim 10M_\odot$ The protostar created by the collapse process detailed previously (Fig 1 1d) can be a low- or intermediate-mass star The high-mass star formation process, however, is significantly different and is discussed later (§1 2 3)

The stellar initial mass function (IMF) describes the distribution of masses with which stars are formed Although its origin and exact form are not fully known it is generally assumed to be invariant both temporally and spatially (Meyer et al , 2000), however Scalo (1998) argues that the large discrepancies found in certain

[2]A protostar can be defined as a central, condensed star-sized object which derives all its energy from the gravitational potential energy of the core collapse Nuclear fusion does not take place within a protostar (Ward-Thompson, 2002)

IMF estimates may actually be variations Numerous observational studies have determined that the IMF flattens at masses less than $1M_{\odot}$ (see Meyer et al , 2000), showing that there is a characteristic stellar mass of the order of $1M_{\odot}$ i e in the low-mass star regime Larson (1999) states that 75% of the mass that forms stars goes into stars of 0 $1M_{\odot}$ to $10M_{\odot}$ (low- and intermediate-mass stars), about 20% goes into forming stars greater than $10M_{\odot}$ (high-mass stars) and about 5% goes into forming stars of less than about 0 1 $M_{\odot}$ The mass distribution for cores bears a resemblance to the IMF (Motte, André, & Neri, 1998), suggesting that stars may derive their masses directly from their pre-stellar cloud cores

1.2.1 Low-Mass YSOs/CTTS

As low-mass YSOs are so numerous they have been well studied, much more so than either intermediate- or high-mass YSOs When optically visible, low-mass pre-main-sequence (PMS) stars are known as T Tauri Stars (TTSs) TTSs have spectral types F5 – G5, with particularly strong Hα emission and are named after the prototypical source, T Tau (Joy, 1945) TTSs can be sub-divided into Classical TTSs (CTTSs) which have strong Hα emission and Weak-line TTSs (WTTSs) which have much weaker Hα emission They can be classified purely on their Hα equivalent width, CTTS have EW(Hα) > 1nm and WTTS have EW(Hα) < 1nm (e g Alcalá et al , 1993) Of course not all low-mass YSOs are optically visible, statistical analysis would suggest that about 90% of them are optically obscured

Low-mass YSOs can be divided into four classes, 0 to III, based on the shape of their spectral èenergy distribution (SED) from 10μm to 100μm (Lada & Wilking, 1984, Lada, 1987), see Fig 1 2 The SED of a YSO can be modelled as an approximate blackbody with an infrared excess upwards of 2μm due to circumstellar dust and gas surrounding the YSO which absorbs substantial amounts of the radiation emitted by the embedded star and reprocesses it at longer (infra-red) wavelengths Originally this scheme just contained Classes I to III, with the subsequent addition of Class 0 suggested by André, Ward-Thompson, & Barsony (1993) for sources with strong submillimetre emission such that $L_{submm}/L_{bol} \gtrsim 5 \times 10^{-3}$ Class 0 sources are undetected m the near-infrared ($\lambda < 10\mu$m) and their SEDs are a close approximation to a blackbody The infrared excess is very strong m the young, embedded

Class I sources and is almost non-existent in the more evolved Class III sources Although low-mass YSOs can be classified using this scheme, the energy distributions are actually quasicontinuous (Lada, 1987)

It was initially thought that this classification scheme was an evolutionary sequence, with sources evolving from Class 0 to Class III via Classes I and II Not long after the scheme was devised however it was suggested that Class II and Class III sources of similar mass could be coeval (Walter, 1986) Recent observational work has argued both for (Gregorio-Hetem & Hetem, 2002, Gras-Velázquez & Ray, 2004) and against (Duvert et al , 2000) a branching off after Class I to become either Class II or Class III

The dominant emission in Classes 0 to III is at submillimetre, far-IR, near-IR and visible wavelengths respectively Class 0 sources are at an early phase of rapid accretion lasting a few $\times$ 10^4 years (André & Montmerle, 1994, Andre, Ward-Thompson, & Barsony, 2000) Protostars are classified as Class 0 if more than half of the total mass of the system is still in the infalling envelope i e $M_*/M_{env} < 1$ (Andre, Ward-Thompson, & Barsony, 1993) When half of the mass of the envelope has fallen on to the protostar it is classified as a Class I source These sources are in the main accretion phase which lasts a few $\times$ 10^5 years (Barsony & Kenyon, 1992) Class II sources are Classical T Tauri stars (CTTSs) The Class II phase lasts up to 10^6 years Class III sources are WTTSs and have no significant circumstellar material (Larson, 2003) WTTSs have approximately similar ages to CTTSs within the same star forming region (Walter et al , 1988), which indicates that Classes II and III may be coeval This simplistic division of CTTS and WTTS into Class II and Class III respectively is not strictly correct, as André & Montmerle (1994) show Nevertheless the majority of CTTSs are Class II sources and the majority of WTTSs are Class III sources

Classes I to III correspond to a spectral index as measured from their SED The spectral index, α_{IR}, can be defined as

$$\alpha_{IR} = \frac{d\ log\ (\lambda\ F_\lambda)}{d\ log\ \lambda} \tag{1 2}$$

From this Class I corresponds to $\alpha_{IR} > 0$, Class II corresponds to -1 5 $\leq \alpha_{IR} \leq 0$

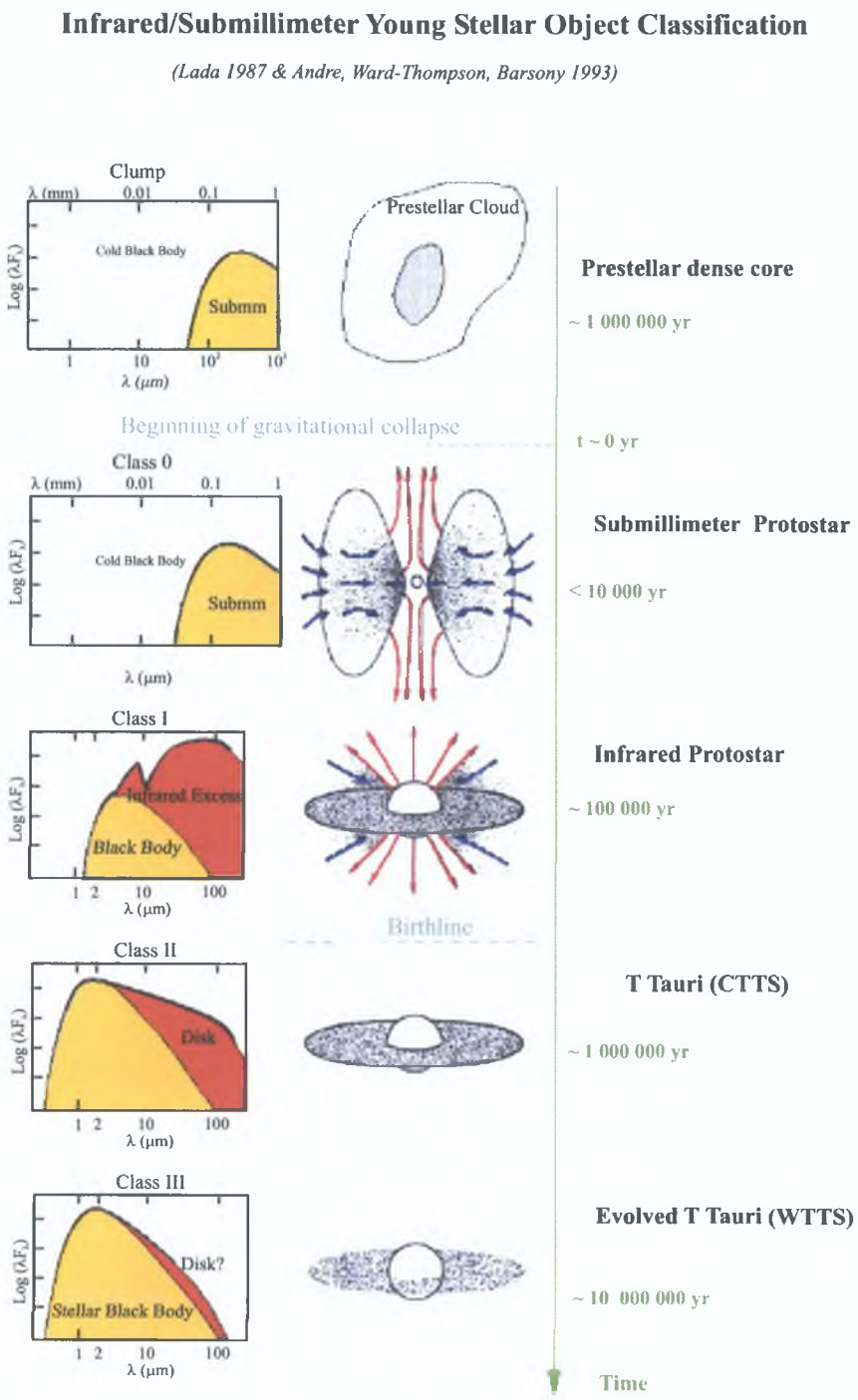

Figure 1.2: Low-mass YSO classification scheme of Lada (1987) and André, Ward-Thompson, & Barsony (1993), assuming an evolutionary transition from CTTS to WTTS. YSOs are classified into four different classes based on the shape of their SED. Taken from André (1994).

and Class III corresponds to α_{IR} < -1 5 (Lada, 1987, Andre & Montmerle, 1994)

1.2.2 Intermediate-Mass Stars/HAeBe Stars

In many cases YSOs or stars more massive than $\sim 2M_{\odot}$ are labelled as high-mass However here I emphasise the distinction between intermediate-mass ($2M_{\odot}$ – $10M_{\odot}$) and high-mass (> $10M_{\odot}$) YSOs as these two mass regimes most probably undergo very different star formation processes In particular the processes involved in creating an intermediate-mass star appear to be similar to those that give rise to low-mass stars, as described previously, while the current understanding of high-mass star formation is described in §1 2 3

The protostar formed in the process outlined in §1 1 (Fig 1 1d) can be either low-mass or intermediate-mass, however the IMF dictates that it will most likely be low-mass Intermediate-mass YSOs are rarer, and therefore tend to be found at greater distances from us requiring higher spatial resolution to observe them The timescale for the protostellar evolution of intermediate- and high-mass stars is much quicker than for low-mass stars, and most of the formation process can occur when these YSOs are still embedded, making them difficult to observe These problems, coupled with a historical bias towards isolated low-mass YSOs, results in many unanswered questions about intermediate-mass star formation

Herbig Ae/Be (HAeBe) stars are the intermediate-mass counterparts of TTSs, first classified by Herbig (1960) HAeBe stars have a spectral type of A or earlier, strong Balmer emission (analogous to TTS), are positioned within a dark cloud and they illuminate a bright nebulosity (Herbig, 1960) Late-type HAeBe stars (Herbig Ae stars – later than B5) become optically visible long before arriving at the main sequence, similar to TTSs, while earlier-type HAeBe stars (Herbig Be stars) remain embedded in their parent core throughout the PMS stage This spectral type/mass division also represents a difference in formation and evolutionary processes (Fuente et al , 2001) Observational evidence shows that while circumstellar disks are frequently found around Herbig Ae stars (Natta et al , 1997), they are rarely detected around Herbig Be stars (Natta, Grinin, & Mannings, 2000), suggesting that either the disks have already been dispersed by the time the central star becomes optically visible, or that the Herbig Be stars are formed through a

different process that does not require a circumstellar disk, such as the coalescence of lower mass stars/protostars (see §1 2 3 for details) Analogous to low-mass stars, optically visible HAeBe stars are the minority within intermediate-mass stars

Intermediate-mass YSOs/HAeBe stars have been classified based on the shape of their SEDs, analogous to the classification for TTSs (Hillenbrand et al , 1992) There are three *groups* in this scheme Group I sources can be modelled as emission arising in a flat, optically thick disk, Group II sources are a star or star/disk system surrounded by an extended envelope, and Group III sources have a small infrared excess which can be modelled by free-free emission from a disk or a stellar wind (Fig 1 3) Hillenbrand et al (1992) argue that the small infrared excess seen in Group III sources excludes the possibility that these are PMS stars surrounded by an optically thick circumstellar disk i e these Group III objects are analogous to low-mass Class III sources Based on the relative luminosity of their Hα lines the relationship between Group III and Group I objects is analogous to that between the low-mass Class III (WTTSs) and Class II (CTTSs) objects This classification scheme represents the progressive decrease of circumstellar material surrounding a forming star and, as Group II objects are thought to be the precursors of Group I objects, the sequence goes from Group II $\rightarrow$ Group I $\rightarrow$ Group III However this scheme is not particularly useful for determining stellar ages

This classification scheme is by no means universally accepted, unlike the TTS scheme A number of studies have suggested that the SEDs of *all* HAeBe stars can interpreted as the emission from a spherical envelope, as opposed to a circumstellar disk (see Natta, Grinin, & Mannings, 2000 and references therein) However (Natta et al , 1993) show that the envelope alone can not explain the observed SEDS, both disk *and* envelope must contribute to the SED – the disk in the near- and mid-infrared and the envelope in the far-infrared

Fuente et al (1998) propose a different classification scheme, based on observations of the parent cloud rather than the YSO Their classification involves three *types*, where Type I sources are still immersed in a dense core and have an age of about 10^5 years, Type II sources are still immersed in a cloud but are not at the peak of a dense core and have an age of typically $0\,1 - 1 \times 10^6$ years, and Type III sources have dispersed most of their surrounding dense gas such that the

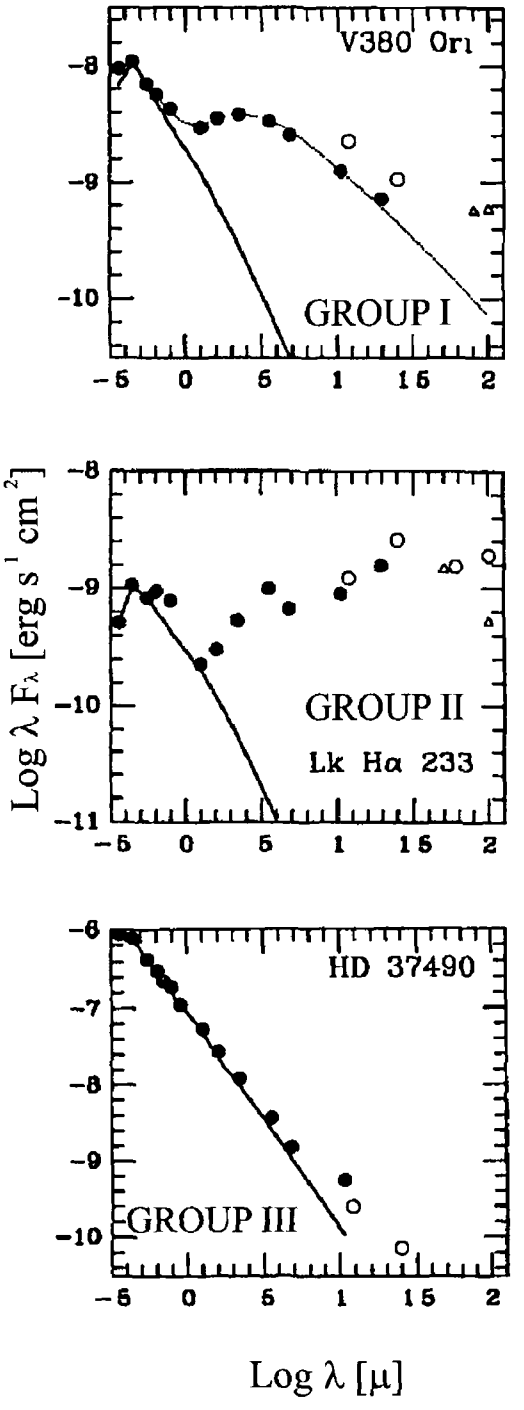

Figure 1 3 SEDs for Group I, Group II and Group III type stars, taken from Hillenbrand et al (1992) Solid circles are ground-based observations, open circles represent large-beam IRAS (Infrared Astronomical Satellite) points, triangles are KAO (Kuiper Airborne Observatory) data The thin line in the Group I type star is a "best fit" disk model Group II, I and III SEDs resemble those of the low-mass Class I, II and III respectively (see Fig 1 2)

central star is in a large cavity, and have an age of $> 10^6$ years Fuente et al (1998) suggest that this scheme gives a simple and independent estimate of the age of a star, based on the "spatial index" which describes the morphology of the cloud

As can be seen, the stages and processes through which an intermediate-mass star is formed is by no means properly understood as yet

1.2.3 High-Mass Stars

The formation of high-mass stars is an area of which relatively little is known - these stars have not been well studied as they are difficult to observe, for the same reasons given in §1 2 2 for intermediate-mass YSOs Their evolutionary timescales are relatively short and in most cases the accretion process has ended before the stars become optically visible However the area of massive star formation has been studied more and more in recent years and it has become clear that the formation process for stars with $M_* > 10M_\odot$ is quite different from that of low- and intermediate-mass (i e Herbig Ae – type) YSOs i e $M_* \leq 6M_\odot$ (Bonnell, Bate, & Zinnecker, 1998, Palla & Stahler, 1990)

The amount of mass that can be directly accreted on to a star is limited by its accretion rate The Eddington limit states that the upper limit on the ratio of luminosity to mass of a stable star is 40,000 ($L_\odot/M_\odot$) If this limit is exceeded the high radiation pressure at the stellar surface will blow away the star's outer layers Eta Carinae, one of the most massive ($80M_\odot$, Corcoran et al , 2001) and most luminous stars in our galaxy is very unstable and has undergone eruptions of its outer layers for this reason (Currie, 2003) While it is now thought to be quite unlikely that many of the stars greater than $10M_\odot$ are formed through accretion (Stahler, Palla, & Ho, 2000) recent observations, including that of a $\sim 20M_\odot$ protostar surrounded by an accretion disk Chini et al (2004), suggest that some of them may be

Bonnell, Bate, & Zinnecker (1998) suggest, and model, a scenario in which high-mass stars are formed through the coalescence of intermediate-mass stars which are themselves formed through accretion For such mergers to be statistically significant they must occur in a high density environment i e the centre of a cluster As high-mass star formation occurs almost exclusively in clusters, and the major-

ity of such stars are found in the centre, this model agrees with the observations Observations also show that many massive stars are in close binary systems (Garmany, Conti, & Massey, 1980), which this model can also explain – if collisions are to occur allowing stars to merge, then there should be many situations where stars come close enough to form a binary system but do no actually collide (Bonnell, Bate, & Zinnecker, 1998) The components within such a binary should both be at least intermediate-mass and possibly more massive if they themselves have already undergone a collisional merge

Potential problems with this coalescence model arise from the timescales needed to create intermediate-mass stars and allow them to then collide, and also from the fact that the stellar radii are so small that direct collisions are improbable, even in a high density environment However the effective cross section can be increased by a number of factors (see Stahler, Palla, & Ho, 2000 and references therein), and comparisons of theoretical collision timescales verses accretion timescales by Bonnell, Bate, & Zinnecker (1998) show that collisions become the dominant mode of increasing a star's mass in a cluster core within 5×10^5 years of its formation

High-mass stars do not have an optically visible PMS phase of evolution (Palla & Stahler, 1990, 1993) The length of time from the onset of gravitational collapse to hydrogen burning in the core of a star is governed by the Kelvin-Helmholtz timescale, τ_{KH}

$$\tau_{KH} = \frac{GM_*^2}{R_* L_*} \tag{1 3}$$

where M_*, R_* and L_* are the mass, radius and luminosity of the star respectively For a $50M_\odot$ star $\tau_{KH} \simeq 10^4$ years, while for a $1M_\odot$ star it is $\simeq 10^7$ years This means that for a high-mass star $\tau_{KH} < \tau_{ff}$, i e hydrogen burning begins while cloud collapse, and hence infall, is still in progress Only low- and intermediate-mass stars, for which $\tau_{KH} \gtrsim \tau_{ff}$, have an optically visible PMS stage

1.3 Outflows from Young Stellar Objects

1.3.1 Function/Importance of Outflows

The mass of a newly formed stellar object obtained *directly* from the collapse of a core is very small and almost all of a star's final mass is accreted from the surrounding cloud as it collapses (Larson, 2003) For a typical mass accretion rate of 10^{-7} $M_{\odot}$ yr^{-1} over a timescale of 10^{6} years, a $1M_{\odot}$ protostar should accrete enough mass to spin the star to $> 0\ 5$ of breakup velocity, V_{bkp} ($V_{bkp} \sim 200$ kms^{-1}) in the absence of any loss of angular momentum (Hartmann & Stauffer, 1989) Observations show however that low-mass stars have a rotational velocity of $\sim 0\ 1\ V_{bkp}$ (Bouvier et al , 1986), so some mechanism by which angular momentum is lost from the star/disk system must be present Mass outflows, ejected from the accretion disk, could be that mechanism

It is now well accepted that mass outflow is a vital part of the star formation process, and occurs simultaneously with accretion (Fig 1 4) A number of studies (e g Hartigan, Edwards, & Ghandour, 1995, Cabrit & Andre, 1991, Cabrit et al 1990) have shown that there is strong evidence for a physical link between outflows and accretion disks and Hartigan, Edwards & Ghandour (1995) show that mass outflow rates are directly correlated with mass accretion rates The exact means by which these outflows are ejected from an accretion disk is still unclear, however I discuss some of the current models later (§ 1 3 3)

As the material accreted comes from the surrounding envelope it follows that accretion rates should decrease with time as the protostar/disk system evolves and therefore the size of both the envelope and the disk decrease with time (Ward-Thompson, 2002) By definition, a protostar becomes a Class I source when about half of the mass of the envelope has been accreted onto the protostar (cf § 1 2 1) As the Class I phase lasts about an order of magnitude longer than the Class 0 phase this implies that about half of the final stellar mass is accreted in about 1/10th of the combined time for the Class 0/I phase (Ward-Thompson, 2002) In addition a study by Bontemps et al (1996) shows that the outflow activity around low-mass YSOs decreases as sources evolve from Class 0 to Class I (see Fig 1 5), as one would expect

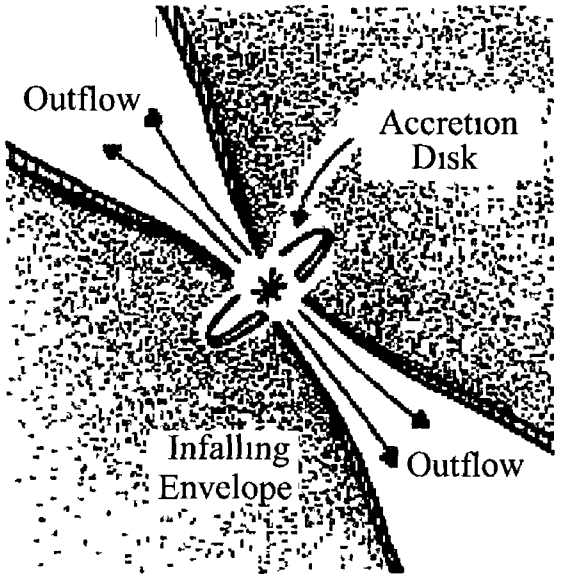

Figure 1 4 Schematic of the accretion disk and bipolar outflows, adapted from Snell, Loren, & Plambeck (1980)

Outflows may have a significant influence on their parent cloud For example, turbulent pressure in a molecular cloud may counterbalance its self-gravity However it has been shown that turbulence, even in the presence of magnetic fields, decays in the order of 10^6 years (Stone, Ostriker, & Gammie, 1998, Mac Low et al , 1998), which is about an order of magnitude smaller than a typical cloud lifetimes (cf §1 1) So somehow turbulence must be replenished in the cloud A number of possible mechanisms by which this could occur have been suggested e g shock waves from supernovae, stellar winds, superbubbles and even outflows from YSOs (Norman & Ferrara, 1996, Ward-Thompson, 2002) The possible contribution from outflows will be discussed further in Chapter 2 Arce & Goodman (2002) show that outflows can also affect the kinematics and distribution of material surrounding them If outflows can have such an influential effect on their surroundings they may even influence subsequent star formation in their vicinity

Parsec-scale outflows, created over thousands of years, are also an important "fossil record" of the mass-ejection (and consequently of the accretion) history of their source This is discussed further in §1 3 4

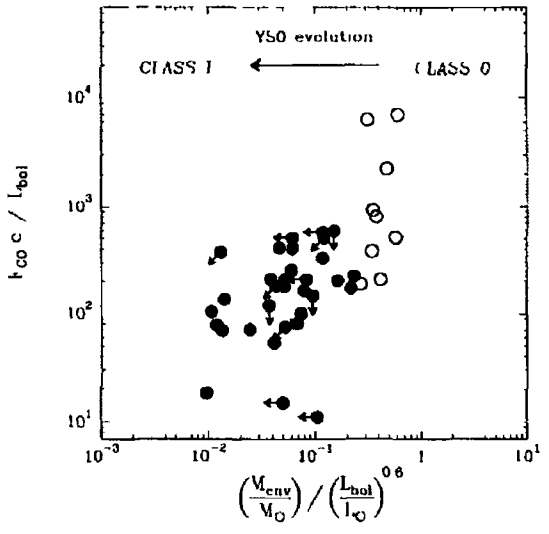

Figure 1 5 $F_{CO}c$ (CO momentum flux)/L_{bol} (dimensionless) versus $M_{env}/L_{bol}{}^{0.6}$ (M_{env} and L_{bol} in units of $M_\odot$ and $L_\odot$ respectively) for 41 embedded low-mass YSOs Class 0 YSOs are plotted as open circles and Class I YSOs as filled circles This diagram provides clear evidence for a decline of outflow strength from Class 0s to Class Is Taken from Bontemps et al (1996)

1.3.2 Observational Aspects

Herbig-Haro objects

Herbig-Haro (HH) objects are the optically visible shock-excited nebulous tracers of outflows These objects were first discovered independently by Herbig (1951) and Haro (1952) and it was soon recognised that they are intrinsically linked to young YSOs (Ambartsumian, 1957, Haro & Minkowski, 1960) However it was Schwartz (1975) who realised that these objects are shock excited due to the interaction of an energetic outflow from a YSO with its surroundings, an idea suggested much earlier by Osterbrock (1958) By 1974 there were 43 HH objects known (Reipurth & Heathcote, 1997) whereas there are approximately 800 known today A thorough review of the history of the discovery of HH objects is given by Reipurth & Heathcote (1997)

HH objects are so-called "working surfaces" (e g see Blondin, Konigl, & Fryxell, 1989, Raga & Cabrit, 1993 and references therein) that can be created in two ways Firstly, when an outflow rams into the undisturbed ambient medium a "terminal working surface" is created which in many cases is bow-shock shaped e g

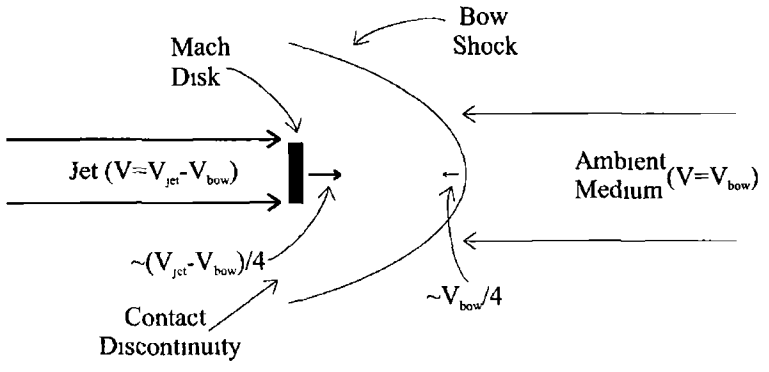

Figure 1 6 Schematic of the structure of the Mach disk and bow shock (in the frame of reference of the shocks)

HH34N and HH34S in Fig 1 8 Secondly, internal interactions within the outflow itself, for example where faster moving ejecta catch up with previously ejected slower material, causes "internal working surfaces" Successive ejecta will have different velocities if there are variations in the jet velocity at the source (Raga et al , 1990, Falle & Raga, 1995)

A working surface consists of two shocks – a reverse shock, or Mach disk, which decelerates the jet flow and a forward shock which accelerates the material with which the flow collides – see Fig 1 6 In the frame of reference of the shock system (Fig 1 6) the jet material leaves the Mach disk with a velocity of $\sim\frac{V_{jet}-V_{bow}}{4}$ while at the bow shock ambient material enters the working surface at $\sim\frac{V_{bow}}{4}$ This describes the adiabatic case, however radition must be included in the case of HH objects In the radiative case a high-density layer builds up in the postshock region (see Fig 1 7) and as this layer cools at constant pressure it radiates Conservation of mass implies that ρV must be constant in the postshock so the velocity of the postshock gas slows rapidly towards zero (as opposed to $\frac{V_{shock}}{4}$) in this high-density region The distance between the shock front and the high-density layer depends on the cooling distance at the shock front however this distance is very small in comparison to the overall size of the HH object In the observer's frame of reference this thin layer of high-density (postshock) material is observed to be moving at V_{shock} It is this radiating layer that we observe as a HH object

HH objects are are observed in both forbidden and permitted lines The cooling and recombination of the postshock gas results in lines of species of successively

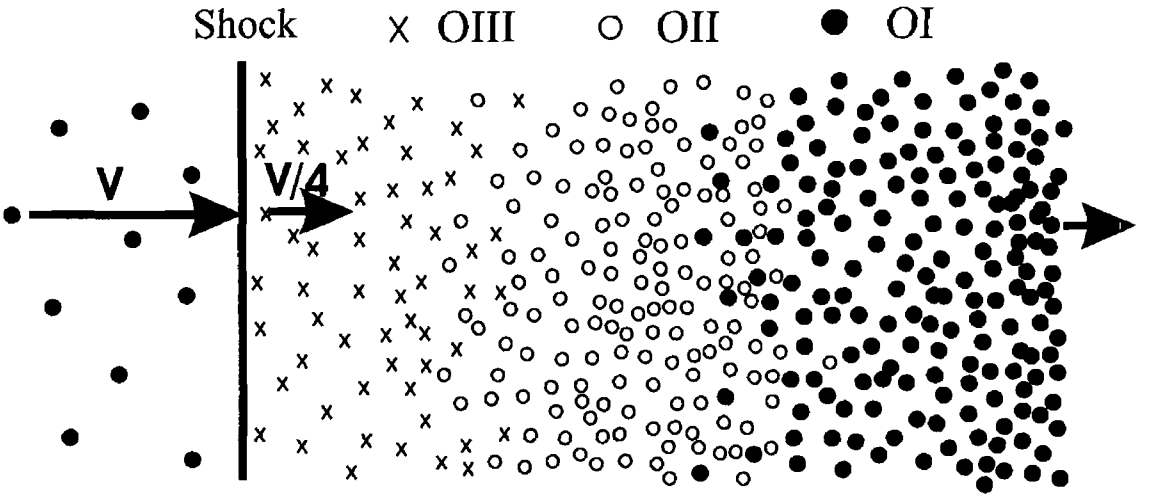

Figure 1 7 The structure of a radiative shock (in the frame of reference of the shock) Material enters the shock front at the left with a velocity V and is slowed by a factor of 4 after crossing the shock The density increases by a factor of 4 at the shock and increases gradually as the gas cools and slows As an example, cooling zones of oxygen are depicted by the crosses, circles and dots Taken from Hartigan et al (2000)

lower excitation dominating the emission at successively greater distances behind the shock front as shown in Fig 1 7 For example the brightness of high-excitation lines such as those of [OIII] should peak closer to the front than low-excitation lines such as those of [SII] Any neutral hydrogen immediately behind such a shock will suddenly encounter a very hot environment, and there is a 10 – 20% chance that it will become collisionally excited before it is ionised Therefore $H\alpha$ emission delineates the leading edge of shock fronts in outflows (Hartigan et al , 2000) A Hubble Space Telescope (HST) image of HH 34 S (Fig 1 8) demonstrates this clearly

Optical (HH) Jets and Outflows

Outflows from YSOs generally take the form of a highly collimated HH jet close to the source with discrete HH objects at larger distances (e g see Fig 1 8) The "internal working surfaces" generated in a jet give the appearance of a series of aligned HH objects rather than a continuous stream of emission Such surfaces also generate the "knotty" structures seen in most HH objects Outflows are emitted approximately orthogonal to the circumstellar disk and are normally seen to be bipolar For the most part, the blueshifted outflow appears brighter and more

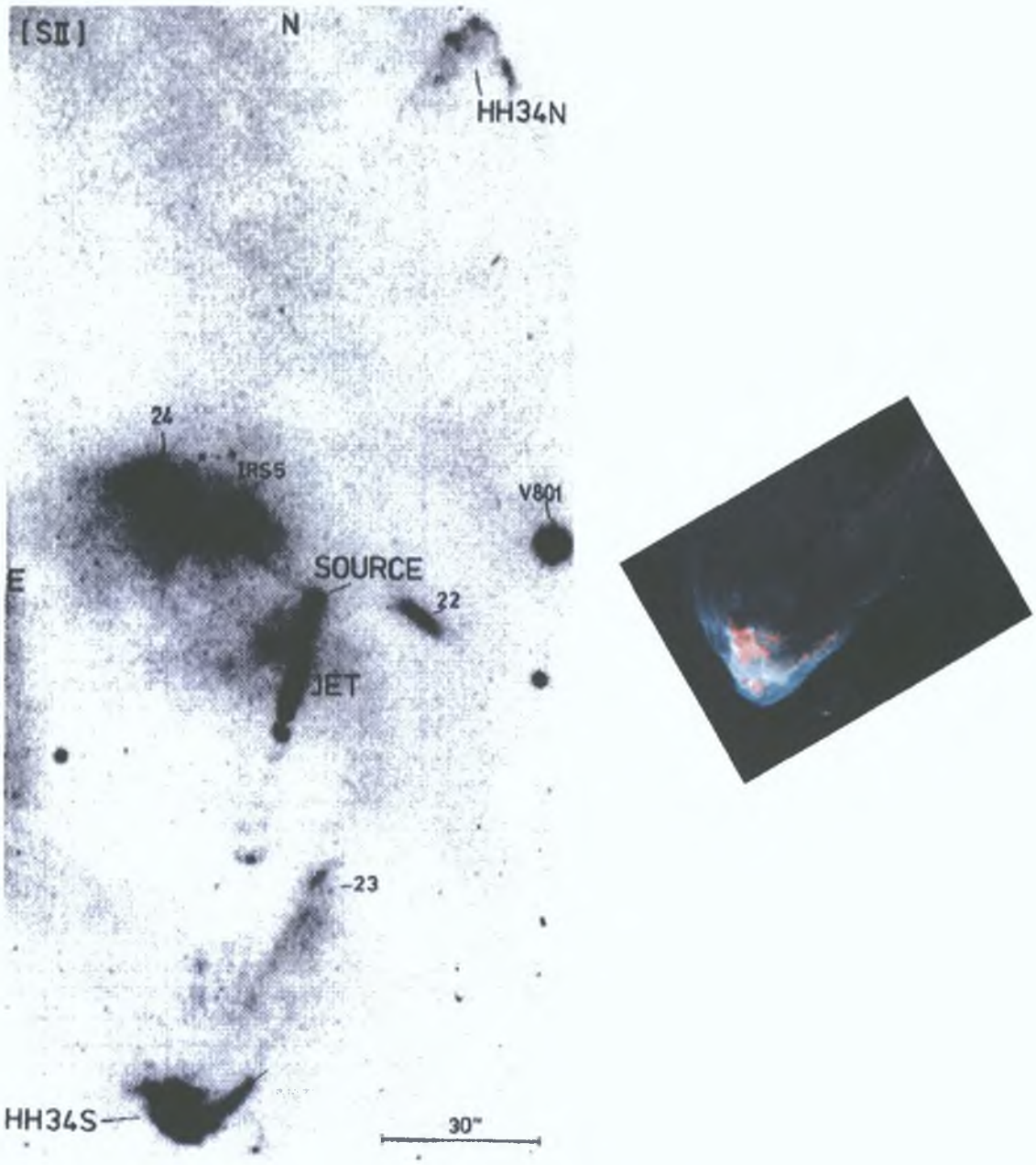

Figure 1.8: The HH 34 outflow. The main image shows the HH 34 jet emanating from a Class I low - mass YSO (HH 34 IRS) (Devine et al., 1997) and two HH shocks to the north (HH 34 N) and south (HH 34 S) of the source. Taken from Bührke, Mundt, & Ray (1988). To the right is a Hubble Space Telescope image of HH 34 S. Hα filaments (*green*), resulting from the collisional ionisation of hydrogen at the shock front, outline the edge of the shock. Fainter [SII] emission (*red*) is seen inside the shock, i.e. in the postshock cooling region. Taken from Reipurth & Bally (2001).

extended than the red shifted outflow, and in some cases the redshifted outflow is not seen at all as it is obscured by dust in the cloud or by the circumstellar disk (depending on its orientation with respect to the line of sight)

The vast majority of outflows known to date are driven by *Class I low-mass sources* Outflows have been observed from intermediate-mass sources, however they are much rarer because their parent sources are less common but in addition such stars have a shorter accretion and outflow phase (§1 2 2) Although outflows have been observed from high-mass YSOs they appear to be quite different from their low- and intermediate- mass counterparts For example, Fig 1 9 shows an outflow from the massive YSO OMC 1 - the outflow is very poorly collimated and appears as a fan of "bullets" rather than a jet (Lee & Burton, 2000) Thus while the degree of collimation of jets from low-mass Class I YSOs is high, typically $\sim$ 5° (Mundt, Ray & Raga, 1991) it is much lower for massive stars – this is discussed in more detail in Chapter 2

Supersonic jet velocities of 200 – 400 kms^{-1} (Mundt, Brugel & Buhrke, 1987) are typically found for jets associated with low-mass sources Generally jet velocity increases with the mass of the source, jets from higher mass YSOs can reach up to $\sim$ 600 kms^{-1} (Edwards, Ray, & Mundt, 1993) Typical radial velocities of jets from low-mass Class I YSOs are 100 – 150 kms^{-1} (Eisloffel & Mundt, 1994)

Molecular Outflows

While the optical emission from species such as [SII], [OII] etc trace the outflow or its immediate environment, molecular emission lines can be used to follow larger scale motion in the ambient cooler surrounding gas The mainly atomic ionised jet drives a molecular outflow which is usually observed in CO as this molecule is both abundant in molecular clouds and has a large dipole moment

As these molecular outflows can be observed at infrared and millimetre wavelengths they have been found around a number of Class 0/I low-mass YSOs which may not have optically visible (HH) outflows Molecular outflows tend to be more poorly collimated than optical outflows (Richer et al , 2000) and in cases where both molecular and optical outflows occur together the optical outflows are often found along the axis of the molecular outflow (for example in the case of the DG

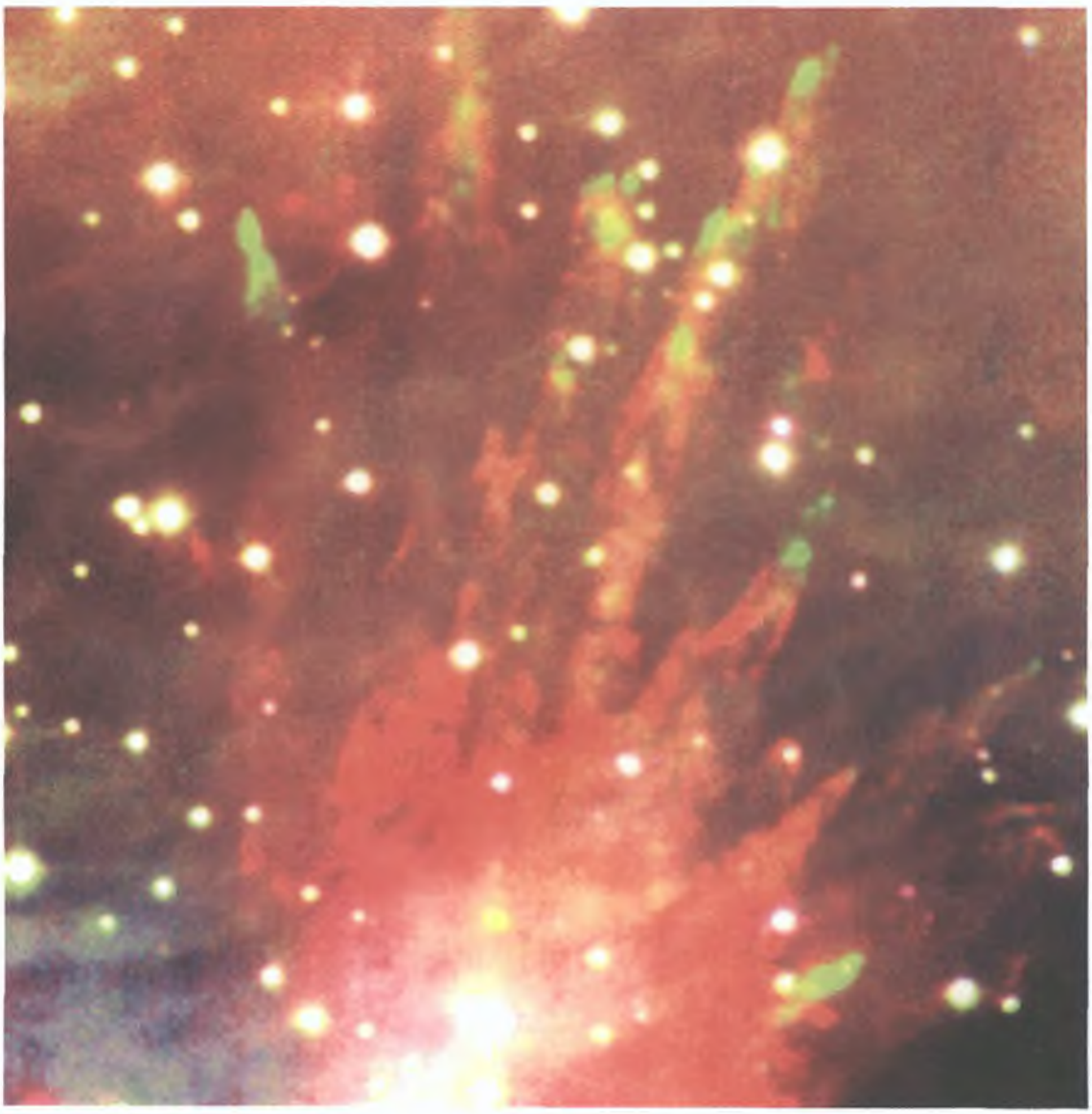

Figure 1.9: Image of the so-called "Orion Bullets" driven by the high-mass source OMC 1. H_2 line emission (2.12 μm) is shown in red, J-band emission in blue and [FeII] (1.64 μm) emission is green. The latter is more pronounced at the tip of the "bullets". The morphology and degree of collimation is remarkably different to that of HH 34 (Fig. 1.8) which is driven by a low-mass source. Picture courtesy of Jung Kyu Lee (Lee & Burton, 2000).

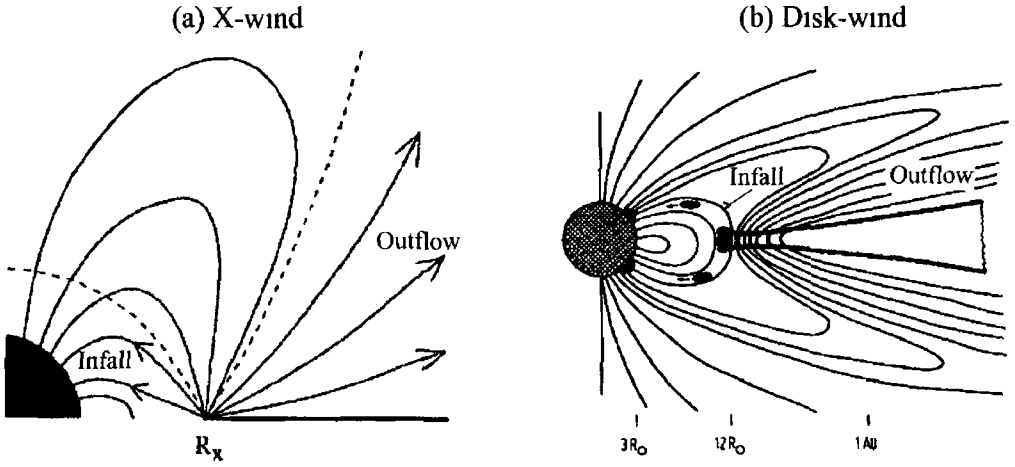

Figure 1 10 (a) Schematic of the X-Wind Model of Shu et al (1994) The circumstellar disk is truncated at a distance of R_X from the star Both an energetic outflow and a funnel flow emerge from the disk truncation region Gas accreting from the disk onto the star in a funnel flow (infall) drags the stellar field into a trailing spiral pattern Adapted from Najita (1995) (b) Schematic of the Disk Wind model The open and closed field lines are similar to those in the X-wind model The jet launch region is at a greater distance from the star than that of the X-wind Taken from Camenzind (1990)

Tau B outflow, see Chapter 3) It is thought that molecular outflows consist of ambient gas swept up by the highly collimated optical outflow How such a narrow, supersonic jet can generate these wide outflows is a fundamental question, and has been addressed by a number of models which are discussed below

1.3.3 Jet Launching Models

The mechanism by which material is accreted and outflows are launched from the YSO/disk system is still unclear Early models were purely hydrodynamic and suggested that the outflow was collimated by the ambient medium or by thermal pressure from a surrounding large-scale flattened structure or disk (Barral & Canto, 1981) However it was soon realised that thermal pressure alone is not enough to focus an outflow (Konigl, 1982, DeCampli, 1981) Current ideas suggest, by analogy with earlier models for extragalactic jets (Blandford & Payne, 1982), that outflows may be launched centrifugally along magnetic field lines In particular, two main approaches are taken

X - Wind Model Here the outflow is launched where the stellar magnetosphere co-rotates with the disk at the so-called "X" point, R_x – Fig 1 10a (see Shu et al (2000) for a review) As the disk spins, material is centrifugally launched along magnetic field lines As the ejected material spins faster the magnetic field lines will start to bend in to the azimuthal direction producing hoop stresses, which then collimate the outflow Angular momentum is lost by by the material launched from the disk which prevents the star from spinning to V_{bkp} Infall of material onto the stellar surface is induced by the YSO's gravitational field and occurs along magnetic field lines

Disk Wind Model In disk wind models the outflow is centrifugally launched from a range of disk radii (Fig 1 10b) again along magnetic field lines threading the disk (Wardle & Konigl, 1993) Infall towards the stellar surface occurs on closed stellar magnetic field lines However these models have been challenged as it may not be physically possible to generate the required strength of the magnetic field in the disk and the external magnetic fields retained in viscous disks are probably insufficient to launch a wind (Bachiller, 1996) A number of different disk wind models exist, see Konigl & Pudritz (2000) for a review

Formation of Molecular Outflows There are two competing mechanisms by which molecular outflows are formed In the first, "prompt" entrainment of ambient material occurs at the head of a collimated jet If the jet direction changes (i e via precession) there will be many locations where this entrainment can occur, creating a wide outflow cavity In this way a highly collimated, time-variable jet can drive a poorly collimated molecular outflow of much lower velocity Various groups have explored this possibility, e g De Young (1986), Masson & Chernin (1993), Raga & Cabrit (1993), Smith, Suttner, & Yorke (1997), Volker et al (1999) As many jets and outflows show some degree of directional variation over time this mechanism is plausible An alternative to this is based on a "steady state" entrainment model (Stahler, 1994, Taylor & Raga, 1995, Raga, Cabrit, & Canto, 1995) Here, entrainment occurs along the sides of the jet by turbulent mixing of the ambient material through Kelvin-Helmholtz instabilities The turbulent layer thickens with distance from the source as more and more ambient gas is pulled into the layer Eventually the jet itself will be completely pinched off and the flow will become fully turbulent (Davis et al , 1997) This model is unsatisfactory in the case

of high Mach number flows, such as the ones we are considering here, as the bow shock formed at the end of a highly supersonic jet will push the ambient gas aside into a high-density "shroud", which will be separated from the beam of the jet by a warm, low density "cocoon", restricting contact between the jet and the ambient gas (Chernin, Masson, Gouveia dal Pino, & Benz, 1994, De Young, 1986)

1 3.4 Parsec - Scale Optical Outflows

Outflow Lengths

It was initially assumed that optical outflows were only of the order of $\lesssim 0\ 1$ pc in length (Mundt, Brugel & Buhrke, 1987) However a number of observations hinted that this may not be the case, e g the discovery of a 1 4 pc outflow from RNO 43 (Ray, 1987) and of the 2 8 pc HH 34 outflow (Bally & Devine, 1994) In the last decade many parsec - scale outflows have been observed (Reipurth & Bally, 2001)

It is not surprising that such outflows can attain these lengths when we consider that they have tangential velocities of between 50 – 200 kms^{-1} (Devine et al , 1997, Reipurth, Bally, & Devine, 1997) and the outflow phase lasts for at least 10^5 years (i e the timescale for a low - mass, Class I source – §1 2 1) In reality, it should be *expected* that most will attain parsec - scale lengths with the fastest moving outflows possibly extending up to 20 pc

Although outflows may reach such lengths, there are a number of reasons why they may be difficult to observe The main observational hindrance in the past was the relatively small fields of view offered by most CCD cameras With the advent of large format CCD mosaics more and more parsec - scale outflows have been discovered Another factor that may be important is the position of the outflow within its parent cloud An outflow may extend beyond the boundary of its parent core and into the ISM or interclump medium Any terminal shocks generated in the outflow/ambient medium interaction will probably be very faint as the density of the ISM/intercloud medium is much less than that of the core However if earlier ejecta has already blown out of the cloud into the surrounding medium, any subsequent ejecta may be optically visible through interactions with it In such a scenario some HH objects may be seen just beyond the edges of the cloud boundary – many of the large - scale outflows presented by Reipurth, Bally, & Devine (1997) demonstrate

this, especially HH 355 in the T Tauri outflow, HH 300 A in the IRAS 04239+2436 outflow and the PV Cep and RNO43 outflows.

Timescales

The dynamical age of an outflow can easily be estimated, based on its velocity and optically observed length. However it must be noted that in most cases its *full* extent has not been observed and its true age is much larger.

As the dynamical age of parsec-scale outflows are typically of the order of 10^4 years they can be a significant fraction of the major accretion period of the source. Therefore they may be used to extrapolate not only the mass ejection but also, to a limited degree, the mass accretion history of the source.

Typical Sources of Parsec-Scale Outflows

The majority of the parsec-scale outflows that have been observed to date are driven by *Class I low-mass* YSOs. Optical outflows are not usually observed from Class 0 sources, presumably due to the extinction caused by the dense envelope of gas and dust that surrounds the forming star. By the time a YSO has evolved to Class II, a significant fraction of this envelope has either been accreted or driven away. As the outflow rate is intrinsically linked to the accretion rate and steeply declines with age (§1.3.1; Fig. 1.5) when outflows are observed from Class II sources they are generally small scale so-called "micro-jets" (Solf, 1997). While jets and outflows have been observed from such sources they have generally not been seen to extend to parsec-scale lengths (however see Chapters 3 and 4). Parsec-scale outflows driven by intermediate-mass YSOs are rare, as discussed earlier (§1.3.2).

This thesis explores the occurrence of parsec-scale optical outflows from both intermediate-mass YSOs (Chapter 2) and Class II low-mass stars (Chapters 3 and 4). Observations of these outflows are presented, and are compared to those from more "typical" sources i.e. low-mass Class I YSOs.

Morphology

One of the most striking morphological trends that parsec-scale outflows exhibit is an exponentially decreasing frequency of HH emission with distance from their source. Rather than signifying a time dependent increase in the rate at which mass

is ejected, this decreasing frequency is almost certainly due to the fact that internal shocks generated by physically smaller ejection events decay quickest so that only the largest, most evolved shocks are seen at great distances from the source As faster ejecta collide with, and sweep up, previously ejected material moving at a slower velocity, large shocks are created followed by regions devoid of any strong emission As a consequence of this, the more distant ejecta in these outflows also tend to be more chaotic and have larger dimensions than the HH objects seen closer to the source The HH 34 outflow (Fig 1 8) demonstrates this – the bow shocks HH 34 N and HH 34 S to the north and south of the jet respectively are much larger and more complex than the HH 34 jet The morphology of these outflows also suggests that the YSO undergoes quiescent phases punctuated by violent mass eruptions giving rise to the HH objects/complexes seen (see Chapter 3)

Parsec-scales outflows also tend to display some degree of bending Most often outflows are "S" shaped with the source in the middle of the "S" The most likely cause of such morphology is precession of the jet or deflection caused by interactions with dense clumps in the ambient medium (Dutrey, Guilloteau, & Bachiller, 1997) In rarer cases the outflows are "C" shaped with the source at the centre and are possibly caused by the motion of the source through the parent cloud (Eisloffel, 2000) While noticeable "S" and "C" shaped outflows are not always the case, *some* changes in outflow direction are generally seen on extended scales

Blow Outs

If outflows can reach lengths of 10 – 20 pc as I estimated earlier, they will be about an order of magnitude greater in size than their parent core, i e they will "blow out" This is indicated in many outflows by the fact that HH objects are often seen at or near the cloud boundaries but much less frequently beyond However *once* they have blown out of the cloud any shocks generated will be too faint to be seen at optical wavelengths

Kinematical Velocities

There is a claimed systematic decrease in the proper motions and radial velocities of HH objects with increasing distance from the source (Reipurth & Bally, 2001) Cabrit & Raga (2000) suggest two possible explanations for this First, the ejection velocity of the jet is slow to build up and so earlier ejecta has a slower velocity

than material currently being ejected A comparison of the dynamical and outflow timescales would suggest that this explanation is rather contrived The second, and more likely, explanation is that the interaction of the jet with the surrounding medium slows down the ejecta In Chapter 4 I present proper motion studies of the HH objects in outflows from CTTSs that are presented in Chapter 3 and I examine whether the claimed decrease in tangential velocities is actually observed

1.4 Summary and Foreword

Parsec-Scale outflows are commonly observed from low-mass Class I, i e embedded, sources These outflows are thought to remove excess angular momentum, preventing the star from rotating to breakup velocities Their dynamical timescales are such that the recent mass-loss and therefore accretion history of the star can be extrapolated from them, i e they are a "fossil record" of the mass-loss history of the source Parsec-scale outflows may also be a replenishing source of turbulence in the parent cloud, and may even affect subsequent star formation in their vicinity

This thesis aims to determine whether parsec-scale outflows occur from intermediate-mass YSOs and also whether they persist into the Class II low-mass phase The morphology and kinematics of these outflows will be compared to the more common parsec-scale outflows from "typical" sources of such outflows (Class I low-mass sources) to establish similarities

In Chapter 2 I present observations of parsec-scale outflows from six intermediate-mass YSOs The morphology, dynamical timescale and degree of collimation of these outflows are noted/estimated and are compared to those of similar length outflows from low-mass Class I sources In Chapter 3 outflows from five CTTS sources are presented and are similarly discussed in comparison to outflows from low-mass Class I sources Proper motion studies are done on these CTTSs outflows and are presented in Chapter 4 These studies not only determine the tangential velocity of the HH objects but also confirm or refute their suggested driving sources How the velocities of HH objects evolves with distance from the source is also examined for these outflows Conclusions drawn from these studies are presented in Chapter 5 with necessary future work also detailed here

Chapter 2

Parsec-Scale Outflows from Intermediate-Mass Sources

As discussed in Chapter 1, the majority of known optical jets have low-mass ($\sim 1 M_\odot$) sources either the embedded (Class I) counterparts of CTTSs or CTTSs themselves (Reipurth, Bally, & Devine, 1997) and these outflows tend to be very highly collimated Turning to higher mass YSOs ($> 10 M_\odot$), such as those driving the Orion OMC1 (Fig 1 9) or Cepheus A outflows, one sees a very different picture (Allen & Burton, 1993, O'Dell et al , 1997, Hartigan, Morse, & Bally, 2000) Their outflows, although highly energetic, often appear poorly collimated and more chaotic (Reipurth & Bally, 2001) than their low-mass counterparts This transformation suggests two obvious inter-related questions at what point does the transition occur and is it a smooth function of mass? To answer these questions one must examine outflows from YSOs of mass greater than $\sim 2 M_\odot$

Optical outflows have been observed from a number of intermediate-mass ($2 M_\odot \leq M_* \leq 10 M_\odot$) YSOs, for example R Mon, LkHα 234, and AFGL 4029 (Ray et al , 1990 and references therein) Such stars, where optically visible, are known as HAeBe stars although their embedded counterparts have also been seen Optical outflows from these YSOs are rare however and there are a number of reasons for this The initial mass function favours the production of low mass stars and therefore intermediate mass YSOs tend to be found at relatively large distances from us More massive stars also have a faster evolutionary timescale – i e they evolve more quickly than low-mass YSOs and so their outflow phase is shorter making

their outflows more difficult to detect Another contributing factor could be that massive stars tend to be more obscured intermediate-mass and massive stars tend to be surrounded by large amounts of circumstellar gas and dust, making it harder to find an outflow at visual wavelengths Finally there may well have been a historical bias towards studying outflows from low-mass stars The situation however has changed in recent years as more and more studies focus on higher mass YSOs

With these ideas in mind, I have investigated the occurrence of large-scale outflows from intermediate-mass stars By large-scale I mean those stretching several parsecs e g the PV Cephei outflow at 2 6 pc (Gomez, Kenyon, & Whitney, 1997, Reipurth, Bally, & Devine, 1997), the HH 80/81 5 3 pc outflow (Martí, Rodríguez, & Reipurth, 1993) and the HH 354 outflow at 2 4 pc (Reipurth, Bally, & Devine, 1997) I emphasise that these outflows have vastly longer associated timescales than the smaller scale outflows that have been "traditionally" observed A small-scale HH jet close to its source has a dynamical timescale of only a few hundred years, whereas the HH objects in these parsec-scale flows trace mass ejection over tens of thousands of years They are, in effect, fossil records of the mass-loss histories of their parent star

Newly detected parsec-scale outflows around five intermediate-mass young stars are discussed here Twenty-six new HH objects were found in this study – their positions and probable sources are listed in Table 2 1 Of these sources LkHα 198, LkHα 233 and LkHα 234 are of spectral type A and 1548C27 is A7-F0 All five of these stars were known to possess small-scale optical outflows The one optically invisible YSO in this sample, IRAS 19395+2313, was not previously known to drive any outflow The lengths and morphologies of these outflows are examined and compared to outflows of comparable length from low-mass sources (which were described in §1 3 4) The degree of collimation and dynamical timescales of these outflows is estimated and discussed Whether these outflows could be a mechanism of replenishing turbulence in the parent cloud (see §1 3 1) is also discussed here

§2 1 describes the observations and method and in §2 2 I present the newly discovered parsec-scale outflows The implications of these findings are discussed in §2 3

Object	Source	α(J2000)	δ(J2000)
HH 800	LkHα 198 IR?	$00^h11^m02\ 0^s$	$+58°55'04''$
HH 801	LkHα 198	$00^h11^m12\ 0^s$	$+58°54'01''$
HH 802	LkHα 198	$00^h11^m44\ 5^s$	$+58°42'39''$
HH 803	1548C27 IRS 1	$19^h42^m47\ 0^s$	$+23°22'19''$
HH 804	IRAS 19395+2313	$19^h42^m10\ 4^s$	$+23°21'49''$
HH 805	IRAS 19395+2313	$19^h41^m41\ 5^s$	$+23°20'34''$
HH 806	UNKNOWN	$19^h42^m03\ 4^s$	$+23°20'02''$
HH 807	UNKNOWN	$19^h42^m07\ 1^s$	$+23°19'54''$
HH 808	LkHα 233	$22^h34^m35\ 6^s$	$+40°39'42''$
HH 809	LkHα 233	$22^h34^m30\ 4^s$	$+40°39'01''$
HH 810	LkHα 233	$22^h34^m21\ 2^s$	$+40°37'34''$
HH 811	LkHα 233	$22^h34^m14\ 5^s$	$+40°36'48''$
HH 812	LkHα 233	$22^h34^m11\ 6^s$	$+40°36'33''$
HH 813	LkHα 233	$22^h34^m06\ 6^s$	$+40°36'18''$
HH 814	LkHα 233	$22^h35^m01\ 4^s$	$+40°43'33''$
HH 815	LkHα 234	$21^h44^m29\ 9^s$	$+66°13'42''$
HH 816	LkHα 234	$21^h44^m26\ 4^s$	$+66°10'58''$
HH 817	LkHα 234	$21^h44^m13\ 3^s$	$+66°10'55''$
HH 818	LkHα 234	$21^h43^m57\ 7^s$	$+66°10'26''$
HH 819	LkHα 234	$21^h44^m01\ 0^s$	$+66°09'52''$
HH 820	LkHα 234	$21^h43^m47\ 9^s$	$+66°09'50''$
HH 821	LkHα 234	$21^h43^m43\ 4^s$	$+66°08'47''$
HH 103 A	LkHα 234	$21^h42^m20\ 7^s$	$+66°03'31''$
HH 822	LkHα 234	$21^h41^m42\ 1^s$	$+66°01'45''$
HH 823	UNKNOWN	$21^h43^m27\ 9^s$	$+66°11'46''$
HH 824	IRAS 21416+6556	$21^h42^m56\ 9^s$	$+66°09'10''$
HH 825	IRAS 21416+6556	$21^h42^m39\ 2^s$	$+66°10'56''$

Table 2.1 Positions and *probable* sources of the HH objects found in the intermediate-mass source survey

2.1 Observations and Method

To carry out this survey the Wide Field Camera (WFC) at the prime focus of the 2 5m Isaac Newton Telescope at El Observatorio del Roque de los Muchachos (La Palma, Canary Islands) was used The WFC consists of four thin-coated EEV CCDs each with 2048 x 4100 pixels which are 13 5μm in size One pixel projects to 0″33 on the sky Three of the CCDs are positioned from north to south with their long axes adjoining The fourth is attached to the west to form a square mosaic (34′2 wide) with its northwestern corner missing (see Fig 2 1)

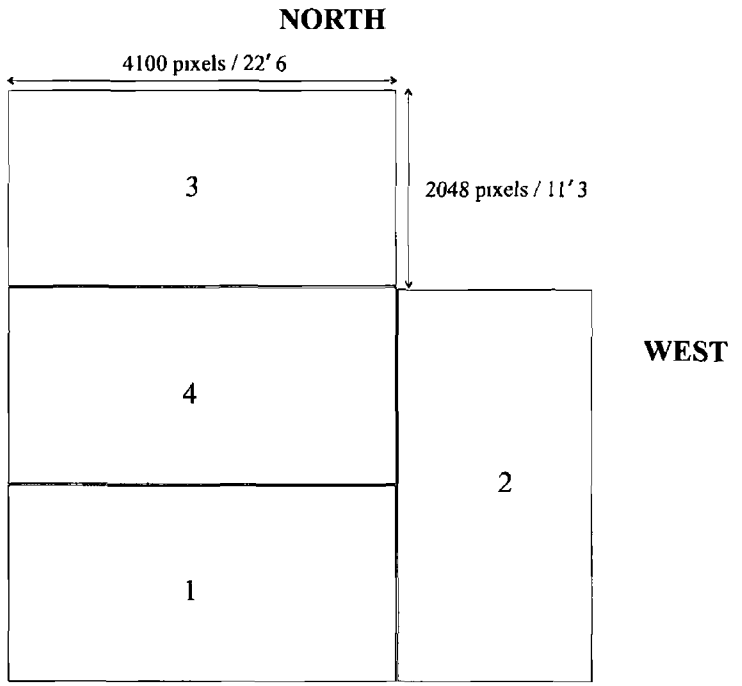

Figure 2 1 Schematic of the four CCD WFC mosaic

The images were taken on nights between the 13th and the 21st of July 1998 Seeing was moderate at 1″15 – 1″5 as measured from the images HH objects were identified using two narrowband emission line filters Hα(λ_c = 656 8nm, $\Delta\lambda$(FWHM) = 9 5nm) and [SII](λ_c = 672 5nm, $\Delta\lambda$(FWHM) = 8 0nm) To distinguish HH emission from reflection nebulosity, broadband images in V and I were also taken Exposure times for the narrowband and broadband images were typically 30 and 10 minutes respectively The data was reduced using IRAF[1] software for bias sub-

[1]IRAF is the Image Reduction and Analysis Facility – software for the reduction and analysis of astronomical data

traction and flat fielding

There are a number of criteria that were used separately or simultaneously to determine a possible driving source(s) for newly detected HH objects Firstly, if a HH object is aligned with a previously known jet or HH object(s) then they are most probably driven by the same source Similarly if a number of HH objects are detected which appear to be aligned then the direction(s) of the driving source can be inferred As discussed in Chapter 1 parsec-scale outflows can undergo some directional changes, however these are usually very gradual and the position of the source can still be estimated Secondly, in certain cases the morphology of the object can allude to its source For example, in the case of a bow shock the outflow direction is more than likely along the apex of the shock (unless part of the shock is optically obscured or the bow shock is asymmetrical due to the impact that caused the shock) If the object is linear, which is most likely only if it is close to its source, then it is probable that the source is also along this linear direction These morphological alignment criteria are used to suggest candidate driving sources (and determine if these new objects are part of extended outflows) for the newly detected objects here and in Chapter 3

The sources observed here are intermediate-mass/HAeBe YSOs and were previously known to possess outflows, with the exception of IRAS 19395+2313 which was discovered in the field of view of the 1548C27 observations Nine such sources were observed, with four of them – LkHα 198, 1548C27, LkHα 233 and LkHα 234 revealing five extended outflows in their fields of view No additional extended optical emission was found in the KK Oph, VV Ser, V1685 Cyg, WW Vul or PV Cep outflows

2.2 Results for Individual Regions

2.2.1 LkHα198 & V376 Cas

LkHα 198 and its nearby companion, V376 Cas, are both Herbig Ae stars (Herbig, 1960) located in the small dark cloud L1265, at a distance of 600 pc (Chavarria-K , 1985) An asymmetrical, bipolar molecular outflow in this region was noted by Canto et al (1984) Strom et al (1986) subsequently found the first optical

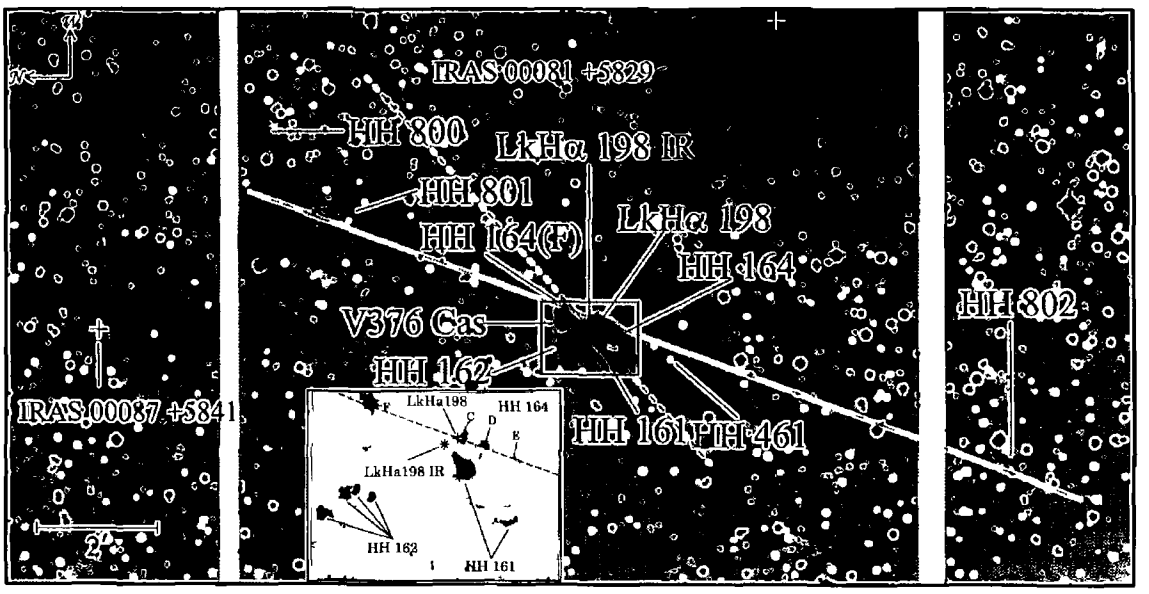

Figure 2 2 *LkHα198 [SII]* Mosaic of the entire outflow around LkHα198, including the three newly discovered HH complexes with the main outflow axis delineated by a dotted line For all images relating to LkHα 198 (Figs 2 2, 2 3 and 2 4) north is to the left and west to the top but for all subsequent images in the thesis north is to the top The continuum subtracted [SII] image of Corcoran, Ray, & Bastien (1995) is inset, showing the HH 164 knots (C, D, E and F), most of which are not seen in the [SII] image due to the presence of the reflection nebula Here, the position of LkHα 198 is indicated by a red cross slightly northeast of knot C The PA of HH 164 at 340° (Corcoran, Ray, & Bastien, 1995) is marked on the inset and it can be seen from the outflow axis on the main image that the PA of the extended outflow is also at 340° The PA of HH 161 with respect to LkHα 198 IR at 132° is marked with a dashed line There are two known optically invisible IRAS sources in the region and their positions are marked The white strips delineate gaps in the WFC CCD mosaic

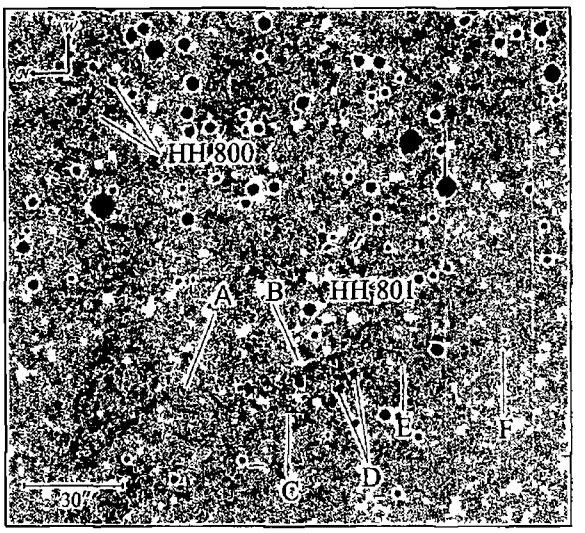

Figure 2 3 *LkHα 198 [SII]* HH 800 and HH 801 showing various features referred to in the text The knotty morphology of HH 801 is clearly seen here

outflow tracer, HH 161, a bright HH object some 12″ from LkHα 198 at a position angle[2] (PA) of 100° (Fig 2 2) Further observations by Goodrich (1993) yielded another HH knot 81″ away at a PA of 153° This object was rediscovered by Aspin & Reipurth (2000) who refer to it as HH 461

The discovery, however, of LkHα 198 IR, a deeply embedded companion to LkHα 198 with a luminosity of $\sim 100 L_{\odot}$, by Lagage et al (1993) raised the question of which of these two stars is the primary outflow source in this region In their study Corcoran, Ray, & Bastien (1995) (hereafter referred to as CRB) concluded there are two separate outflows with their origin in the vicinity of LkHα 198 one driven by LkHα 198 itself and the other by LkHα 198 IR Their observations of HH 161 revealed a tail pointing back towards LkHα 198 IR and they also discovered a suspected bow shock 39″ southeast of this source The bow shock, HH 161 and its tail are all aligned and appear to constitute a one-sided outflow from LkHα 198 IR To date no counterflow has been seen CRB also found a number of faint HH knots (HH 164 C, D and E – see inset in Fig 2 2) with the same PA from LkHα 198 as HH 461 Thus HH 164 C, D and E and HH 461 appears to delineate an outflow from LkHα 198 To the north they also discovered a faint knot (HH 164 F) which may be a tracer of the counterflow from LkHα 198 Finally to the east of V376 Cas a

[2]Position angle is measured from North through East

Object	Source LkHα 198	Angular Separation[a]	PA[b] /°	Spatial Extent[c]
HH 800	LkHα 198 IR?	6′25	330	0′1 × 0′6
HH 801	LkHα 198	4′95	340	0′5 × 1′2
HH 802	LkHα 198	6′2	160	0′8 × 2′

Table 2 2 Angular separations, PAs and spatial extent of newly discovered HH objects in the LkHα 198/LkHα 198 IR region
[a] Angular distance from the presumed source
[b] PA with respect to the presumed source
[c] Width and length of the object respectively

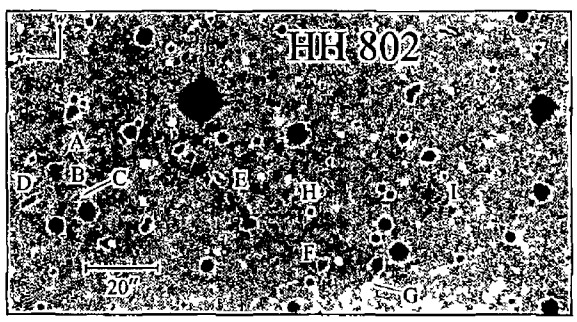

Figure 2 4 *LkHα198 [SII]* HH 802, to the southeast of LkHα 198

number of bright HH emission knots, HH 162, were also found by CRB These knots were seen again in these new images, although their origin remains unclear

Two of the three HH complexes found here (see Table 2 2) are extensions of the outflow from LkHα 198 discovered by CRB, while the third may be part of the LkHα 198 IR outflow HH 801 has the same PA of 340° with respect to LkHα 198 as HH 164 F and is therefore almost certainly part of the same flow It appears to be an asymmetrical bow shock of which primarily the western wing is seen (B in Fig 2 3) some 45″ in length, at a distance of 4′95 (∼ 0 9 pc) from LkHα 198 There are also a number of more easterly knots, C - F Knot A may also be part of the western wing

In the diametrically opposite direction from HH 801 through LkHα 198 is HH 802 It consists of a number of features, A – I (Fig 2 4) which look somewhat chaotic Feature E, however, like its counterpart in HH 801, could be the western wing of an asymmetrical bow shock The total length of HH 802 is 2′ It has a PA of 160° with respect to LkHα 198 and is aligned with knots C, D and E of HH 164 (CRB)

and HH 461 i e it is the counterflow of HH 801 and HH 164 Knot F The furthest knot in HH 802 (Knot I) is at a distance of 8′ 16 (1 4 pc) from LkHα 198, implying the total projected extent of the flow, from HH 801 to HH 802, is 2 3 pc

HH 800 to the northwest of HH 801 is unlikely to be part of the HH 801 – HH 802 outflow unless the outflow direction has changed abruptly Although changes in flow direction have been observed in other parsec-scale outflows (Reipurth & Bally, 2001), they tend to be more gradual Moreover HH 802 is even further from LkHα 198 than HH 800 (at least in projection) and the flow associated with the former appears to have maintained a constant outflow direction HH 800 may be part of the counterflow from LkHα 198 IR which should be at a PA of 312° if it is aligned with its outflow (at 132°) while HH 800 is at ∼ 330° with respect to this source It is possible that the outflow axis may have swung through 18° over the distance of 6′ 3 from LkHα 198 IR to HH 800 Alternatively, it could have been produced by either of the two optically invisible IRAS sources in the region (Fig 2 2) IRAS completeness[3] in this region is of the order of $5L_{\odot}$ Proper motion studies would clearly help to identify its origin

2.2.2 1548C27

The cometary-shaped reflection nebula 1548C27, and its associated Hα emission line jet (HH 165) were first noted by Crane, Byard, & Boeshaar (1981) The optical jet, at a PA of 54°, was later confirmed by Mundt et al (1984) A low-mass, poorly collimated molecular outflow was also observed in the region by Dent & Aspin (1992)

Near-infrared photometry in the immediate vicinity of 1548C27 by Vilchez et al (1989) yielded two potential sources One of these appears to be a foreground star but the other, IRS 1, is located near the apex of the nebula, and they suggest this to be the driving source of HH 165 (see Fig 2 5) The IRAS PSC (point source catalogue) shows IRAS 19407+2316 to be located close to, but not coincident with, IRS 1 Vilchez et al (1989) however conclude that both near- and far-infrared

[3]However this obviously depends on the temperature of the YSO/star and whether it peaks in the 12μm – 60μm range where the IRAS completeness is calculated from i e completeness is $5L_{\odot}$ for mainly Class 0/I YSOs (see Fig 1 2)

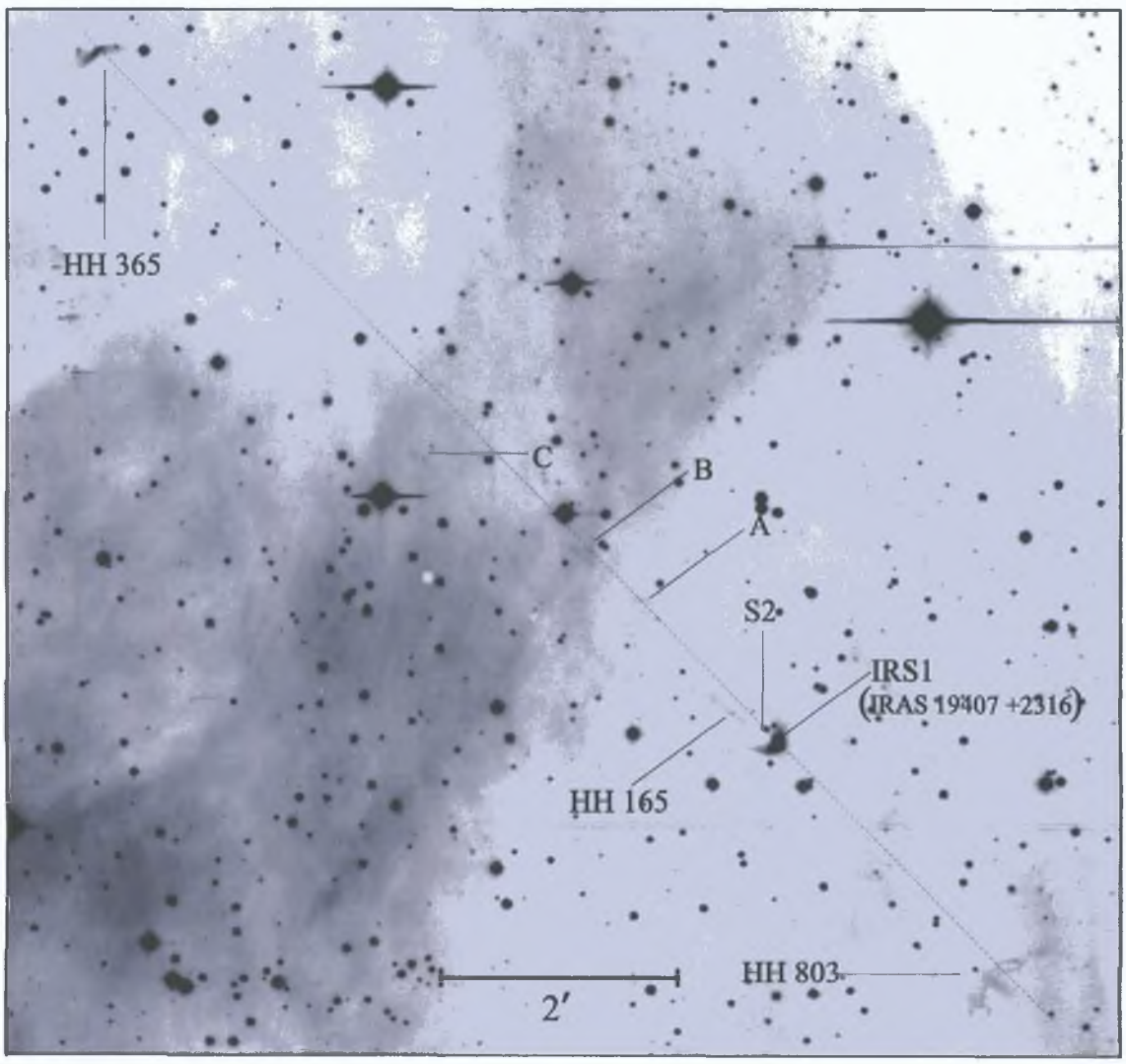

Figure 2.5: *1548C27 Hα:* Entire outflow around 1548C27 IRS 1. Note that north is to the top and east to the left in this and subsequent images. An approximate outflow axis is marked here, at a PA of $\sim 45°$, however the outflow appears to be precessing – see text.

Object	Source	Angular Separation[a]	PA[b] /°	Spatial Extent[c]
HH 803	1548C27	2'6	223	50″× 13″
Knot A	1548C27[d]	1'6	44	13″× 5″
Knot B	1548C27[d]	2'2	48	10″× 13″
Knot C	1548C27[d]	3'8	53	10″× 12″

Table 2 3 Angular separations, PAs and spatial extent of newly discovered HH (and HH-like) objects in the 1548C27 region
[a] Angular distance from the presumed source
[b] PA with respect to the presumed source
[c] Width and length of the object respectively
[d] Alignment with HH 165 suggests that these knots are driven by 1548C27 IRS1 *if* they are HH objects

sources are the same object, which, for convenience, I will refer to here as IRS 1

The optical jet (HH 165) is very narrow, with a width of 2″ - 3″ and its length is estimated to be $\sim$ 45″ There is a gap of $\sim$ 13″ between the source and the jet and two bright knots are visible at 23″ and 29″ from the source (Mundt et al , 1984) The kinematic distance of 1548C27 is 2 4 kpc Dent & Aspin (1992) which implies a luminosity for IRS 1 of approximately 580 $L_{\odot}$

Another star S2, 10″ northeast of 1548C27, was found by Scarrott, Rolph, & Tadhunter (1991) This star illuminates the nebula along with IRS 1 Scarrott, Rolph, & Tadhunter (1991) suggest HH 165 curves towards this star, implying that it is the driving source, however I find no evidence in these images to support this

HH 365 to the northeast of 1548C27 was briefly referred to by Alten et al (1997) as being bow-shaped and possibly associated with HH 165 This object was mentioned in their paper but no image of it was included Its morphology is clearly seen here in Figs 2 5 and 2 6 HH 365 is 8'13 (5 7 pc) from IRS 1 at a PA of 46° i e close to that of the HH 165 jet From these images it appears to consist of two bright regions, Knot A and Feature B that extends to the northwest some 8″ (Fig 2 6) The overall shape of Feature B is suggestive of an asymmetrical bow, the axis of which points roughly back towards 1548C27

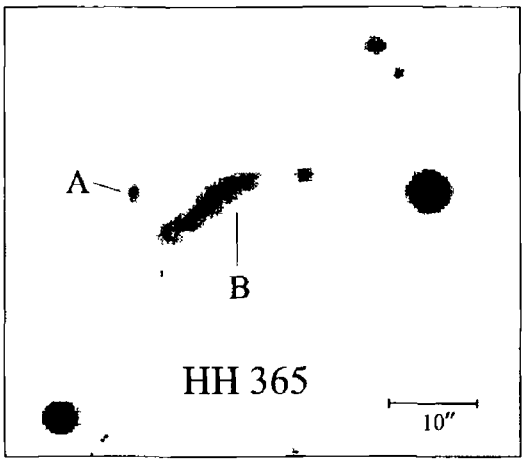

Figure 2 6 *1548C27 Hα* HH 365, to the northeast of 1548C27 IRS 1

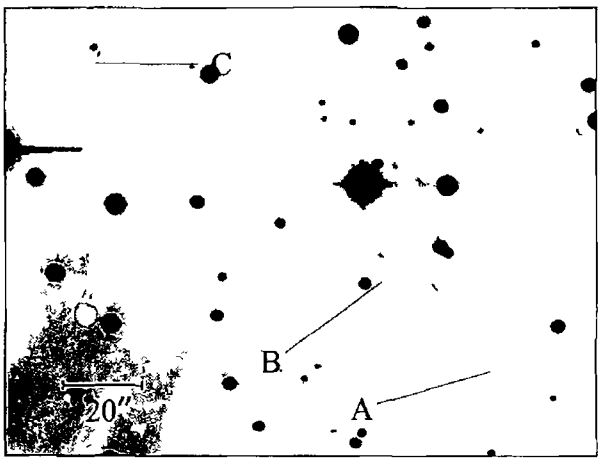

Figure 2 7 *1548C27 Hα* Possible HH knots A, B and C to the northwest of HH 165

This survey also revealed a number of possible new HH objects (see Fig 2 5 and Table 2 3) although several are very faint Moreover, it is unclear whether Knots A, B and C (Fig 2 7) to the northeast of HH 165 are HH objects, as there is a lot of contaminating HII nebulosity in the region However the fact that these lie on the path between HH 165 and HH 365 would suggest they might be Further study is necessary, however, to determine their nature and for this reason I will refrain from assigning them HH numbers In any event it seems likely that HH 165 and HH 365 are part of the same outflow from IRS 1 and that Knots A, B and C may also be part of this flow

A counterjet from IRS 1 was found recently in the near-infrared (Whelan, private communication) It lies along the same line as HH 165 at a PA of 234° and extends for at least 5″ A number of faint [FeII] emitting knots were also seen beyond the counterjet Neither the counterjet nor any of these knots are observed in these optical images, presumably because of extinction

HH 803 (Fig 2 8), 2′63 (1 85 pc) southeast of IRS 1 at a PA of 223°, has a very interesting morphology It appears to be bow-shaped but convex towards IRS 1 It is 50″ in width and contains a 13″ "jet-like" feature bisecting the bow The "ring" at the southern edge of the bow and the diffuse appearance of Knot A to the west add to the complexity of this object Note that the jet-like feature does not quite point back towards IRS 1 I should also add that apart from IRS 1, no other IRAS

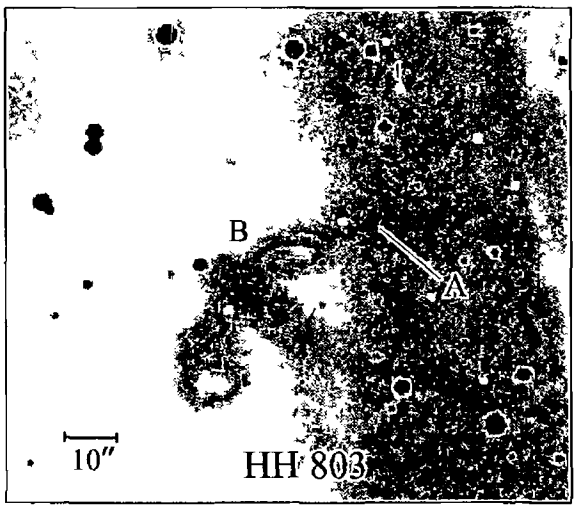

Figure 2 8 *1548C27 Hα* The morphology of HH 803 is clearly seen here

sources were found in the region strengthening the possibility that HH 803 is driven by IRS 1 However IRAS completeness at this distance is $\geq 100 L_{\odot}$[4]

If Knots A, B and C are included as part of the HH 165/HH 365/HH 803 outflow then its overall appearance suggests that it may be slowly precessing with shifts in the outflow direction of at least 10° The sense of precession (i e point-like symmetry through IRS 1) to the northeast is also consistent with the position of HH 803 to the southwest

2.2.3 The IRAS 19395+2313 Region

A number of HH objects and possible sources were found in this region (see Fig 2 9 and Table 2 4), which lies approximately 18′ west of 1548C27 and is in the vicinity of the young open cluster NGC 6823, as is 1548C27 It is highly unlikely that any of these newly-discovered HH objects are part of the 1548C27 IRS 1 outflow although I will assume they are at the same distance, i e 2 4 kpc

Two of the newly discovered HH objects are found close together - HH 806 is 30″ west of HH 807 (Fig 2 9) The region between them coincides with a gap in the CCD mosaic although a cursory inspection of the Palomar Sky Survey Red

[4]As previously explained in this Chapter, the accuracy of the IRAS completeness depends on the temperature peak of the sources

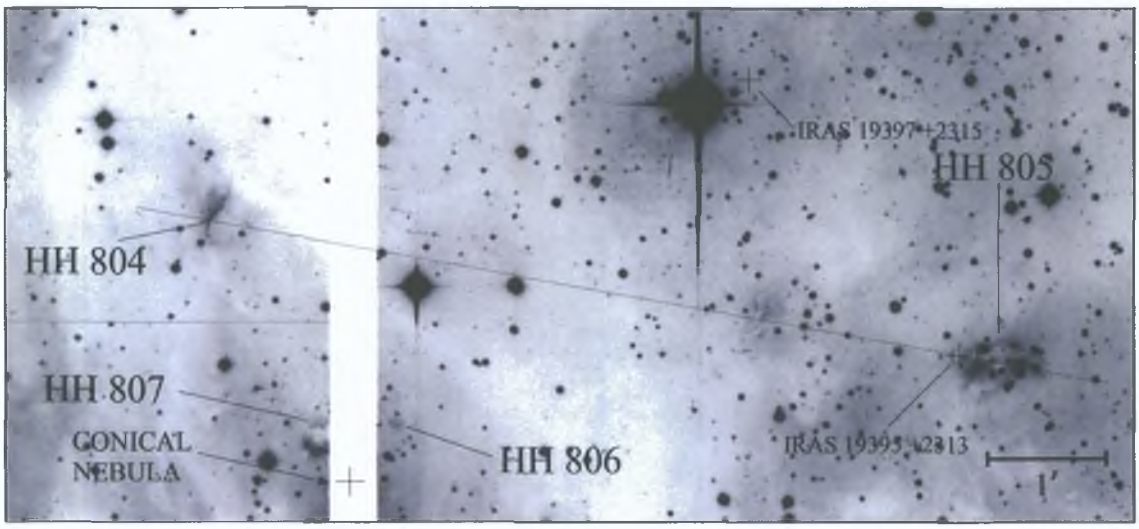

Figure 2.9: *IRAS 19395+2313 Hα:* The region around IRAS 19395+2313, including all known additional IRAS sources in its vicinity. IRAS completeness at this distance is $\geq 100 L_{\odot}$. Four newly discovered HH objects are marked. The position of the conical nebula, visible on the Palomar Sky Survey Red (E) plate which might be associated with the driving source for HH 806, is indicated. The possible outflow from IRAS 19395+2313 is marked with a dotted line at a PA of 80°.

(E) plate shows there is a star in the "gap", ALS 10422 or IRAS 19399+2312 (at $19^h42^m05.5^s$ +23°18′59″, J2000) which, at first sight, might be a possible YSO. This object is however an AGB star (Parthasarathy, Vijapurkar, & Drilling, 2000) so it can be disregarded. On the Palomar Sky Survey red (E) plate, a conical nebula is seen $\sim 36''$ southeast of HH 806 (at $19^h42^m02.12^s$ +23°19′30″, J2000) which may be associated with the HH 806 source. In fact HH 806 lies along the major axis of this conical nebula. Although this nebula is not seen in Fig. 2.9, its position is marked. There is no obvious driving source for HH 807.

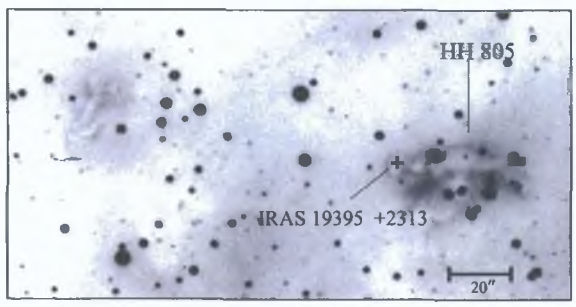

Figure 2.10: *IRAS 19395+2313 Hα:* HH 805 and its candidate driving source.

Object	Source	Angular Separation[a]	PA[b] /°	Spatial Extent[c]
HH 804	IRAS 19395+2313	6′3	80	20″× 3″
HH 805	IRAS 19395+2313	∼ 0	260	16″× 45″
HH 806	conical nebula[d]	0′6	322	10″× 3″
HH 807	?			10″× 2″[e]

Table 2 4 Angular separations, PAs and spatial extent of newly discovered HH objects in the IRAS 19395+2313 region

[a] Angular distance from the presumed source

[b] PA with respect to the presumed source

[c] Width and length of the object respectively

[d] Details of this possible source for HH 806 is given in the text

[e] As direction of motion is unknown, width and length may be in reverse order

HH 805 has an interesting morphology (Fig 2 10) and IRAS 19395+2313 seems an obvious candidate to be powering it, given its position I have estimated the luminosity of IRAS 19395+2313 to be ∼ 320 $L_{\odot}$ The angular extent of HH 805 is approximately 45″ (0 5 pc) and it can be seen from Fig 2 10 that this outflow is poorly collimated Morphologically it appears to have a knotty ring-like structure and is reminiscent of the HH complex associated with V380 Ori (Corcoran & Ray, 1995) HH 804 (Fig 2 9) may be part of the counterflow from IRAS 19395+2313 although I emphasise that this association is *highly* uncertain It is at a PA of 80° with respect to the latter HH 804 is at a distance of 6′3 from IRAS 19395+2313, implying the total projected extent of the flow, assuming HH 804 is part of it, is ∼ 5 pc

2.2.4 LkHα 233

LkHα 233 is an A5e-type pre-main sequence star (Corcoran & Ray, 1997) at a distance of 880 pc and is associated with a bipolar nebula that is approximately 0 1 pc in size (Calvet & Cohen, 1978, Staude & Elsasser, 1993) The nebula has a distinct X-like morphology with bright reflection limbs at 50°/90° and 230°/270°

The discovery by Leinert, Haas, & Weitzel (1993) of a light scattering "halo" ∼ 1″ in size around LkHα 233 led them to suggest that the star is highly embedded and optically visible largely through scattered light Corcoran & Ray (1998) discovered a bipolar jet and counterjet (HH 398) spectroscopically at PAs of approx-

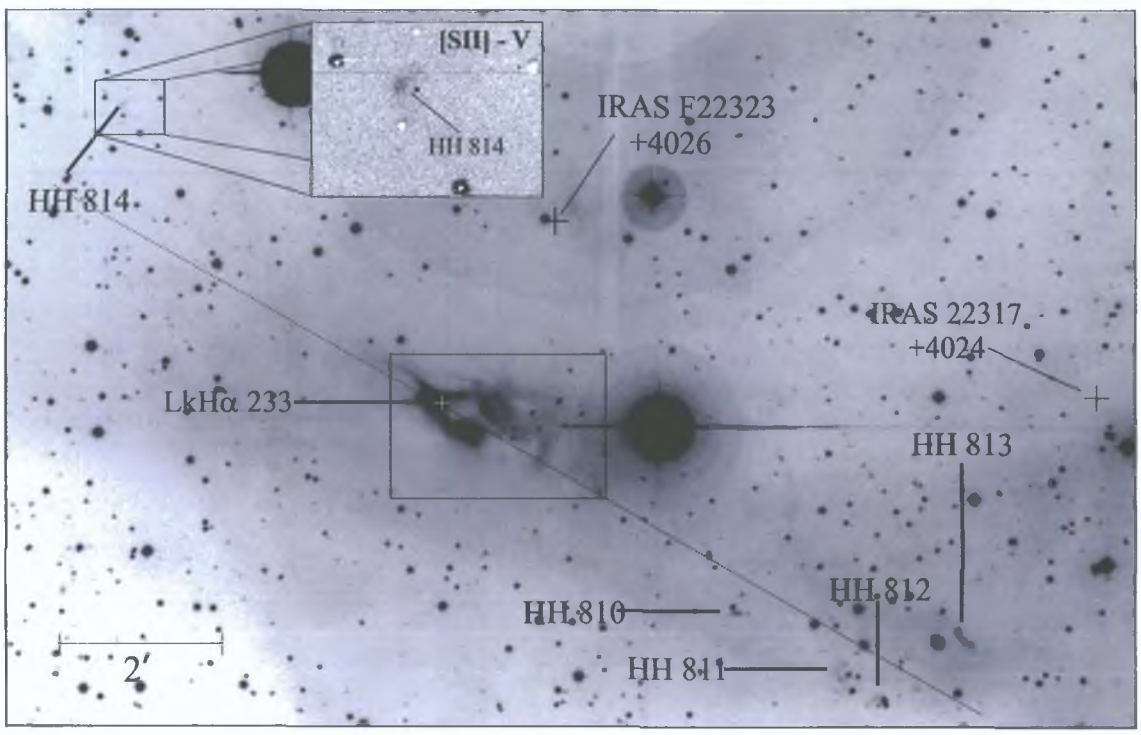

Figure 2.11: *LkHα 233 [SII]:* The entire outflow around LkHα 233 including all known optically invisible IRAS sources in the region. The approximate axis of the outflow at 62° through the source is indicated by a dotted line. The continuum subtracted ([SII]-V) image in the top left corner shows HH 814 more clearly. The area around LkHα 233 (marked by a box) is seen in more detail in Fig. 2.12.

Object	Source	Angular Separation[a]	PA[b] /°	Spatial Extent[c]
HH 808	LkHα 233	1′1	250	2″× 3″
HH 809	LkHα 233	2′2	241	2″× 5″
HH 810	LkHα 233	4′5	236	15″× 5″
HH 811	LkHα 233	6′	236	19″× 14″
HH 812	LkHα 233	6′5	236	12″× 12″
HH 813	LkHα 233	7′	247	6″× 17″
HH 814	LkHα 233	5′2	47	7″× 4″

Table 2 5 Angular separations, PAs and spatial extent of newly discovered HH objects in the LkHα 233 region
[a] Angular distance from the presumed source
[b] PA with respect to the presumed source
[c] Width and length of the object respectively

imately 245° and 65° that bisect the X-shaped nebula In their spectrograms, the redshifted counterjet is seen to begin 0″7 from the centre of the stellar continuum, whereas the blueshifted jet can be traced right back to the continuum peak

Evidence for the presence of a large "polarisation disk" centred on LkHα 233 with a radius of about 15000 AU was found by Aspin, McCaughrean, & McLean (1985) The position angle of this disk is about 155°, which places it perpendicular to the observed optical outflow The existence of this "polarisation disk" combined with the fact that the counterjet is not seen spectroscopically close to the star leads to the conclusion that there is a circumstellar disk present that obscures the beginning of the receding flow

Close to LkHα 233 the [SII] emission can be resolved into two velocity components (Corcoran & Ray, 1998) The high velocity component is identified with the optical jet while the low velocity component, which extends to < 2″ from the star, may be modelled as a rotationally broadened disk wind (Kwan & Tademaru, 1995)

This survey revealed a number of previously unknown HH objects in the vicinity of LkHα 233 (Table 2 5) It is possible that not all of these objects can be attributed to LkHα 233 and the positions of a nearby IRAS source, IRAS 22317+4024, complicates the analysis (see Fig 2 11) Candidate driving sources for all the new HH objects are suggested here

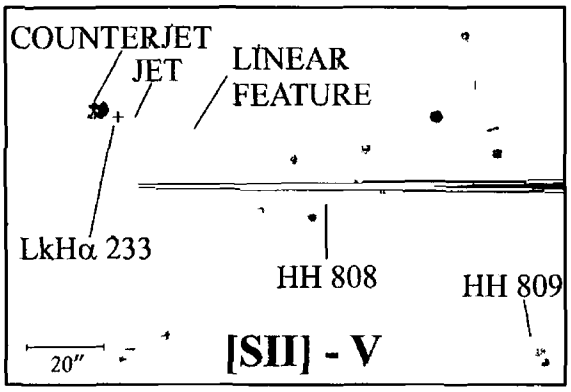

Figure 2 12 *LkHα 233 [SII]* Continuum subtracted image of the LkHα 233 nebula The jet is optically visible here, along with a number of other emission features close to the source including HH 808 and HH 809

Continuum subtracted images of the nebula surrounding LkHα 233 reveal a number of HH features which are not seen, at least so clearly, in the [SII] image alone Fig 2 12 shows the first optical images of an $\sim 7''$ jet emerging from the LkHα 233 nebula at a PA of $\sim 248°$, which is relatively close to the PA of the jet as spectroscopically determined by Corcoran & Ray (1998) A possible counterjet to the northeast of LkHα 233 is also seen in this image But it is difficult to determine whether this is actually a counterjet or simply a residual of the continuum subtraction process There are two other emission knots to the southwest of the source The first of these, HH 808, is situated close to a diffraction spike from a bright star to the west of LkHα 233 HH 808 is 1′05 from the source at a PA of 250° The second knot, HH 809, is 2′2 from the source at a PA of 241° Two other objects were seen to the northeast of LkHα 233 at a distance of $\sim 2'$, the first has a PA of 63° and the second is at 65° These objects are outside the area shown in Fig 2 12 and it is unclear at present whether these are HH objects

Also to the northeast of LkHα 233 I discovered HH 814 (Fig 2 11) at a distance of 5′18 (1 3 pc) The morphology of this object may be studied more clearly in the continuum subtracted image inset in Fig 2 11 HH 814 appears to be a broad bow shock facing back towards LkHα 233 at a PA of 47° with respect to LkHα 233 Corcoran & Ray (1998) determined a PA of approximately 65° for the counterjet, suggesting that if HH 814 is part of the same flow, its direction has changed by $\sim$ 20° Note however that the PA determined by Corcoran & Ray (1998) is very crude

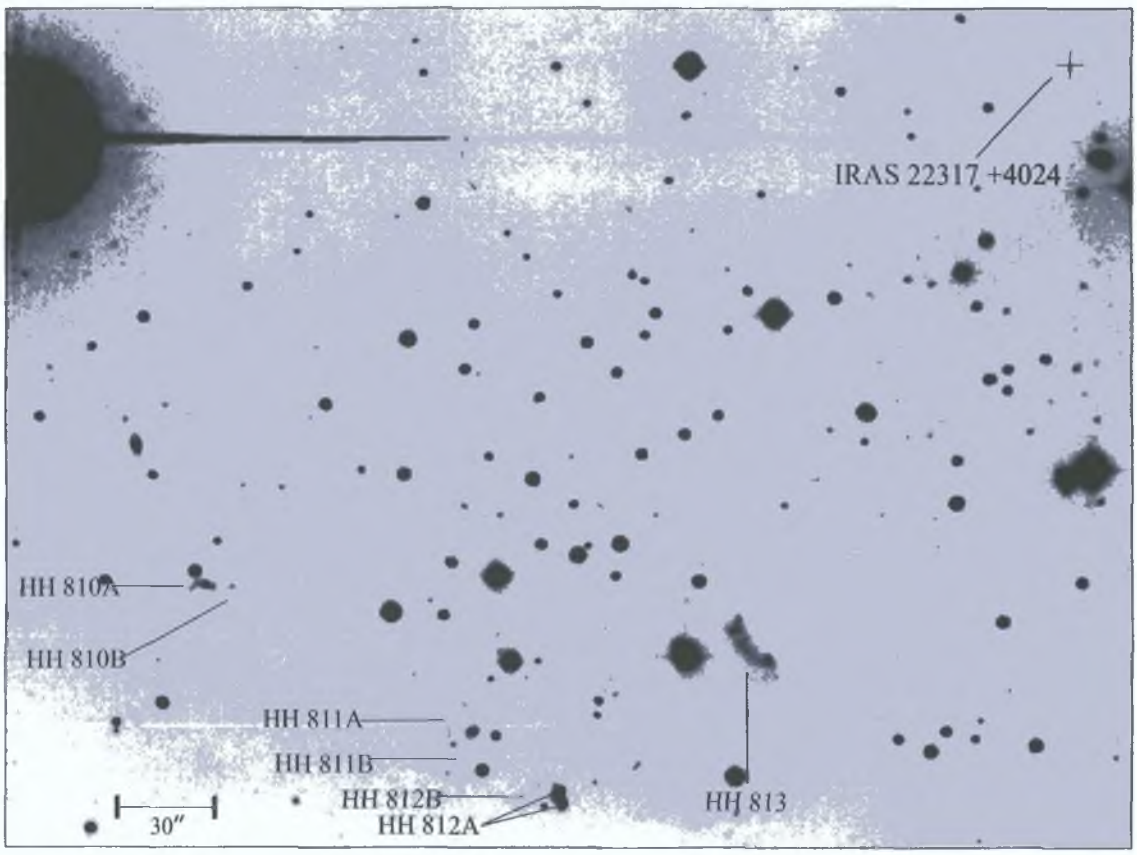

Figure 2.13: *LkHα 233 [SII]:* HH 810 – HH 813, to the southwest of LkHα 233.

as it was deduced by slit sampling at various PAs.

A number of other objects were discovered to the southwest of LkHα 233 (see Fig. 2.13). HH 810, HH 811 and HH 812, are at 4′.5 (1.2 pc), 6′ (1.5 pc) and 6′.5 (1.7 pc) respectively from LkHα 233, all at a PA of 236°. HH 813, at a distance of 7′ (1.8 pc) has a PA of 247° with respect to LkHα 233. Considering the possibility that outflows from higher mass stars may not be as collimated as those from low mass stars, HH 810 - HH 814 could be the optical tracers of the edges of a moderately collimated flow driven by LkHα 233. The axis of this outflow with respect to LkHα 233 is $\sim$ 62° (marked on Fig. 2.11), which agrees well with the estimate of the PA of the jet closer to the source. It is also possible that HH 813 is a bow shock facing back towards IRAS 22317+4024 (Fig. 2.13). Proper motion studies could conclusively determine whether this is the case.

Object	Source	Angular Separation[a]	PA[b] /°	Spatial Extent[c]
HH 815	LkHα 234/cluster	11′	53	1′2 × 1′1
HH 816	LkHα 234/cluster	8′9	63	30″× 7″
HH 817	LkHα 234/cluster	7′7	58	2″× 3″
HH 818	LkHα 234/cluster	6′2	55	3″× 2″
HH 819	LkHα 234/cluster	6′2	63	2″× 2″
HH 820	LkHα 234/cluster	4′9	55	2″× 3″
HH 821	LkHα 234/cluster	3′7	63	10″× 23″
HH 103 A	LkHα 234/cluster	5′6	234	10″× 7″
HH 822	LkHα 234/cluster	10′7	238	17″× 57″
HH 823	?			5″× 5″[d]
HH 824	IRAS 21416+6556	2′	143	3″× 6″
HH 825	IRAS 21416+6556	0′9	294	6″× 3″

Table 2 6 Angular separations, PAs and spatial extent of newly discovered HH objects in the LkHα 234 region

[a] Angular distance from the presumed source

[b] PA with respect to the presumed source

[c] Width and length of the object respectively

[d] As direction of motion is unknown, width and length may be in reverse order

2.2 5 The NGC 7129 region

A large number of YSOs are known in the NGC 7129 cluster which lies at a distance of 1 25 kpc (Shevchenko & Yakubov, 1989) Aside from optically visible young stars such as LkHα 234, there are many embedded ones For example, a 160 μm survey by Bechis et al (1978) revealed two far infrared sources and although one of them is spatially coincident with LkHα 234 (FIRS 1), the other is 3′ further south (FIRS 2) and optically invisible Additional infrared (Weintraub, Kastner, & Mahesh, 1994, Cabrit et al , 1997) and submillimetre sources (Fuente et al , 2001) are also known

Associated with these sources one finds the usual host of phenomena typical of star formation including reflection nebulae (Bertout, 1987), molecular outflows (Edwards & Snell, 1983, Bertout, 1987, Mitchell & Matthews, 1994), HH objects (Ray, 1987, Miranda, Eiroa, & Gómez de Castro, 1993), HH jets (Ray, 1987, Ray et al , 1990, Cabrit et al , 1997) and shocked H_2 flows (Eisloffel, 2000)

Looking at the distribution of previously known HH objects in the region, and

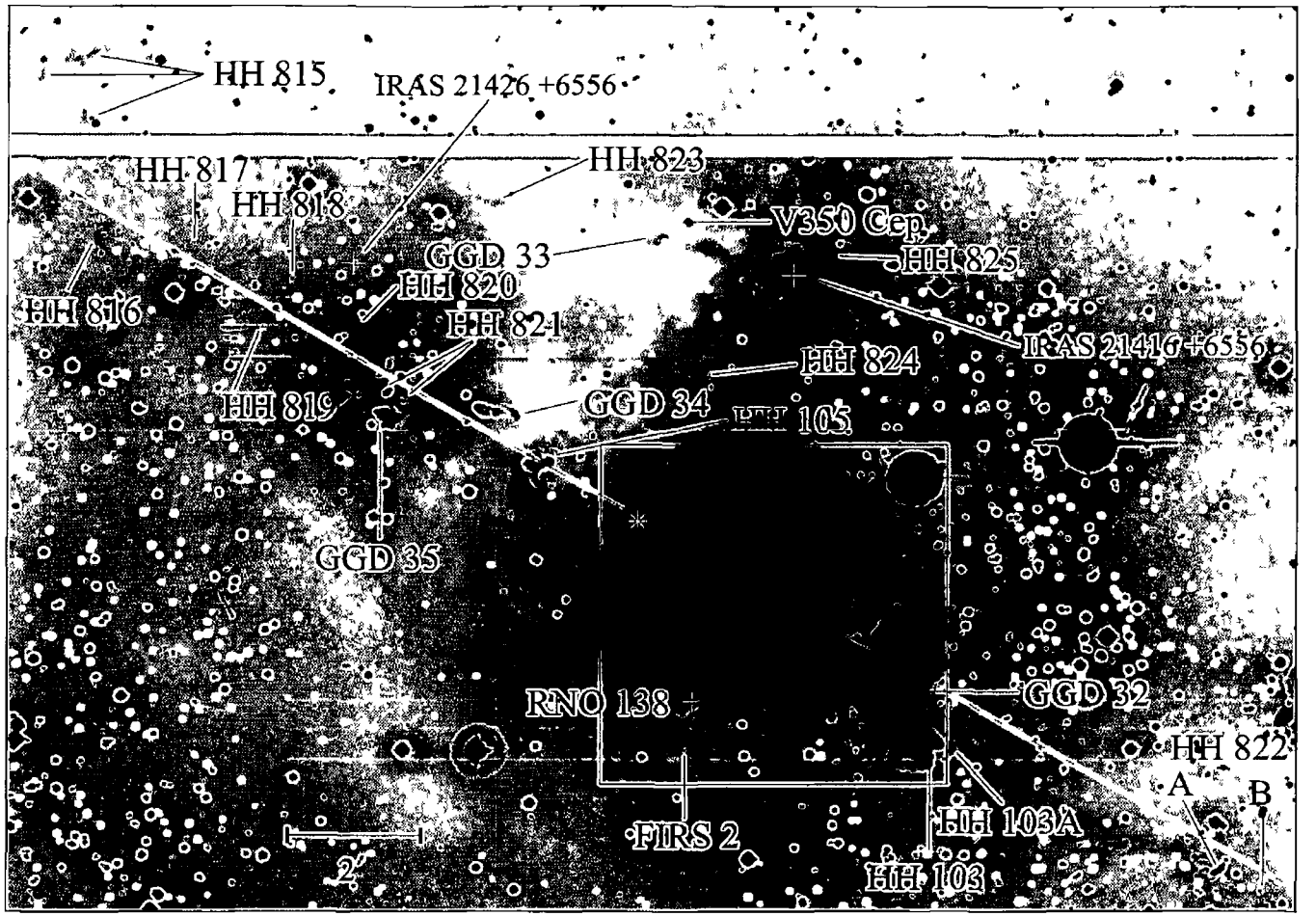

Figure 2 14 *LkHα 234 [SII]* Mosaic of the entire outflow around LkHα 234 The position of LkHα 234 is marked with a white star - the area surrounding LkHα 234 indicated by the box can be seen more clearly in Fig 2 15 The dotted line marks the apparent primary outflow axis flow at 60°/240° Other known sources in the cluster are indicated in Fig 2 15

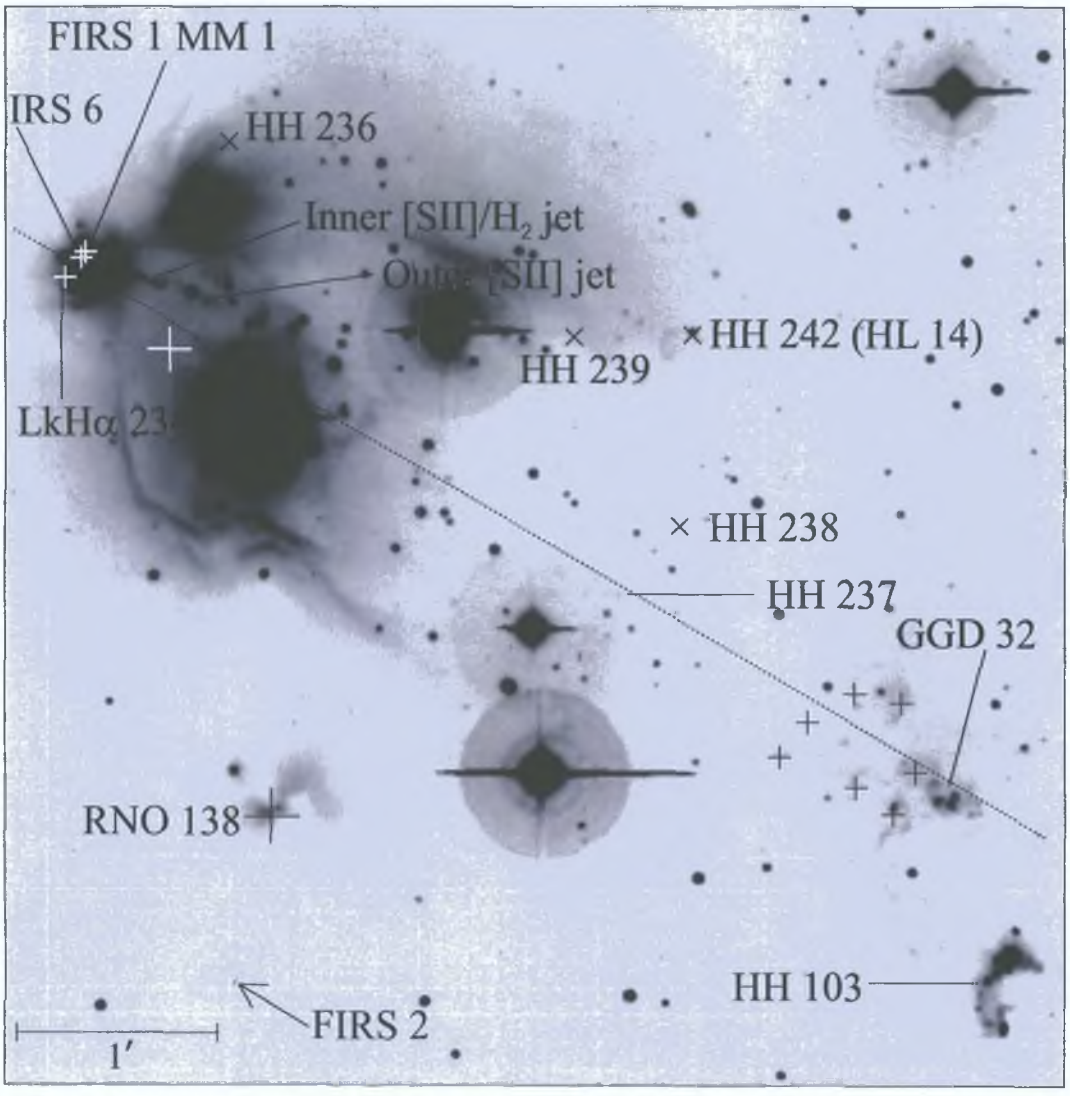

Figure 2.15: *LkHα 234 [SII]:* The NGC 7129 cluster region (indicated in Fig. 2.14) including the "inner" and "outer" optical jets discovered by Ray et al. (1990) and Cabrit et al. (1997). The contrast has been changed here with respect to Fig. 2.14 so that more objects within the cluster core are visible. The white cross to the southwest of LkHα 234 marks the position of an infrared source, IRAS 21814+6552. In the southwest corner of the image, Black crosses and X's are used to mark the positions of HH objects found by Eiroa, Gómez de Castro, & Miranda (1992) and Miranda, Eiroa, & Gómez de Castro (1993) respectively. The apparent primary outflow axis through the cluster at 60°/240° is marked.

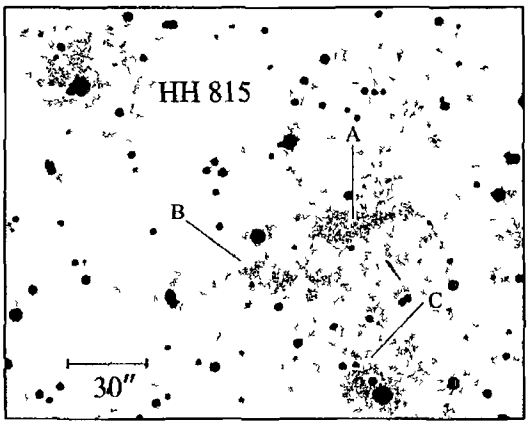

Figure 2 16 *LkHα 234 [SII]* HH 815, to the northeast of the cluster, is the most distant outlying HH object in this region and may be a bow shock (see text) Its relative position is seen in Fig 2 14

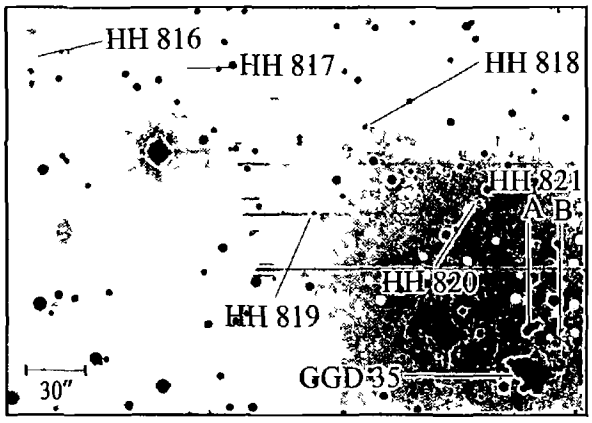

Figure 2 17 *LkHα 234 [SII]* HH 816 – HH 821 (A and B), to the northeast of LkHα 234

the new ones discovered here (see below and Table 2 6), one gets the impression (see Figs 2 14 and 2 15) that the primary outflow axis, or axes, is roughly in a northeast to southwest direction and centred on the cluster core Caution however is necessary Proper motions studies have shown that some HH objects like GGD 32 and HH 103 are not moving to the southwest, as one might suspect, but instead to the west (Ray et al , 1990) Moreover others, like GGD 34 (Gómez de Castro & Robles, 1999) and possibly GGD 33 (Cohen & Schwartz, 1983, Goodrich, 1986), have their own sources outside the cluster core

The HH 815 complex (Fig 2 16) is over 1′ in size and is at a distance of 11′ (4 pc) from LkHα 234 The three emission regions in HH 815 (A, B and C) appear to form the edges of a large bow shock that is concave towards the cluster core HH 816 (Fig 2 17) may be another bow trailed by a series of faint HH knots i e HH 817 - HH 820 HH 821, $\sim$ 15″ north of GGD 35, is aligned with HH 819 and HH 816 and so could form part of the same flow Note also that HH 105, is on the same axis from the cluster core and that no source for HH 105, at least in its immediate vicinity, is known

The most distant HH object to the southwest of the cluster discovered here is HH 822 (Fig 2 18) It is at a PA of 238° with respect to LkHα 234 and the morphol-

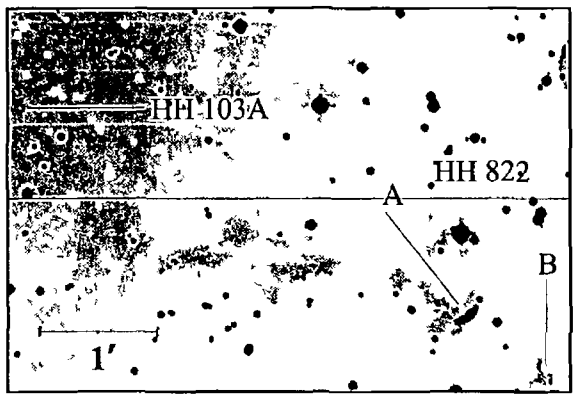

Figure 2 18 *LkHα 234 [SII]* HH 103 A and HH 822 to the southwest of LkHα 234

ogy of its brightest component (HH 822 A), i e a bow concave towards the cluster, suggests it is part of an outflow that originated there An additional knot close to HH 103 was also found and I shall refer to it as HH 103 A (Fig 2 14) Given its location, it seems likely it is part of the same flow that drives HH 822 Moreover faint emission can be seen linking HH 103 A to HH 822 A reinforcing this conclusion HH 822 B is at a distance of 10′7 (3 9 pc) from LkHα 234

The large number of sources in this region makes it extremely difficult, without detailed kinematic studies, to determine the origin of individual HH complexes As previously mentioned there are a number of low-mass YSOs, like the one that drives GGD 34, present and this complicates the analysis That said, it seems likely, purely on morphological grounds as well as location, that many of the newly discovered HH objects are driven by a source(s) in the cluster core Because of their large distance from the core, however, it may prove impossible, even with good proper motion data, to determine their precise origin Several possible candidates exist including LkHα 234, IRS 6 and FIRS 1-MM1 If an imaginary axis is drawn through the core at a PA of 60°/240° it roughly delineates the region where most of the new HH objects, HH 816 to HH 822, are located (see Fig 2 14) Assuming we are dealing with one outflow here, that originates in the cluster, then its overall angular size is 21′8 i e $\sim$ 8 pc in projected length

There are three other HH objects which are not situated along the major axis marked in Fig 2 14 HH 824 and HH 825 are located on either side of IRAS 21416+6556 at 143°/294° with respect to this source, suggesting a possible bipolar

outflow driven by IRAS 21416+6556 These objects are 2′ and 51″ respectively from IRAS 21416+6556 The driving source of HH 823 is unclear as is its association with any of the other outflows in this region

2.3 Discussion

2.3.1 Outflow Lengths

It has been stated, albeit somewhat tongue-in-cheek, that the apparent length of optical outflows from YSOs is a function of CCD chip size! Early chips were small and sampled only a small angular patch of the sky This, in combination with the episodic nature of the flows themselves, conspired to suggest outflow lengths measured in tens of thousands of AU rather than parsecs In a number of cases however CCD mosaicing did hint that some flows were at least in the parsec league (Ray, 1987) Large format CCDs in focal-plane mosaics can cover fields of view larger than 30′ which, at a distance of 1 kpc, corresponds to more than 8 7 pc Flows can therefore be detected to beyond the peripheries of their parent cloud

Table 2 7 lists parameters such as distance, source luminosity, outflow length, cloud size, dynamical timescale and degree of collimation for both the intermediate-mass sources discussed here and several other well-studied outflows powered by both intermediate- and low-mass YSOs In some regions, the projected lengths of the outflows are similar to the sizes of the clouds from which they emerge This correlation of length scales is to be expected and there should also be a tendency for shocks to be seen near the cloud edges where extinction by dust is minimal

If an average tangential velocity for outflows of 100 kms^{-1} is assumed, in 10^5 yrs material originally at the source will be transported $\sim$ 10 pc i e typically to the edge of the clouds Using the evolutionary tracks of Palla & Stahler (1993), such a period corresponds to about 10% of the time an average Herbig Ae/Be star spends in the pre-main sequence phase It follows that only in the case of the more massive YSOs, i e those with the shortest evolutionary timescales, do HH outflows represent a "fossil record" of activity over the totality of the outflow phase

Source	Distance /pc	Ref	L_{bol} /$L_\odot$	Ref	Outflow length /pc	Ref	Associated Nebula	Cloud size[a] /pc	τ_{dyn}[b] / $\times 10^4$ yr	θ_{flow}[c] /°
LkHα 198	600	2	$\geq$ 160	2	2 3	1	L1265	2	1 12	2 8
1548C27 IRS 1	2400	4	580	4	7 5	1	NGC 6823	33	2 79	11 6
IRAS 19395+2313	2400	4	320	1	5	1	NGC 6823	33	2 15	30 2
LkHα 233	880	5	$\geq$ 121	5	3 1	1	ANON	3 2	0 88	6 3
LkHα 234	1250	6	1200	7	8	1	NGC 7129	5 1	1 96	6 2
IRAS 18162-2048[d]	1700	8	1700	9	5 3	8	L291	15	2 59	1
HH 354 IRS	750	10	120	10	2 4	11	L1165	1 8	1 17	4 04
PV Cephei	500	12	100	13	2 6	11,14	L1617	28	1 27	6 7
IRAS 05491+0247[e,f]	460	11	25	11	7 7	11	L1617	28	3 76	7 4
HH 1/2 VLA 1[f]	460	15	50	16	5 9	17	L1641	25	2 89	10 3
HH 34 IRS[f]	460	15	28	18	3	19	L1641	25	1 47	1 5

Table 2 7 Parameters of newly discovered, and some previously known, parsec-scale outflows from low- and intermediate-mass YSOs

[a] This is the diameter of the cloud where diameter = [major axis + minor axis]/2

[b] Based on the assumption that the velocity of the most distant objects is 200 kms^{-1}, which may be an upper limit

[c] θ_{flow} is calculated by taking the width of the most distant shock in both the outflow and counterflow and dividing by the projected distance from the source The mean value of θ_{flow} for the outflow and counterflow is given here

[d] The source of HH 80/HH 81

[e] The source of HH 111

[f] These YSOs are low-mass sources and are included here for comparison purposes only

References 1 this work, 2 Chavarria-K (1985), 3 Lagage et al (1993), 4 Dent & Aspin (1992), 5 Calvet & Cohen (1978), 6 Shevchenko & Yakubov (1989), 7 Harvey, Wilking, & Joy (1984), 8 Rodríguez, Moran, & Ho (1980), 9 Martí, Rodriguez, & Reipurth (1993), 10 Schwartz et al (1991), 11 Reipurth, Bally, & Devine (1997), 12 Cohen, Kuhi, Spinrad, & Harlan (1981), 13 Mundt & Ray (1994), 14 Gomez, Kenyon, & Whitney (1997), 15 Hester, Stapelfeldt, & Scowen (1998), 16 Harvey, Joy, Lester, & Wilking (1986), 17 Ogura (1995), 18 Reipurth et al (1993), 19 Bally & Devine (1994)

2.3.2 Outflow Morphology

HH outflows are episodic they are clearly not continuous phenomena For the most part, the shocks we see are generated by supersonic jet material ramming into previously ejected slower gas This process produces a series of "working surfaces", radiative shock systems that fade with time and therefore with distance from their source Only the strongest shocks survive to produce dramatic, often chaotic, structures on parsec scales It has even been suggested that the FU Orionis phenomena[5] may signal the dramatic change in output needed at the source to produce such a shock (Reipurth, 1989), at least in the case of low-mass sources (see Chapter 3) Thus the spacing between HH objects increases with distance from the source at least amongst low-mass YSOs (Reipurth & Bally, 2001) Such a trend is also visible here amongst the flows from intermediate-mass YSOs such as LkHα 198 and 1548C27 Another phenomenon that occurs with HH outflows from low-mass YSOs is that the shock structures become larger and apparently more chaotic with distance Again this is something which is replicated in their intermediate-mass YSO counterparts

A phenomenon that is found in parsec-scale outflows from lower mass YSOs is that the flow often exhibits "S" or "C" shape symmetry (Reipurth, 1989) possibly as a result of jet precession or source motion through the parent cloud respectively In this small sample, I do not find any clear-cut examples of either although, as previously mentioned, the parsec-scale outflow from 1548C27 IRS 1 may be slightly "S-shaped"

2 3.3 Degree of Collimation

As alluded to at the beginning of this Chapter, one of the most striking differences between parsec-scale outflows from low and massive YSOs is the relative lack of collimation seen in the latter (Shepherd, Churchwell, & Wilner, 1997, Hunter, Phillips, & Menten, 1997, Shepherd, Watson, Sargent, & Churchwell, 1998) This point is well illustrated by the archetypal example of an outflow from a high luminosity YSO the Orion IRC2 flow (Allen & Burton, 1993) Its opening angle is $\sim 90°$ (Burton & Allen, 1994) which is a sharp contrast to the angles (typically a few

[5]See §3 3 4 for details of this phenomenon

degrees) seen in outflows from low-mass YSOs

Table 2.7 lists "final" opening angles for this small sample. Values are determined by dividing the width of the most distant HH object by its projected source separation. Note that as projected separations are used the quoted values must be upper limits, however these observations only reveal the brightest portions of the shocks and fainter outer parts may be missed, so the opening angles may actually be greater than what is optically observed. Observed opening angles range from 2.8° to 12° suggesting a degree of collimation comparable to that seen in outflows from low-mass YSOs. The degree of collimation of the IRAS 19395+2313 is greater than this at 30° due to its unusual morphology i.e. a very large object so close to the (suspected) driving source. A very important finding is that *this suggests that the transition from well-collimated outflows to poorly-collimated outflows occurs at higher masses than the sources observed here*.

2.3.4 The Frequency of Blow-Outs

The true size of an outflow, in comparison to that of its parent cloud, is an important factor in determining whether the outflow's energy and momentum is transported into the ISM or remains within the cloud itself. A cursory examination of this data shows a clear tendency for HH objects to lie close to the edges of the parent cloud or at least close to the edges of clumps. As already mentioned, such an effect is to be expected considering the low extinction near cloud peripheries and the very low ISM densities beyond the cloud boundaries.

More importantly, it is clear that actual outflow timescales are very long in comparison to apparent dynamical ones which are given in Table 2.7. Here dynamical timescales are derived by dividing the projected length of an outflow by its estimated tangential velocity (assumed here to be 200 kms^{-1}). This, and the observation of HH objects near cloud boundaries, immediately suggests that most, if not all, of the flows studied here have blown-out of their parent cloud.

2.3.5 Are Outflows a Source of Cloud Turbulence?

I mentioned in §1.3.1 that large-scale outflows may be an important source of turbulence in molecular clouds. As the outflows presented in this chapter are comparable

in length to the dimensions of their parent cloud (see Table 2 7) I will discuss this possibility here

The parsec-scale HH outflows imaged here appear largely well-collimated and therefore one might think they could affect only a narrow cone of ambient material One has to remember however that these flows are supersonic and that we are viewing only the most highly collimated outflow component The same flows "imaged" in the CO J = 1→0 line would normally appear much less collimated, especially at low velocities That these flows affect cloud structure on parsec scales is evident from features such as the large CO "cavity" in NGC 7129 (Eisloffel, 2000) No doubt they also affect cloud dynamics Arce & Goodman (2001) for example has found that molecular outflows associated with parsec-scale HH flows can possess kinetic energies comparable to the turbulent and gravitational binding energies of their parent clouds Armstrong & Winnewisser (1989) suggested that the kinetic energy of a parsec-scale outflow could generate up to 6 times the turbulent energy in a cloud! Although this seems phenomenally high, Arce & Goodman (2001) show that the outflow power of the molecular outflow associated with HH 300 is only about a factor of 10 below the power needed to drive MHD turbulence However the driving source of HH 300 is a 1 $3L_{\odot}$ Class I YSO (Arce & Goodman, 2001), a more massive source may drive even more turbulence

Although this shows that parsec-scale outflows may significantly affect their surrounding cloud, this only proves that they are a *potentially* important source of turbulence Unfortunately we do not understand the coupling between outflows and their ambient medium well enough to be sure Numerical simulations (Downes & Cabrit, 2003) are helping to address this problem but further studies are required

Chapter 3

Parsec-Scale Outflows from Classical T Tauri Stars

As mentioned earlier (Chapter 1) many of the parsec-scale outflows that have been observed to date are driven by young, Class I i e embedded, low-mass YSOs This classification scheme is based on the shape of the SED of the YSO from 10μm to 100μm (Lada & Wilking, 1984, Lada, 1987) The SED can be modelled as an approximate blackbody with an infrared excess beyond 2μm due to circumstellar gas and dust The infrared excess is very strong in the young, embedded Class I sources and is almost non-existent in the more evolved Class III sources Here I report on wide field observations of a number of Class II low-mass sources – i e Classical T Tauri stars (CTTSs) to see whether the parsec-scale outflow phenomenon persists into this phase These sources have a smaller infrared excess than Class I sources i e they have less circumstellar material (see §1 2 1 for more details on the classification scheme for low-mass YSOs)

The CTTSs investigated here were not previously associated with parsec-scale outflows, in fact many were only known to drive "micro-jets" of the order of $\sim 5''$ to $40''$ ($\lesssim 0\ 03$ pc assuming a distance of 140 pc to the Taurus-Auriga Cloud where all of the CTTSs are located) Although outflows from these more evolved sources are not nearly as spectacular as those from Class I YSOs, CTTSs are no longer surrounded by significant amounts of dust and so their outflows can be traced right back to the origin These Class II sources are still actively accreting and ejecting matter, albeit at rates 10-100 times smaller than Class I sources (Hartigan,

Edwards & Ghandour, 1995) In this Chapter I present and discuss a number of possible parsec-scale outflows from CTTSs

As previously stated the morphology of parsec-scale outflows yields valuable information about their driving sources They are, in effect, a fossil record of the mass-loss history of their parent star over their dynamical timescales ($\sim 10^3$ to $\sim 10^5$ yr) They suggest, for example, quiescent phases between periods of violent mass ejection that give rise to the large HH complexes we see today The morphology of an outflow can also indicate whether it is precessing and, if so, the rate of precession Here I also investigate whether these CTTSs show evidence for having undergone FU Orionis-like outbursts, based on the morphology of their outflows

Details about the observations are given in §3 1 In §3 2 I report the discovery of five possible parsec-scale outflows from CTTSs in the Taurus-Auriga Cloud which is at a distance of 140 pc (Elias, 1978, Wichmann et al , 1998) I also include serendipitous observations of a parsec-scale outflow from a less evolved Class I source These results are discussed in §3 3

3.1 Observations

This data was acquired using the Wide Field Camera (WFC) on the 2 5m Isaac Newton Telescope – this camera is described in §2 1 The filters used and the exposure times of the images are the same as those detailed in Chapter 2 These images were taken during two separate observing runs, the first between the 10^{th} and 13^{th} of February 2001, and the second between the 24^{th} and 27^{th} of November 2003 Seeing for the February 2001 run was moderate at $1''-2''$ as measured from the images The seeing in November 2003 was better at $0''9-1''1$ The method used to determine driving sources for the newly detected HH objects is described in §2 1 The sources observed here are CTTSs with previously known "micro-jets" or short outflows of $\lesssim 1'$ All are in the Taurus-Auriga Cloud, chosen for its abundance of isolated CTTSs and proximity Seven such sources were observed, with five of them – CW Tau, DG Tau, DO Tau, HV Tau C and RW Aur – revealing extended outflows of the order of 1 pc No *extended* optical emission was found in the UY Aur and DP Tau outflows

Object	Source	α(J2000)	δ(J2000)
HH 826 A	CW Tau	$04^h14^m17\ 8^s$	$+28°10'40''$
HH 826 B	CW Tau	$04^h14^m19\ 8^s$	$+28°09'52''$
HH 827	CW Tau	$04^h14^m15\ 1^s$	$+28°03'55''$
HH 826 C	CW Tau	$04^h14^m15\ 3^s$	$+28°11'39''$
HH 828	CW Tau	$04^h14^m10\ 3^s$	$+28°14'54''$
HH 829 A	CW Tau	$04^h14^m03\ 0^s$	$+28°25'36''$
HH 829 B	CW Tau	$04^h14^m04\ 8^s$	$+28°26'53''$
HH 829 C	CW Tau	$04^h14^m07\ 3^s$	$+28°27'37''$
HH 830 A	DG Tau	$04^h27^m37\ 3^s$	$+26°12'27''$
HH 830 B	DG Tau	$04^h27^m44\ 8^s$	$+26°12'56''$
HH 830 C	DG Tau	$04^h27^m51\ 7^s$	$+26°15'33''$
HH 831 A	DO Tau	$04^h39^m13\ 2^s$	$+26°13'48''$
HH 831 B	DO Tau	$04^h39^m15\ 2^s$	$+26°13'55''$
HH 832	DO Tau	$04^h39^m02\ 0^s$	$+26°12'21''$
HH 833	HV Tau C	$04^h38^m44\ 0^s$	$+26°14'42''$
HH 834	?	$04^h39^m05\ 9^s$	$+26°03'23''$
HH 835	RW Aur	$05^h07^m30\ 4^s$	$+30°27'11''$
HH 836 A	DG Tau B	$04^h27^m13\ 5^s$	$+26°04'16''$
HH 836 B	DG Tau B	$04^h27^m19\ 7^s$	$+26°03'07''$
HH 837	DG Tau B	$04^h27^m44\ 8^s$	$+26°00'49''$
HH 838	?	$04^h26^m56\ 4^s$	$+26°05'58''$
HH 839	?	$04^h27^m43\ 8^s$	$+26°04'35''$

Table 3 1 Positions and *probable* sources of the HH objects found in the CTTS survey

3.2 Results

3.2.1 CW Tau

CW Tau has a spectral type of K3 (Cohen & Kuhi, 1979), with $M_\star = 1.40\ M_\odot$ and $L_\star = 2.6\ L_\odot$ (Gomez de Castro, 1993). A "micro-jet" (HH 220) propagating southeast from this source was discovered in optical images by Gómez de Castro (1993), with a gap of $\sim 1''.3$ between the source and the jet. A full opening angle of 3.3° is derived for this blueshifted jet at 3″ from the source (Dougados et al., 2000). Long-slit spectroscopic observations by Hirth, Mundt, & Solf (1994) showed the outflow to extend at least 4″ - 6″ on either side of the source. The blueshifted HH 220 outflow is at a PA of 144° ± 2° with respect to CW Tau (Gómez de Castro, 1993, Dougados et al., 2000) and I estimate the redshifted jet to be at ∼ 329° with respect to CW Tau from the [SII] images of Dougados et al. (2000).

These wide field images of the region around CW Tau (Fig. 3.1) reveal that this outflow may be much more extended than just the HH 220 bipolar jet – see Table 3.2 for details of the newly discovered objects in the CW Tau outflow. Two knots are found to the south of CW Tau at 22″ (HH 826 A) and 1′.27 (HH 826 B). HH 826 A is only seen in [SII] emission while HH 826 B is seen in both [SII] and Hα. Both are at a PA of ∼ 153° with respect to the source and are reasonably well aligned with the blueshifted HH 220 jet (Fig. 3.2). Further out is HH 827 at 6′.1 and a PA of 184° with respect to CW Tau. Precession of the outflow may explain this directional change. HH 827 consists of a bright knot with a trail of emission stretching to the northeast and a fainter trail of emission to the southwest (see Fig. 3.3) and is much brighter and more extended in Hα emission than in [SII]. The total length of this object in Hα is ∼ 1′.8. It is possible that HH 827 is not driven by CW Tau in which case IRAS 04113+2758 to its northeast (marked on Fig. 3.1) is a candidate source, however the trail of emission from HH 827 does not point back to this source. Assuming HH 827 is driven by CW Tau then the projected length of the blueshifted outflow is 7′.08 (0.29 pc).

The [SII] images also show that the redshifted HH 220 jet extends to ∼ 46″ from CW Tau at a PA of 326° (Fig. 3.1). The jet first extends to ∼ 9″ from the source, then there is a gap of almost 20″ where the jet is too faint to be seen. It becomes

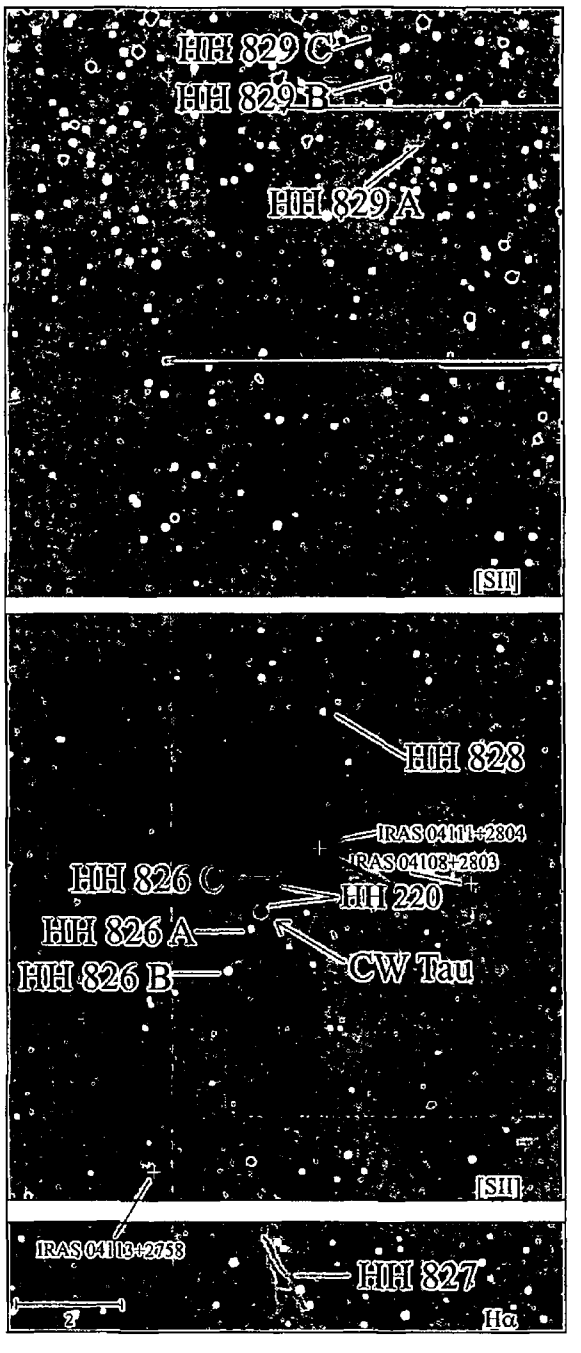

Figure 3 1 *CW Tau* Mosaic of the entire CW Tau outflow The top and middle frames are in [SII] and the bottom frame is in Hα as HH 827 is much stronger in this emission line All known IRAS sources in the region are marked with white crosses The individual knots can be seen more clearly in Figs 3 2 to 3 4 Any information in the gaps between the CCDs (white strips) is lost The northern edge of this image is the northern edge of the field of view of the CCD Mosaic Note that the faint linear object to the east of HH 829 B is an asteroid trail

Object	Source	Angular Separation[a]	PA[b] /°	Spatial Extent[c]
HH 826 A	CW Tau	0'.37	153	2″× 2″
HH 826 B	CW Tau	1'.27	153	2″× 5″
HH 827	CW Tau	6'.2	184	1'.8 × 16″
HH 826 C	CW Tau	0'.77	326	4″× 3″
HH 828	CW Tau?	4'.52[c]	342[c]	3″× 2″(E)[d]
	CW Tau?	4'.27[c]	338[c]	2″× 3″(M)[d]
	CW Tau?	4'.33[c]	334[c]	5″× 3″(W)[d]
HH 829 A	CW Tau?	14'.9	348	29″× 5″
HH 829 B	CW Tau?	16'.12	351	3″× 4″
HH 829 C	CW Tau?	16'.8	353	3″× 6″

Table 3.2 Angular separations, PAs and spatial extent of newly discovered HH objects in the CW Tau region

[a] Angular distance from the presumed source

[b] PA with respect to the presumed source

[c] Width and length of the object respectively

[d] The three knots in HH 828 (see Fig. 3.2) are labelled here as the Eastern-most Knot (E), the Middle Knot (M) and the Western-most Knot (W)

visible again for a distance of $\sim 17''$ before terminating in the bright knot HH 826 C. Further out a trio of knots (HH 828) are found at $\sim 4'.3$ from CW Tau and are only seen in [SII] (Figs. 3.1 & 3.2). The most western knot is at a PA of 334° from CW Tau and the most eastern is at 342°. There are two known IRAS sources in the vicinity of HH 828 (marked in Fig. 3.1) and it is possible that the source of the HH 828 Knots is one of these or CW Tau itself. Proper motion studies would help distinguish between these possibilities (see Chapter 4).

There is a projected distance of $\sim 10'.8$ (0.44 pc) between HH 828 and the next HH object along this direction, HH 829 A (Figs. 3.1 & 3.4). HH 829 A, B and C are 14'.9, 16'.12 and 16'.8 at 348°, 351° and 353° from CW Tau respectively. The edge of this complex is approximately 37″ from the northern edge of the field of view of the WFC CCD so it is possible that further emission is present beyond this. While HH 829 A is comparable in brightness in both Hα and [SII] emission, Knots B and C are brighter in [SII] and Hα respectively (Fig. 3.4). IRAS 04111+2820 (slightly outside the field of view of Fig. 3.1) is $\sim 1'.5$ at a PA of 78° from HH 829 C is also a candidate source. The projected length of this assumed CW Tau redshifted outflow is 0.69 pc (16'.8). This gives a total projected length of the CW Tau blue-

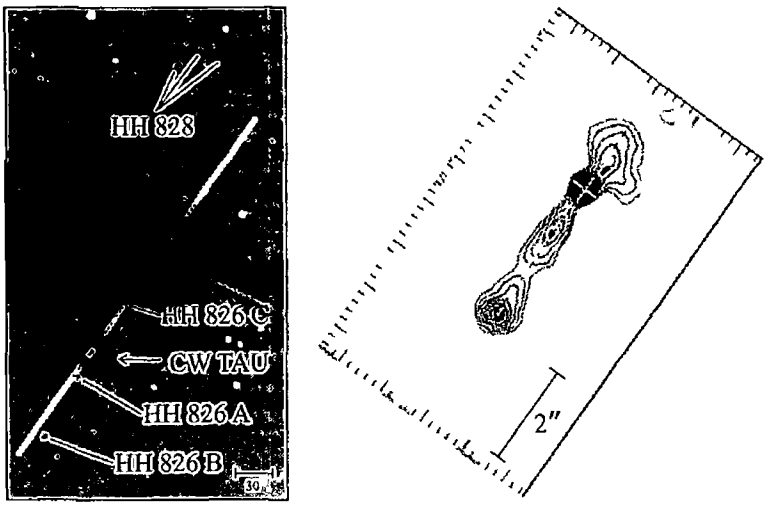

Figure 3 2 *CW Tau Left* [SII] image showing CW Tau and the newly discovered HH 826 and HH 828 Knots The small white box superimposed on CW Tau marks the region shown on the right *Right* CW Tau and the HH220 jet taken from Dougados et al (2000) A dotted line shows the PA of 144° determined by Dougados et al (2000) and a similar line at 144° is superimposed on the [SII] image to show the slight change in direction of the outflow close to the source

and redshifted outflows of $\sim$ 0 98 pc although the reader is referred to the proper motion studies in Chapter 4 for more information

The variation in PA in the blueshifted outflow is 40° and is 24° in the redshifted outflow This change in direction gives the extended outflow an inverted 'S' shape Similar morphologies are seen in many large-scale outflows from less evolved low-mass sources (see §1 3 4) and suggests outflow precession The change in direction is approximately symmetrical about CW Tau which substantiates the suggestion that both HH 827 and HH 829 may be part of this outflow (however see Chapter 4) CW Tau is surrounded by a dark cloud (Fig 3 1) so the majority of the outflow is presumably obscured It is interesting to note however that the more distant objects in this outflow, HH 827 and HH 829, are found at the cloud edges

3.2.2 The DG Tau region

DG Tau is a low luminosity star with $L_* \simeq 8L_\odot$ (Cohen & Kuhi, 1979) and was one of the first TTSs to be associated with an optical jet (HH 158), noted by Mundt & Fried (1983) HST/STIS observations show HH 158 to be at a PA of 223° with

Figure 3 3 *HH 827 Hα* Continuum subtracted Hα image of HH 827 to the south of CW Tau The trail of emission to the northeast is clearly seen and the fainter trail to the southwest extends for $\sim 31''$ from the southern end of the bright knot

respect to DG Tau (Bacciotti et al , 2002) and that the blueshifted HH 158 "micro-jet" can be traced to within $\sim 0''1$ from the star (Bacciotti et al , 2000) Larger scale studies show the HH 158 outflow to extend to $\sim 16''$, with a number of resolved knots (Eisloffel & Mundt, 1998) A redshifted jet $\sim 1''$ in length is detected $\sim 0''45$ from the source (Lavalley et al , 1997) There is a semi-circular nebula associated with DG Tau (Mundt, Brugel & Buhrke, 1987) which HST data resolves as three nested arcs of reflection at $2''$, $5''$ and $10''$ from the star (Stapelfeldt et al , 1997) The PA of the axis of symmetry of all three arcs is $\sim 225°$ with respect to DG Tau which is well aligned with the PA of HH 158, suggesting that these arcs are the illuminated edges of a cavity carved by the blueshifted jet

The most spectacular object in this extended outflow is HH 702 - an $\sim 4'$ long shock system to the southwest of DG Tau This object has already been noted independently by Sun et al (2003), however these new Hα images show much more detail than the [SII] image of Sun et al (2003) HH 702 consists of five bright knots (Fig 3 5d) (one of which (E) was not noted by Sun et al 2003), two fainter Knots (F and G) and a trail of emission to the northeast In these images, the trail of emission is first seen $7'9$ from DG Tau at a PA of 218°, pointing back towards DG

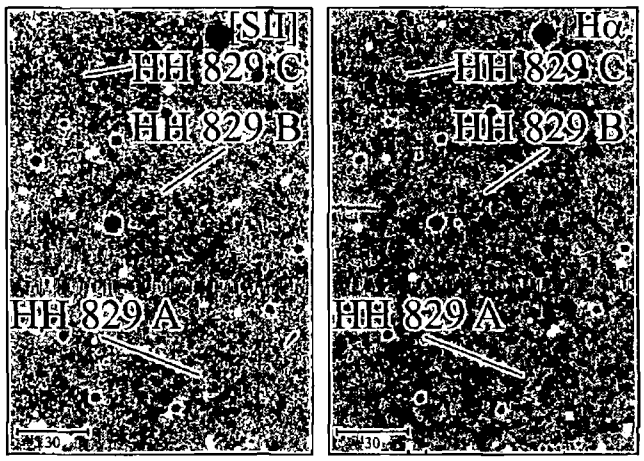

Figure 3 4 *HH 829* Image of HH 829 A, B and C to the north of CW Tau in [SII] (left) and Hα (right) HH 829 C is stronger in Hα emission and HH 829 B is stronger in [SII] emission, while HH 829 A is comparable in both

Tau, and stretches a distance of 2′75 to Knot A Knot A is an intense emission knot at 10′6 from DG Tau, with a star directly to the east Knots C and E are on either side of a star and can be seen more clearly in the continuum subtracted image inset in Fig 3 5d While a number of IRAS sources in the vicinity have been previously suggested as possible sources for HH 702 (Sun et al , 2003), I think it is more likely that this object is driven by DG Tau given the alignment between HH 702 and HH 158 The most distant optically visible object in the blueshifted outflow, Knot G of HH 702, is 12′32 from DG Tau which is 0 5 pc in projected length at a distance of 140 pc to the Taurus - Auriga cloud

These observations reveal a possible new HH complex (HH 830) in the DG Tau outflow (however see Chapter 4), details of which are given in Table 3 3 HH 830 is a faint complex 9′6 to the northeast of DG Tau and consists of three separate emission objects A – C (Fig 3 5b & c) HH 830 A is a 44″ long linear object orientated east/west and dips southwards towards its western edge HH 830 B is $\sim$ 11′3 from DG Tau and is brighter than HH 830 A but is much smaller in size (Fig 3 5b) HH 830 C is the most distant optically visible object in this outflow and appears to be two separate emission regions at 14′1 (PA of 47°) and 14′4 (PA of 50°) from the source (Fig 3 5b) This object is at the eastern edge of the image and there might be more emission further east The HH 830 knots are comparable in Hα and [SII] emission Both HH 830 A and the centre of HH 830 C are along a PA of $\sim$ 48° with

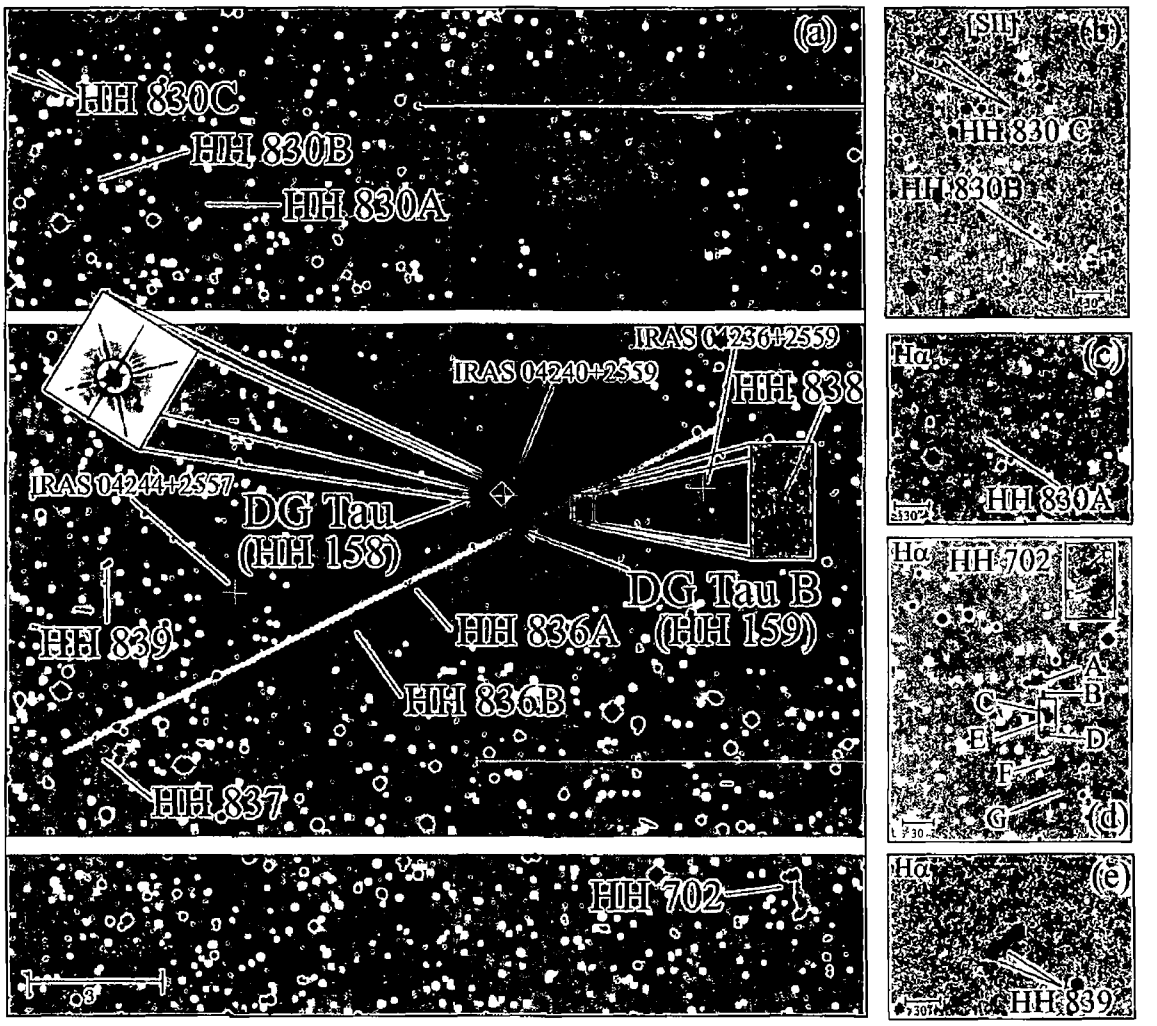

Figure 3 5 *DG Tau* (a) Mosaic image of the region surrounding DG Tau and DG Tau B in Hα The new objects discovered in both the DG Tau outflow (HH 830) and the DG Tau B outflow (HH 836 and HH 837) are indicated here HH 838 and HH 839 appear to be separate outflows in this region A HST image of HH 158 (21″7 by 22″05) is included here as an inset and has been rotated such that north is up The dotted line through the centre of the main image is at 116° and marks the blueshifted DG Tau B outflow The three known IRAS sources in the region are marked with white crosses (b) HH 830 B and C in [SII] HH 830 C can be seen here to be two distinct regions of emission, and HH 830 B is a small knot The left hand edge of the image is actually the eastern edge of the field of view so it is possible that HH 830 C is more extended (c) HH 830 A in Hα HH 830 A is a faint, linear emission object extending $\sim 28''$ and dips southwards towards the western edge for another 16″ (d) HH 702 in Hα An image taken in February 2001 is used here as it shows the whole of HH 702 in one CCD field Knots A, B, C and D (discovered by Sun et al 2003) can clearly be seen The newly discovered Knots E to G are also marked here There is a star to the north of Knot E but this knot can be seen more clearly in the Hα continuum subtracted image (inset) (e) HH 839 in Hα

Object	Source	Angular Separation[a]	PA[b] /°	Spatial Extent[c]
HH 830 A	DG Tau?	9′6	48	5″× 44″
HH 830 B	DG Tau?	11′3	48	2″× 2″
HH 830 C	DG Tau?	14′1	47	21″× 9″
		14′4	50	6″× 3″
HH 836 A	DG Tau B	2′6	116	14″× 7″
HH 836 B	DG Tau B	4′4	122	12″× 3″
HH 837	DG Tau B	10′4	117	21″× 32″[d]
		10′4	117	19″× 18″[e]
HH 838	?			43″× 4″[f]
HH 839	?[g]		126	3″× 10″

Table 3 3 Angular separations, PAs and spatial extent of newly discovered HH objects in the DG Tau and DG Tau B region

[a] Angular distance from the presumed source

[b] PA with respect to the presumed source

[c] Width and length of the object respectively

[d] The morphology of HH 837 is different in Hα and [SII] emission, this is the width and length of this object in Hα

[e] The morphology of HH 837 is different in Hα and [SII] emission, this is the width and length of this object in [SII]

[f] As direction of motion is unknown, width and length may be in reverse order

[g] The source of this outflow appears to be a stellar object at its base (see text)

respect to DG Tau Thus they are reasonably well aligned with the redshifted jet which I estimate to be at 44° from the images of Lavalley et al (1997) HH 830 B is slightly off this axis, at a PA of 52° The total length of the redshifted outflow is 14′4 i e 0 59 pc, giving the total projected length of the DG Tau bipolar outflow to be 1 09 pc (however see the proper motion studies in Chapter 4)

The outflow direction changes by 5° in the blueshifted outflow and 8° in the redshifted outflow giving the extended outflow a 'C' shaped morphology, with DG Tau at the apex of the 'C' Similar morphologies have been noted in a small number of large-scale outflows from less evolved sources, for example the HH 366 outflow in Barnard 5 (Bally, Devine, & Alten, 1996) This morphology may be analogous to the head-tail extragalactic radio sources where a curved morphology is created between the radio source (head) and the bipolar jet (tails) due to the motion of the source through the ISM (Edge & Rottgering, 1995) In the YSO case, typical

stellar velocities of around 5 – 10 kms^{-1} with respect to the parent cloud, combined with jet velocities of approximately 150 kms^{-1}, might produce a similar effect (Lim & Raga, 1998, Canto & Raga, 1995)

DG Tau B is located 47″ south and 28″ west of DG Tau and is a low luminosity *Class I* source (i e it is *not* a CTTS and is only included here as it is in the field of view of the DG Tau outflow) with $L_* = 0\,88 L_\odot$ (Jones & Cohen, 1986) It is the driving source of an optical jet (HH 159) also found by Mundt & Fried (1983) and seen to be bipolar by Jones & Cohen (1986) HST images have resolved DG Tau B as a compact bipolar reflection nebula with no optically visible star (Stapelfeldt et al , 1997) The eastern lobe of the reflection nebula is 'V' shaped and the PA of its axis of symmetry is 122° (Padgett et al , 1999) The 56″ redshifted jet and 15″ blueshifted jet have been observed both in imaging mode (Mundt & Fried, 1983, Mundt, Ray & Raga, 1991, Eisloffel & Mundt, 1998) and spectroscopically (Jones & Cohen, 1986, Mundt, Brugel & Buhrke, 1987, Eisloffel & Mundt, 1998) Position angles of 122° for the blueshifted jet and 296° for the redshifted jet were determined by Mundt, Ray & Raga (1991) However examination of these images would suggest that the PA of the blueshifted jet is closer to 116° i e the two jets are diametrically opposed as one might expect In either case, the blueshifted jet is approximately coincident with the axis of symmetry of the reflection nebula, suggesting that the 'V' delineates the walls of a cavity cleared by it The redshifted jet passes through the centre of a well collimated redshifted CO emission lobe (Mitchell et al , 1994, Mitchell, Sargent & Mannings, 1997)

These observations reveal two faint new objects to the southeast of DG Tau B, with a third more evident one further out in the same direction (Figs 3 5 & 3 6), details of which are given in Table 3 3 HH 836 A is at $\sim 2'6$ from the source and is seen only in Hα HH 836 B is at $4'4$ from DG Tau B and is seen in both Hα and [SII] A trail of emission appears to curve back towards HH 836 A from HH 836 B in the Hα image These objects are quite faint and diffuse The most distant optically visible object in the blueshifted outflow is HH 837 at $10'4$ from DG Tau B In [SII] it appears to have a 'V' shaped morphology pointing eastwards In Hα it is much stronger and is clearly bow shaped with some emission over-lapping the [SII] emission to the west of the bow (Fig 3 6) There is no indication of this bow shock in the [SII] emission HH 836 A and HH 837 are at PAs of 116° and 117°

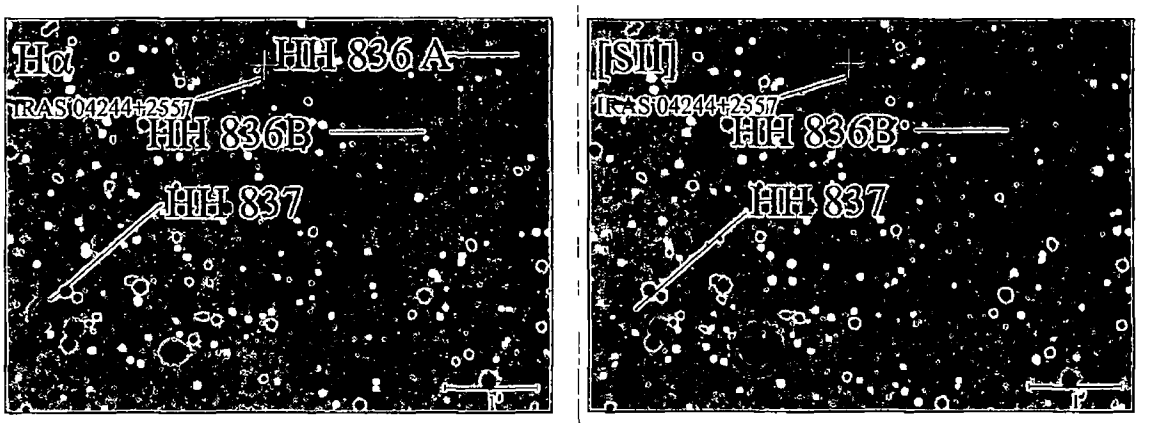

Figure 3 6 *HH 836 and HH 837* The objects to the southeast of DG Tau B are shown here in both Hα and [SII] See Fig 3 5a for the extended DG Tau B outflow HH 836 A is only seen in Hα, and HH 836 B is stronger in Hα than in [SII] There is a distinct difference between HH 837 in Hα and [SII] The nearby IRAS source, which is also marked on Fig 3 5a, is marked here

respectively with respect to DG Tau B and are well aligned with the blueshifted HH 159 jet HH 836 B is slightly off this axis at 122° suggesting that the direction of the blueshifted outflow has only varied slightly over the 10′4 distance from the source Although IRAS 04244+2557 is a possible driving source for some of these HH objects it seems more than coincidental that all three are aligned with the DG Tau B jet (Fig 3 5) The length of this outflow, from the redshifted HH 159 jet to HH 837, is 11′3 which is a projected length of 0 46 pc It is interesting to note that the opening angle for the blueshifted jet was initially estimated to be $\sim$ 17° i e almost four times that of the redshifted jet at $\sim$ 4 5° (Mundt, Ray & Raga, 1991) These images of the extended blueshifted outflow show that it has clearly recollimated, the opening angle (to HH 837) is now 3°

Two other HH objects are found in this region which do not appear to be related to either the DG Tau or the DG Tau B outflows HH 838 is 1′6 at a PA of 286° from DG Tau B and is a faint, 43″ by $\sim$ 4″ linear HH object running north/south (Fig 3 5a) seen only in Hα emission All known IRAS sources in the regions are marked on Fig 3 5a but none of these appear to be a likely driving source for HH 838 These images do not show any other HH emission aligned with HH 838 The second HH object, HH 839 to the east of DG Tau B, consists of three "knots" (seen clearly in Fig 3 5e), of which the most northwestern one appears to be a mixture of continuum and HH emission and is probably the location of the source

driving the outflow The other two knots, which are at a PA of 126° with respect to the assumed source, appear to be an $\sim 10''$ long outflow and are equally strong in Hα and [SII] This outflow is approximately parallel to the DG Tau B outflow HH 839 is quite bright in the I band images so it possibly contains some reflection nebulosity as well I can find no other obvious driving source for this outflow

3.2.3 The DO Tau and HV Tau region

DO Tau is a CTTS associated with an arc-like nebula A bipolar jet (HH 230) extending for approximately $2''$ to $4''$ was observed spectroscopically from DO Tau by Hirth et al (1994) with the redshifted jet at a PA of $\sim 70°$ (Hirth et al , 1994) DO Tau is an M0 star (Herbig & Bell, 1988) with a mass in the range $0\,3 - 0\,7\ M_{\odot}$ and an age of about $1\,6 \times 10^5$ years (Beckwith et al , 1990, Hartigan, Edwards & Ghandour, 1995) To the east of DO Tau is the triple system HV Tau consisting of a close binary, A and B (Simon, Holfeltz, & Taff, 1996), and a third component C $\sim 4''$ northeast of the close binary HV Tau C is an actively accreting CTTS (Woitas & Leinert, 1998) and a bipolar "micro-jet" $\sim 1''5$ in length has recently been observed emerging from it (Stapelfeldt et al , 2003) I have estimated the PA of its northern jet to be at 25° with respect to the source from the images of Stapelfeldt et al (2003)

Four HH objects were found in this region and are marked on Fig 3 7a with details given in Table 3 4 Neither the DO Tau nor the HV Tau C jets are seen in these optical images because of the bright nebulosity around both stars HH 831 is found roughly northeast of DO Tau and is seen in both [SII] and Hα although there are morphological differences between these two images HH 832 and HH 833 are also seen to the northeast of DO Tau however they are only visible in [SII] HH 834 is the only object to the southeast and is seen only in Hα

In Hα images (Fig 3 8) HH 831 A is a $52''$ long structure consisting of three small joined arcs and is fainter towards the northwest and HH 831 B is a diffuse knot In [SII] images (Fig 3 9) HH 831 A is seen as two separate emission regions, the most distant of which is at $10'8$ from DO Tau HH 831 B contains a number of bright emission regions in [SII], more than are seen in Hα and is at a distance of $11'$ from DO Tau HH 831 B is only $\sim 36''$ from the eastern edge of the field of

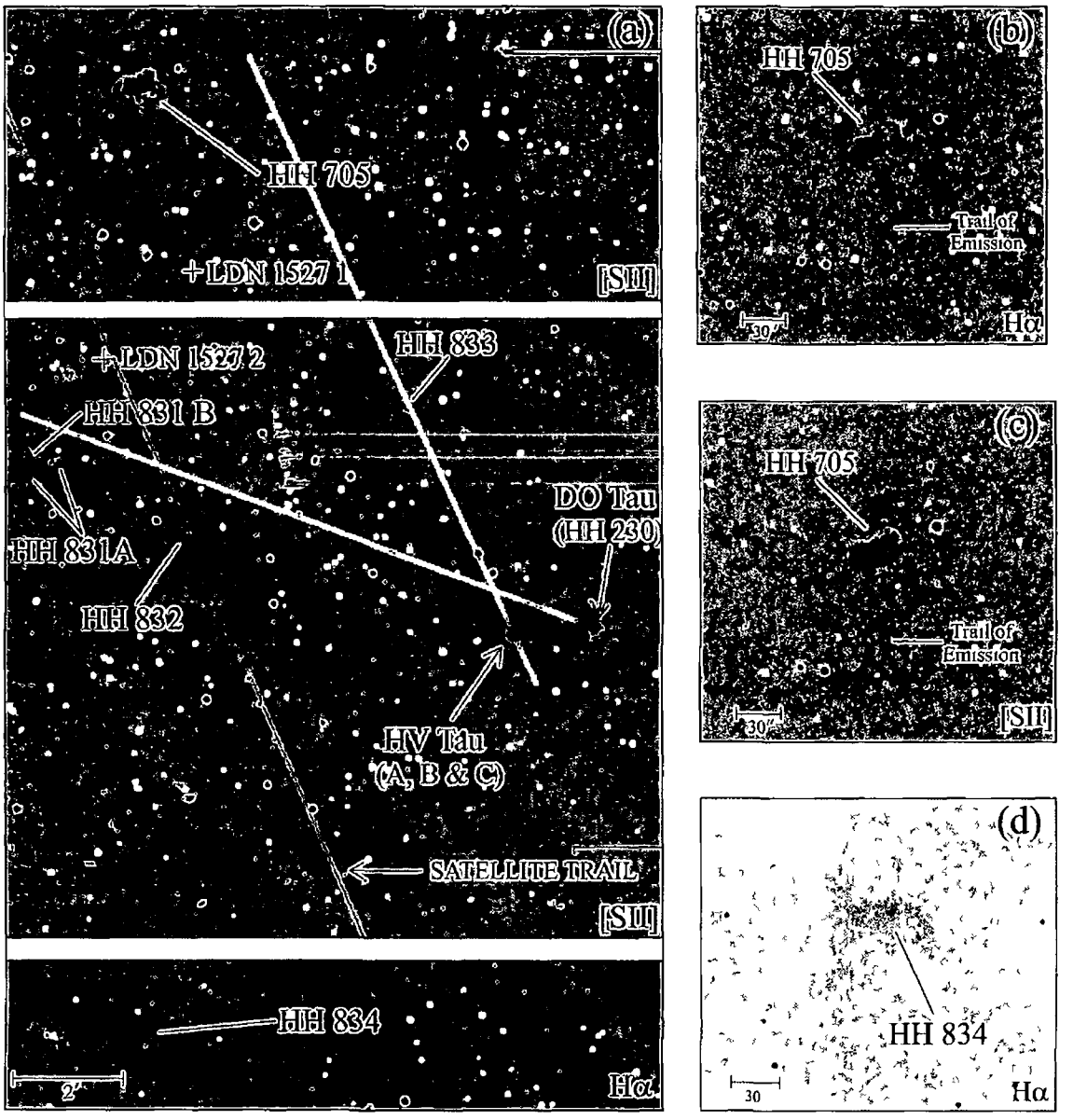

Figure 3 7 *DO Tau/HV Tau* (a) Mosaic of the DO Tau and HV Tau C regions showing the newly discovered HH objects HH 831 – HH 834 The positions of candidate sources for these HH objects are marked HH 230 is not seen in these optical images because of the DO Tau nebulosity, however the dashed line from DO Tau is at 70° marking the direction of the redshifted jet There is also a dashed line at 25° from HV Tau C marking the PA of its northern "micro-jet" HH 831 and HH 832 can be seen more clearly in Figs 3 8 and 3 9 (b) HH 705 in Hα emission (c) HH 705 in [SII] emission (d) HH 834 in Hα Note that HH 834 is not seen in [SII] emission

Object	Source	Angular Separation[a]	PA[b] /°	Spatial Extent[c]
HH 831 A	DO Tau ?	10′8	74	4″× 52″
HH 831 B	DO Tau ?	11′	74	14″× 8″
HH 832	DO Tau	7′7	78	4″× 29″
HH 833	HV Tau C	4′6	25	10″× 8″
HH 834	?			42″× 6″[d]

Table 3 4 Angular separations, PAs and spatial extent of newly discovered HH objects in the DO Tau and HV Tau C region
[a] Angular distance from the presumed source
[b] PA with respect to the presumed source
[c] Width and length of the object respectively
[d] As direction of motion is unknown, width and length may be in reverse order

view so it is very possible that there is more emission in this direction HH 831 is at a PA of $\sim$ 74° with respect to DO Tau and is well aligned with the redshifted jet (however see Chapter 4)

HH 832 (Fig 3 9) is seen only in [SII] and is at 78° and 7′7 from DO Tau It is an $\sim$ 6″ long linear object with faint emission to the northeast There is a nearby trail from a passing satellite

HH 833 (Fig 3 7a) is a diffuse region 4′6 from HV Tau C at a PA of 25° and is seen only in [SII] HH 705, to the north of HH 831, is a complex object containing a number of bright emission regions (Figs 3 7b and c) This object was independently discovered by Sun et al (2003) however these images show it to be more intense and complex than their [SII] images This object may be a bow shock, with faint emission trailing to the southeast and southwest forming the wings and there is a 1′3 long trail to the south Its total width, as measured between the edges of the wings, is $\sim$ 1′ and its total length is 1′9 HH 834 is very faint and seen only in Hα (Fig 3 7d) It is linear and has a total length of 42″

The locations of these new objects in relation to previously known outflows suggests possible links HH 230 is at $\sim$ 70° with respect to DO Tau so it would seem likely that HH 831 at 74°, and possibly HH 832 at a PA of 78°, are part of the same outflow (however see Chapter 4) There is a gap of $\sim$ 7′7 (0 43 pc) between the

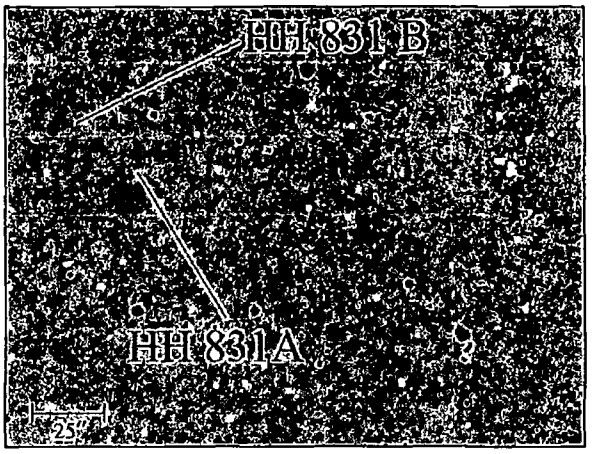

Figure 3 8 *HH 831 Hα* HH 831 as seen in Hα emission Note that this object is much fainter in Hα emission than in [SII] (Fig 3 9) and there is no indication of HH 832 here

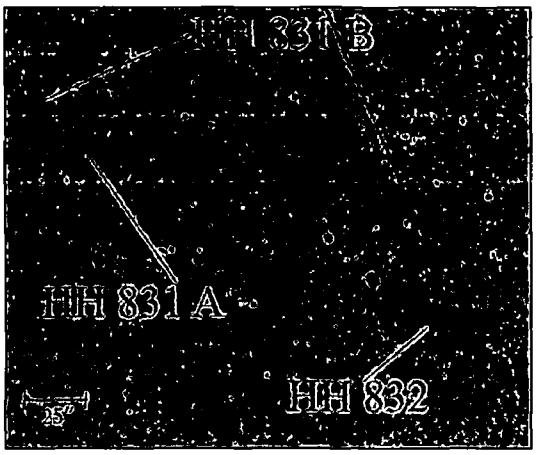

Figure 3 9 *HH 831 and HH 832 [SII]* [SII] image of HH 831 and HH 832 The morphology of HH 831 is quite different to the Hα image (Fig 3 8) and HH 832 is clearly seen here

4″ redshifted HH 230 jet and HH 832 where no HH emission is seen If HH 831 and HH 832 are driven by DO Tau then the length of the redshifted outflow would be $\sim 11'07$ (0 45 pc)

Considering its very close alignment with the previously known "micro-jet" from HV Tau C, it is would seem likely that HH 833 is driven by this source HH 705 could also be part of this outflow (although again see Chapter 4) Both the blueshifted jet from HV Tau C and HH 833 are at 25° with respect to HV Tau C whilst HH 705 is at $\sim 36°$ with respect to this source at a distance of 12′ from it HH 705 is $\sim 7'7$ from HH 833 and it is possible that the outflow direction could have changed by 11° over this distance The southern trail of emission from HH 705 might suggest that its driving source is situated to its south rather than southwest In this case the radio sources LDN 1527 1 or LDN 1527 2 in LDN 1527 (Anglada et al , 1992) are possible driving sources (as suggested by Sun et al , 2003), however it is unlikely that LDN 1527 1 could generate such a large object so nearby Assuming HH 833 and HH 705 are driven by HV Tau C, the projected length of this outflow would be 0 49 pc (12′) However the reader is referred to the proper motion studies in Chapter 4 At present there is no obvious driving source for HH 834

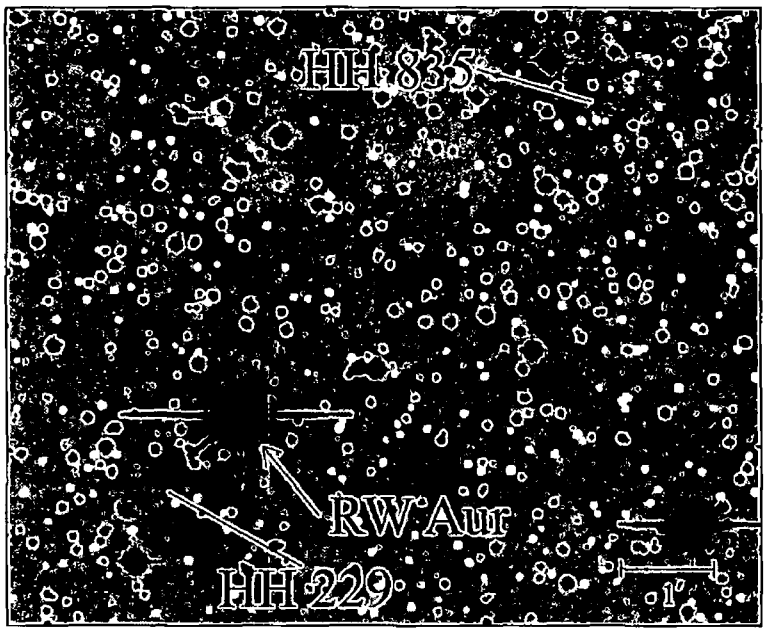

Figure 3.10 *RW Aur Hα* In this image of the RW Aur outflow, the HH 229 jet (and its direction) is clearly seen as is the newly discovered object HH 835, which is seen in more detail in Fig 3.11

3.2.4 RW Aur

RW Aur is a hierarchical triple system, with component A about 1″.4 at a PA of 76° from the close binary B and C (Ghez, Neugebauer & Matthews, 1993) Both RW Aur A and B are actively accreting CTTSs (Duchêne et al , 1999) Although it was suggested as early as 1986 that RW Aur A itself might be a close binary (Hartmann et al , 1986) it is only in recent years that this has been confirmed with evidence of a low-mass secondary companion, possibly a brown dwarf (Gahm et al , 1999, Petrov et al , 2001) The HH 229 bipolar jet is the only indication of an outflow in the vicinity of RW Aur to date (Hamann, 1994, Hirth et al , 1994) Furthermore, long slit spectroscopy confirms RW Aur A as the source of this outflow (Hirth et al , 1994, Hirth, Mundt & Solf, 1997) as does the 0″.1 resolution images of Dougados et al (2000) Recently rotation has been observed at the base of the HH 229 jet – one of the first such outflows where rotation has been detected (Coffey et al , 2004)

The blueshifted component of the HH 229 bipolar jet is at a PA of $\sim 130°$ with respect to RW Aur A (Dougados et al , 2000, Mundt & Eisloffel, 1998, Hirth, Mundt & Solf, 1997) [SII] images of Mundt & Eisloffel (1998) show the redshifted and

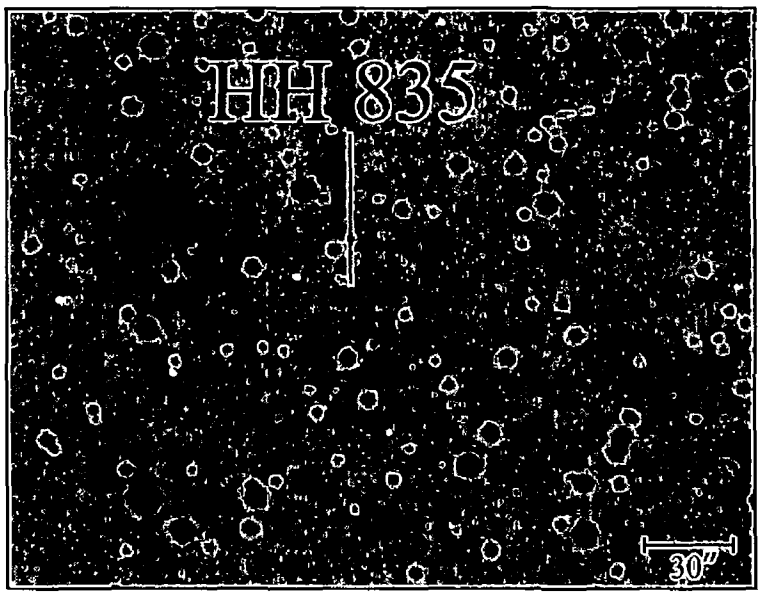

Figure 3 11 *HH 835 Hα* HH 835 to the northwest of RW Aur I suggest that this is the northern wing of a bow shock, with the southern wing being much fainter in these optical images

blueshifted outflows to have lengths of 50″ and 106″ respectively, implying a total projected length of $\sim$ 0 1 pc at a distance of 140 pc Both sides are well collimated, with a full opening angle for the redshifted jet of less than 6° (Woitas et al , 2002) The detection of emission in the redshifted jet can be traced back to 0″1 from the source which implies an upper limit of 15 AU for the projected radius of its circumstellar disk

These images reveal a large object (HH 835) 5′37 to the northwest of RW Aur (See Fig 3 10 and Table 3 5) I suggest that this object is a bow shock with only the $\sim$ 30″ long northern wing visible in these Hα images (Fig 3 11) Given the position of HH 835 on the known axis of the RW Aur outflow (both at a PA of 310° with respect to RW Aur) I suggest that this object is part of the redshifted RW Aur A outflow There is a distance of $\sim$ 4′6 between the end of the redshifted jet and HH 835 in which there is no optical evidence for outflow activity The total observed projected length of the RW Aur outflow from the end of the blueshifted outflow to HH 835 is 0 29 pc (7′)

Object	Source	Angular Separation[a]	PA[b] /°	Spatial Extent[c]
HH 835	RW Aur	5'37	310	30″× 12″

Table 3 5 Angular separations, PAs and spatial extent of the newly discovered HH object in the RW Aur outflow
[a] Angular distance from the presumed source
[b] PA with respect to the presumed source
[c] Width and length of the object respectively

3.3 Discussion

I have shown that five of the seven CTTSs examined in the Taurus-Auriga Cloud (namely CW Tau, DG Tau, DO Tau, HV Tau C and RW Aur) may drive outflows of the order of 0 5 – 1 pc in length I have estimated the length, dynamical timescale and degree of collimation for all six of the outflows discussed in §3 2 and these are presented in Table 3 6 Here I examine the parameters and the morphological trends of these CTTS outflows in more detail, and compare them to large-scale outflows from more embedded Class I sources These trends can be used to infer details about the source, the propagation of the outflow into the ambient medium, and the evolution of the outflow with time

3 3.1 Outflow Morphology

Typically many large-scale outflows from Class I sources are either 'S' shaped with the driving source approximately in the middle of the 'S' - for example the HH 47 outflow (Heathcote et al , 1996), HH 34 outflow (Bally & Devine, 1994) and the PV Cephei outflow (Reipurth, Bally, & Devine, 1997) to name but a few, or the rarer 'C' shaped with the source at the apex of the 'C' - for example the HH 366 outflow in Barnard 5 (Bally, Devine, & Alten, 1996) Some possible scenarios that explain these morphologies are discussed in §1 3 4 It can be seen from the images presented in §3 2 that many of the outflows from CTTSs show evidence for some variations in PA with time, the effect being most evident in the CW Tau outflow This outflow delineates an approximate inverted 'S' shape centered on CW Tau (however see Chapter 4) with the northern part of the 'S' more elongated than the southern part The change in outflow direction is possibly due to precession of the outflow axis (Raga et al , 2001, Masciadri & Raga, 2002) Also, the DG Tau outflow

Source	L_{bol} / $L_\odot$	Reference	Outflow Length / pc	Associated Nebula	Cloud Size[a] /pc	τ_{dyn} $\times 10^4$ yr	θ_{flow}[b] /°
DG Tau	$\geq$7 6	1	1 09	LDN 1521	7 4 × 5 4	1 2	10 6
DG Tau B	0 88	2	0 46	LDN 1521	7 4 × 5 4	0 8	1 8
CW Tau	2 6	3	0 98	LDN 1495	3 9 × 3 2	1 4	3 8
HV Tau C[c]	$\sim$0 5	4	0 49	LDN 1527[d]	0 03 × 0 01	1 0	4 1[e]
DO Tau[f]	3 5	1	0 45	LDN 1527[d]	0 03 × 0 01	0 9	3 1[g]
RW Aur	$\lesssim$ 1 1[h]	5	0 29	Anonymous		0 4	4

Table 3 6 Outflow lengths, dynamical timescales and degree of collimation for the five newly discovered parsec-scale outflows from (Class II) CTTSs and for the serendipitously discovered outflow from the Class I source DG Tau B

[a] Visual estimate of the approximate width and length of the associated nebula for each source

[b] θ_{flow} is calculated by taking the width of the most distant shock in both the red- and blueshifted outflows and dividing by the projected distances from the source The mean value of θ_{flow} for both outflows, where both are seen, is given here

[c] Here I assume that HH 833 and HH 705 are part of the HV Tau C outflow (see §3 2 3)

[d] The source is at the edge of this nebula, however I estimate the larger cloud surrounding this source to be approx 0 4 pc × 0 4 pc

[e] This is the opening angle for the blueshifted outflow only – the redshifted jet is too short to measure accurately

[f] Here I assume that HH 230, HH 831 and HH 832 are part of the DO Tau outflow (see §3 2 3)

[g] This is the opening angle for the redshifted outflow only – there is no optically visible blueshifted outflow (see §3 2 3)

[h] This is the luminosity of the RW Aur A binary and so is an upper limit for the binary component driving this outflow (see §3 2 4)

References 1 Cohen & Kuhi (1979), 2 Jones & Cohen (1986), 3 Gómez de Castro (1993), 4 Stapelfeldt et al (2003), 5 Petrov et al (2001)

may be "C" shaped, as discussed in its results (§3 2 2)

It has also been noted from large-scale outflows driven by less evolved sources that the size and complexity of the HH shocks increases with distance from the source (§ 1 3 4) As the supersonic outflow propagates through the parent cloud it interacts with both the ambient medium and slower, previous ejecta producing the HH shocks observed Many of these shocks fade quickly with time, it is only the strongest and largest shocks that remain As a consequence of this, the gap between consecutive HH objects/complexes increases with distance as the majority of the more distant shock quickly fade leaving just a few, larger shocks (Reipurth & Bally, 2001, Bally & Devine, 1997) As these extended shocks have undergone many interactions with their surroundings, and have had time to evolve, they will often be complex, chaotic objects rather than the simple knot-like structures seen closer to the young star Most of the outflows from CTTSs presented here also demonstrate these trends, as do the parsec-scale outflows from intermediate-mass YSOs (Chapter 2)

3.3 2 Outflow Length

From Table 3 6 it can be seen that the length of the outflows from CW Tau, DG Tau, DO Tau and HV Tau C are of the order of $\sim$ 1 pc This represents an increase over the previously known values by a factor of 480 for the HV Tau C outflow, and factors of between 120 and 160 for the other three (however see Chapter 4) The RW Aur outflow was previously known to be $\sim 2'7$ in length and this revised value is a factor of $\sim$ 2 6 larger ($7'$) Outflows of the order of 1 pc should readily be expected from Class II low-mass stars, the typical age of which is 10^6 years Even if an outflow has an average velocity of around 50 kms^{-1} (i e the minimum velocity required to excite the shocks seen) then over 10^6 years it could extend up to 50 pc

The field of view captured by the Wide Field Camera is $\sim 34'$ square which projects to a maximum detectable outflow length of 1 4 pc at the distance of the Taurus-Auriga Cloud Outflow morphology suggests that the distance between consecutive HH objects complexes increases exponentially with distance from the source so if there is emission beyond the field of view then it may easily be on scales of tens of parsecs, near the edges of the Taurus-Auriga Cloud boundaries, and well

beyond the field of view of the WFC

The apparent dynamical timescales for these outflows is estimated in Table 3 6, assuming the most distant objects are moving at a velocity of 50 kms^{-1} which is a lower limit (see Chapter 4) Values of around 10^4 years are derived thus we are only observing a fraction of the stars' outflow histories

These observations suggest that, in all cases, the outflows have blown out of the associated clump Many of the most distant objects in the outflows are at the clump edges while a few, most notably HH 830 and HH 702 in DG Tau are clearly well beyond There is little doubt based on statistically estimated lifetimes that these outflows are even larger than the field of view, and thus this data supports the idea that they have blown out of their parent cloud Large-scale outflows blowing out of their parent cloud is also a well documented occurrence in outflows from Class I low-mass sources (cf §1 3 4) as the observations presented here of DG Tau B show and in outflows from intermediate-mass sources as shown in Chapter 2

3.3.3 Degree of Collimation

For the CTTSs outflows discussed here I find a degree of collimation of the order of $\sim 5°$ (see Col 8 of Table 3 6) This value is in good agreement with the degree of collimation of large-scale outflows from more embedded Class I stars (Mundt, Ray & Raga, 1991) Although this sample of outflows from Class II stars is small, this suggests that *collimation remains high even as the source evolves*

3.3 4 Have these CTTSs gone through the FUor Phase?

The morphology and location of the HH objects/complexes associated with these CTTSs suggest long quiescent outflow phases punctuated by mass ejections of varying strength According to this scenario, the most violent of the latter have given rise to the most distant (from the YSO), long-lasting and extended HH complexes that we see today Reipurth & Aspin (1997, and references therein) have suggested that these major ejection events occur when the parent star undergoes FU Orionis-type outbursts, or FUor events as they are sometimes known Before addressing whether this is the case, and explaining why I think this sample, albeit small, lends

considerable weight to the hypothesis, it is worthwhile saying a few words about the FU Orionis phenomenon

When a YSO undergoes an FUor outburst, its optical brightness increases by several orders of magnitude before decaying back to the pre-outburst luminosity over 50-100 years (Hartmann & Kenyon, 1996) These outbursts are not fully understood but are believed to be associated with thermal instabilities in the accretion disk (for a detailed review of FUor objects and outbursts see Hartmann & Kenyon, 1996) The spectra of these so-called FUors in quiescence is that of a CTTS and there are at least nine known FUors (Hartmann & Kenyon, 1996) including the prototypical source – FU Orionis itself (Herbig, 1977) Almost immediately after their discovery it was suggested that FUor events could give rise to Herbig-Haro outflows (Dopita, 1978, Reipurth, 1985) More recently, as already stated, Reipurth & Aspin (1997) investigated this possible connection, basing their conclusions largely on a sample of embedded Class I sources As it is accepted that in quiescence FUors are CTTSs it seems more appropriate to examine *outflows of the latter* for any "fossil record" of FU Orionis-type outbursts In particular it is not obvious *apriori* that the outburst timescales for Class I and Class II stars are similar

Examining Table 3 6 we see that the dynamical timescales of the *extended* HH complexes, associated with these CTTSs, are typically 10^4 years Herbig (1977) and Herbig, Petrov, & Duemmler (2003) have estimated the mean time between successive FUor outbursts to be approximately 10^4 years, suggesting a clear link Moreover the relative number of FUors in comparison to CTTSs also supports such a link To conclusive determine if this is the case, the dynamical time between the current most distant HH objects in these outflows, and the next, more distant HH object/complex would have to be found However as any more distant objects will have blown out of the parent cloud their interactions with the less dense ISM/interclump medium will be very faint in optical wavelengths, making this very difficult to determine It would however be useful to test this hypothesis further using large-scale simulations to see whether, given the typical energies involved in such outbursts, we might expect the development and survival of a series of giant HH complex with such timescales

Chapter 4

Kinematical Studies of CTTS-Driven Outflows

In Chapter 3 I examined a number of more evolved, Class II low-mass sources (CW Tau, DG Tau, DO Tau, HV Tau C and RW Aur) and found they may drive parsec-scale outflows despite being previously only known to drive "micro-jets" or small-scale outflows of $\leq 1'$ (0 04 pc at the distance to the Taurus-Auriga Cloud) Here I use multi-epoch observations to determine proper motions and hence tangential velocities for the HH objects associated with these outflows to test whether my conclusions in Chapter 3, largely based on morphology and alignment, are correct Additionally, the tangential velocities of HH objects at relatively large distances from their source is poorly known In particular, how tangential velocities evolve with distance from the source is not well understood Both of these issues are addressed here in light of the results of the proper motions studies

Details about the observations and proper motion method used are given in §4 1 and §4 2 respectively The results of this study are reported in §4 3 and the implications of these results are discussed in §4 4

4.1 Observations

Using multi-epoch observations the velocity and direction of motion of many of the more distant HH objects in the CW Tau, DG Tau, DO Tau, HV Tau C and RW Aur outflows are determined The observations used here were taken on a *num-*

Region	Line	1st Epoch	2nd Epoch	3rd Epoch
DG Tau	[SII]	1999 91	2001 12	2003 91
	Hα	2001 12	2003 91	
CW Tau	[SII]	2001 12	2002 98	2003 91
	Hα	2001 12	2002 98	2003 91
DO Tau	[SII]	2001 12	2002 98	2003 91
	Hα	2001 12	2002 98	2003 91
HV Tau C	[SII]	2001 12	2002 98	2003 91
	Hα	2001 12	2002 98	2003 91
RW Aur	[SII]	2001 12	2003 91	
	Hα	2001 12	2003 91	

Table 4 1 Log of observations used for each source in the proper motions study

ber of different observing runs using the Wide Field Camera on the Isaac Newton Telescope, La Palma (Canary Islands) This camera is described in §2 1 The same CCDs and hence the same angular resolution is used for all observations – 1 pixel projects to 0″33 The observing runs occurred in November 1999 (epoch 1999 91), February 2001 (epoch 2001 12), December 2002 (epoch 2002 98) and finally November 2003 (epoch 2003 91), however not all regions were targeted during each run Narrow band filters were used to observe the HH objects, both [SII](λ_c = 672 5nm, $\Delta\lambda$(FWHM) = 8 0nm) and Hα(λ_c = 656 8nm, $\Delta\lambda$(FWHM) = 9 5nm) are used here, but again not all objects were observed using both of these filters Table 4 1 lists the different observations for each source Exposure time for the narrow band images was typically 30 minutes The data was reduced using standard IRAF procedures for bias subtraction and flat fielding

4.2 Proper Motion Method

A *cross-correlation method* was devised[1] to determine the proper motions of the HH objects found in Chapter 3 The images from two different epochs are initially aligned using star positions obtained from the SExtractor software (Bertin & Arnouts, 1996) The method then maps one of the images onto the other using a polynomial fit (up to third order) and the IRAF task *geomap* This procedure ensures the correction of any systematic effects such as stretching, rotation, etc of

[1]with the assistance of Dirk Froebrich, currently a postdoctoral fellow in DIAS

the image

The programme then moves one of the aligned images relative to the other over a number of pixels in steps of 0 1 pixel Each time this image is moved the two images are multiplied A box is pre-defined around each HH object and the intensity within this box in the product image is noted for each of the steps When all steps have been completed, the position which generates the greatest intensity for each box is taken to be the position of the object in the moved image The difference in pixels between the "moved" image and the "static" image at this position yields the proper motion of the HH object

There are two main sources of error in these measurements The first is due to the accuracy of the alignment of the images This is typically 0 2 – 0 4 pixels in both x and y directions, generating errors of about 20 – 40 kms^{-1} and about 15° – 30° However the errors in the central frame of the CW Tau region (i e HH 826, HH 220 NW and HH 828, see Fig 4 1) are much higher than this There are very few stars in this field of view and consequently the alignment is poorer Alignment errors for these objects are about 1 pixel in x and y i e $\sim$ 110 kms^{-1} and 55° The second source is due to the error in the position of the HH object (due to its signal-to-noise ratio, PSF (point spread function) and extent) This seems to be the limiting error for most of the objects observed here, especially the faint objects as one would expect Typically these errors are about 0 2 – 0 5 pixels in x and y, relating to $\sim$ 20 – 55 kms^{-1} and 16° – 35° The most noticeable exception is the frame containing HH 830 (in the vicinity of DG Tau) which in [SII] has errors of about 1 1 pixels, i e $\sim$ 120 kms^{-1} and 58°, and in Hα has errors of $\sim$ 0 7 pixels in x and y i e $\sim$ 80 kms^{-1} and 45°

4.3 Results

A detailed introduction to the CTTSs DG Tau, CW Tau, DO Tau, HV Tau C and RW Aur and their "micro-jets"/small-scale outflows is given in Chapter 3 The newly discovered objects (HH 826 – HH 835) that may be extensions to these outflows are also presented there Here, a brief summary is given for each outflow before the proper motion results are discussed

			[SII]		Hα	
HH Object	Source [a]	Ang Sep	Velocity /kms^{-1}	Direction /°	Velocity /kms^{-1}	Direction /°
HH 826 A	CW Tau (B)	0′4	132	159		
HH 826 B	CW Tau (B)	1′2	207	156	282	166
HH 827 A	CW Tau (B)	6′1			347	180
HH 827 B	CW Tau (B)	6′9	199	198	151	188
HH 220 NW	CW Tau (R)	0′6	323	287		
HH 826 C	CW Tau (R)	0′8	261	321	111	26
HH 828 M			118	144		
HH 828 E			103	159		
HH 828 W			173	208		
HH 829 A			116	108		
HH 829 B			113	163		

Table 4 2 Tangential velocity and direction of motion of HH 220, HH 826, HH 827, HH 828 and HH 829 in the vicinity of CW Tau assuming a distance of 140 pc (Elias, 1978, Wichmann et al , 1998)

[a] B and R denotes whether the object is aligned with the blue or redshifted jet

4.3 1 CW Tau

The HH 220 bipolar "micro-jet" from CW Tau was first discovered by Gómez de Castro (1993) Hirth, Mundt, & Solf (1994) show this outflow to be 4″ – 6″ on either side of CW Tau In Chapter 3 I presented a number of HH objects which appear to be an extension to this outflow HH 826 A, HH 826 B and HH 827 are to the south of CW Tau, with HH 826 C, HH 828 and HH 829 to the north (see Fig 4 1) Assuming all of these objects are driven by CW Tau the total projected length of the outflow would be $\sim$ 1 pc

The PA of the blueshifted HH 220 jet is at $\sim$ 144° with respect to CW Tau (Gómez de Castro, 1993, Dougados et al , 2000) and I previously measured the redshifted jet to be at $\sim$ 329° from the images of Dougados et al (2000) Here I measure the proper motions of HH 826 to HH 829 in both [SII] and Hα These objects are fainter in Hα, with the exception of HH 827 which is much stronger HH 826 A and HH 828 are not seen at all in Hα emission However the errors in alignment of the central frame (HH 826, HH 220 NW and HH 828) in [SII] and Hα are quite high due to the low number of stars in the field that are used to align the images

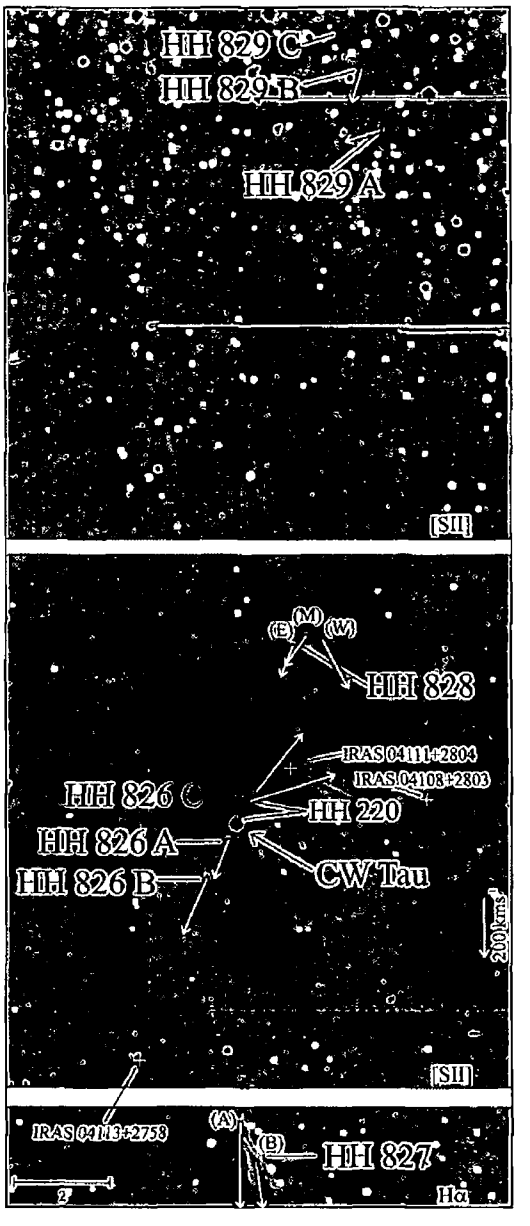

Figure 4 1 Proper motions of HH 826 – HH 829 in the vicinity of CW Tau in [SII] emission Just below HH 826 C is the vector representing the 17″ long northwestern (NW) segment of HH 220 For all images in this chapter the direction of motion is represented by white arrows The relative length of these arrows in each image denotes the relative velocities of the HH objects These vectors clearly show that HH 826 is driven by CW Tau, and that HH 827 is probably also driven by this source if the outflow is gradually changing direction However this study also shows that HH 828 and HH 829 are not driven by CW Tau Other possible sources for these objects are suggested in the text The errors associated with HH 826, HH 220 NW and HH 828 are quite high (typically 110 kms^{-1} in velocity and 55° in direction of motion) and are due to the difficulties in aligning these images, as there are very few stars in the field of view of the middle frame

From Table 4 2 it can be seen that HH 826 A, which is quite close to the source, is moving at a direction of 159° i e it is well aligned with the blueshifted HH 220 jet HH 826 B is moving at 156° in [SII] and 166° in Hα and so is well aligned with both HH 826 A and the blueshifted jet Similarly HH 826 C, moving at 321° (in [SII]), is well aligned with the redshifted HH 220 jet This knot appears to be moving $\sim$ 60° further east (at 26°) in Hα, however this direction is approximately within the associated errors

There are two optically visible parts to the extended redshifted HH 220 jet First, it extends to 9″ from the source, there is then a gap before the second part of the jet is seen at 20″ to 37″ from the source, ending in HH 826 C (cf Chapter 3) The 9″ long segment close to CW Tau was too faint to measure, however the longer segment (HH 220 NW (northwest)) was measured in [SII] and has a direction of 287° Allowing for associated errors, this direction is roughly aligned with HH 826 C (at 321°) and with the PA of the redshifted "micro-jet" closer to the source (329°)

HH 827 is much stronger in Hα, and these proper motion studies show it to be moving at 184° (average of Knot A & B) I refer to the brightest and largest part of HH 827 as Knot B, while Knot A is the closest bright knot to CW Tau – see Fig 4 1 Although HH 827 B is much smaller and fainter in [SII], its direction of motion is still in good agreement at 198° Knot A is too faint to measure in [SII] These directions rule out IRAS 04113+2758 as a possible source of HH 827 (suggested in Chapter 3) As we do not know if and where this outflow starts to bend beyond HH 826 B it is difficult to know if this object is part of the CW Tau outflow It was suggested in Chapter 3 that CW Tau could be driving this object if the outflow is precessing and these results are consistent with this scenario

The HH 828 knots to the north of CW Tau are quite faint and diffuse and their proper motions are not easily measured The western, middle and eastern knots are moving at 208°, 144° and 159° respectively, although the western knot is is very faint and its measured direction of motion will have larger errors While these directions rule out the possibility of them being driven by CW Tau, IRAS 04111+2804 or IRAS 04108+2803 (see Fig 4 1) as suggested in Chapter 3 they do suggest a

common source for the east and middle knots at least IRAS 04111+2820 is 13′ at a PA of 4° from the middle knot and is a strong candidate source for HH 828 This source is beyond the field of view of Fig 4 1 and was suggested in Chapter 3 as a possible source for the HH 829 knots

The most distant objects in the redshifted outflow is HH 829 HH 829 C is too faint to measure in both [SII] and Hα and Knots A and B were measured in [SII] only Knot A is moving in a direction of 108° and B is at 163°, ruling out CW Tau as the driving source I previously noted that IRAS 04111+2820, to the northeast of HH 829 (Chapter 3), could be driving one of the HH 829 knots, however this now looks unlikely given the direction of motion of these knots[2]

In the blueshifted CW Tau outflow the velocity appears to vary widely from object to object HH 826 B is moving at a velocity of ~ 207 km^{-1} in [SII], HH 827 B at 151 kms^{-1} in Hα and HH 827 A is almost 200 kms^{-1} faster than HH 827 B (in Hα) HH 826 A appears to be moving more slowly than any of the more distant knots at 132 kms^{-1} The redshifted outflow appears to just consist of HH 220 NW and HH 826 C, and there is ~ 60 kms^{-1} difference between these two knots which have velocities of 323 kms^{-1} and 261 kms^{-1} respectively

While this proper motion study confirms that HH 826 and HH 827 are driven by CW Tau, it also shows that HH 828 and HH 829 are not This reduces the length of the known outflow from 24′ (0 98 pc), as suggested in Chapter 3, to 7′9 (0 32 pc)

4 3.2 DG Tau

HH 158, a "micro-jet" close to DG Tau, was originally discovered by Mundt & Fried (1983) and extends for $\sim 16''$ (Eisloffel & Mundt, 1998) at a PA of 223° (Bacciotti et al , 2002) In Chapter 3 I suggested that the DG Tau outflow is much longer than just HH 158 and may also consist of two other HH objects which are approximately aligned with HH 158 – HH 702 which was also independently discovered by Sun et al (2003) and HH 830 (see Fig 4 2) If this is the case then the DG Tau outflow actually extends a total length of 27′ (1 09 pc) Here I present proper motion studies confirming that HH 702 is indeed driven by DG Tau, however studies of HH 830

[2]I have just proposed this source as a candidate source for HH 828 instead

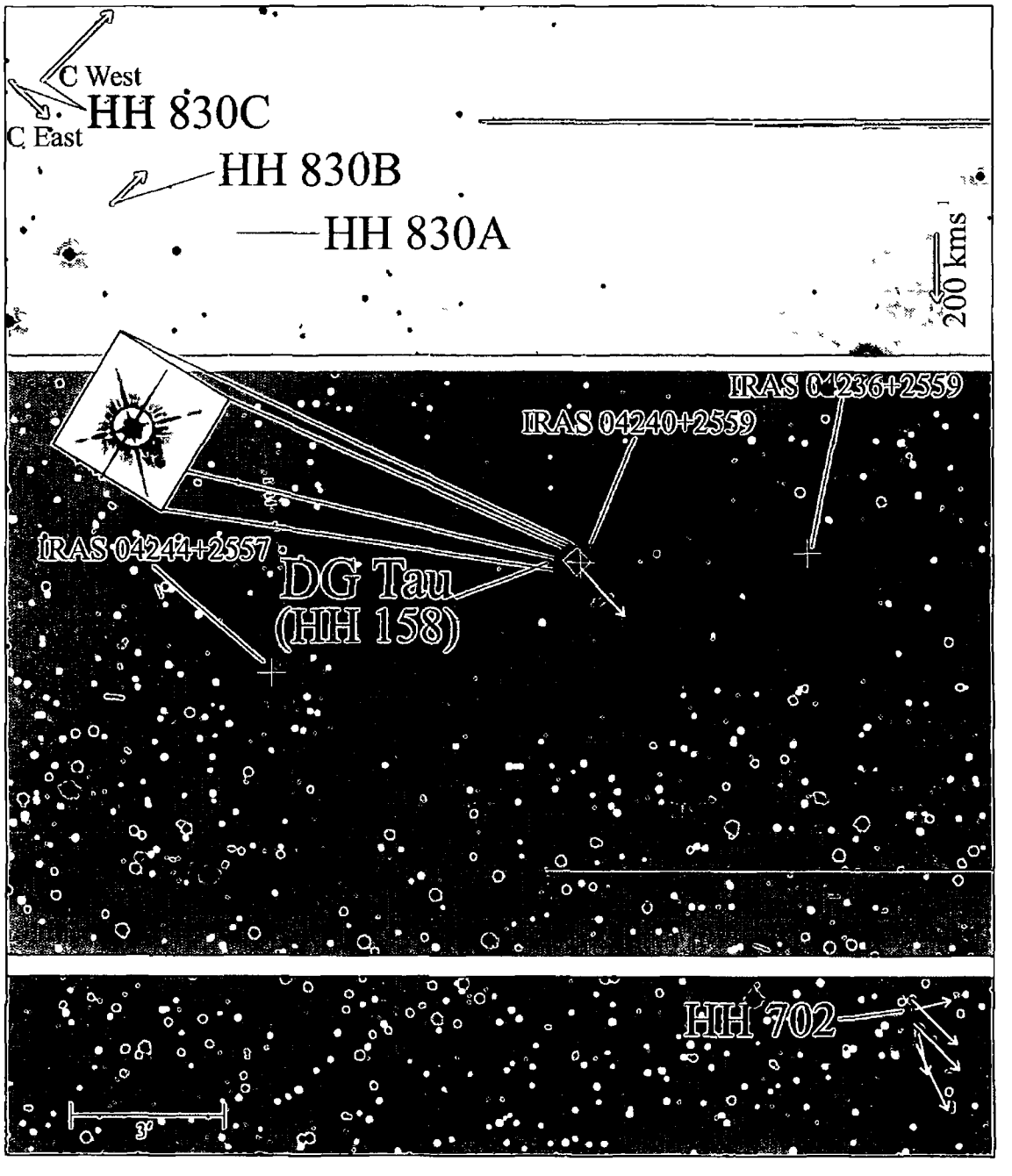

Figure 4 2 Proper motions of HH 702 and HH 830 in the vicinity of DG Tau in [SII] emission, showing that HH 702 is driven by DG Tau, but that HH 830 is not HH 830 C (West) and B appear to be driven by a source to their southeast however I am unable to suggest any possible sources The left hand side of the image is the eastern edge of the field of view of the mosaic, which may affect the accuracy of the results for HH 830 C East

HH object	Source [a]	Ang Sep	[SII] Velocity /kms^{-1}	[SII] Direction /°	Hα Velocity /kms^{-1}	Hα Direction /°
HH 158 C	DG Tau (B)	12″[b]	197[c]	223[d]		
HH 702 A	DG Tau (B)	10′6	203	225	129	194
HH 702 B	DG Tau (B)	10′9	97	285	45	250
HH 702 C	DG Tau (B)	11′1	204	224	149	128
HH 702 D	DG Tau (B)	11′4	219	205	190	269
HH 702 E	DG Tau (B)	11′4	125	191	186	117
HH 830 C West			298	314		
HH 830 C East			161	226	348	314
HH 830 B			142	313	327	233

Table 4 3 Tangential velocity and direction of motion of HH 158, HH 702 and HH 830 in the vicinity of DG Tau assuming a distance of 140 pc (Elias, 1978, Wichmann et al , 1998)

[a] B and R denotes whether the object is aligned with the blue or redshifted jet

[b] Angular separation based on values in Eisloffel & Mundt (1998)

[c] Eisloffel & Mundt (1998)

[d] Bacciotti et al (2002)

suggest that it is not part of this outflow

Table 4 3 shows the velocity and direction of motion of Knots A – E in HH 702 In [SII] emission Knots A, C, D and E are moving at between $\sim$ 191° and $\sim$ 225° These knots are well aligned with HH 158 which has as a PA of 223° with respect to DG Tau (see Fig 4 2) Knot B appears to be moving at 285° and so is not aligned with the other knots in HH 702 Knots A, C and D have comparable velocities between $\sim$ 203 kms^{-1} and $\sim$ 219 kms^{-1} while knots B and E have velocities of only approximately half of this, at 97 kms^{-1} and 125 kms^{-1} respectively

The direction of motion found in Hα emission for the HH 702 knots range from 117° for Knot E to 269° for Knot D (Fig 4 2) Knots A and B are moving within $\sim$ 30° of the direction found in [SII] emission, which the associated errors for both measurements would account for, whereas Knots C, D and E are significantly different Knots A and C have comparable velocities of $\sim$ 129 kms^{-1} and 139 kms^{-1} in Hα while knots D and E are also comparable at $\sim$ 186 kms^{-1} and 190 kms^{-1} Only Knot D has comparable velocity in both Hα and [SII] of 190 kms^{-1} and 215 kms^{-1} Knot B has a velocity of 45 kms^{-1} in Hα, which is a lower limit for the

velocity needed to induce optically visible shocks

HH 830 to the northeast of DG Tau consists of knots A, B and C, with Knot C containing two separate emission regions (C West and C East) Table 4 3 shows the results of the proper motion study of HH 830 B and C only as Knot A is too faint to measure Fig 4 2 shows that Knots B and C West are moving in the same direction at 314°, suggesting a common source Knot C East is moving orthogonally to these however this knot is at the eastern edge of the field of view of the WFC CCD mosaic which makes it more difficult to determine accurate proper motions Also, as mentioned in §4 2, the errors in the position of HH 830 in both [SII] and Hα is quite high, about 80 – 120 kms^{-1} and 45° – 58° These direction of motions prove that these knots are not driven by DG Tau They suggest a source to the southeast, however I am unable to suggest any candidate sources Therefore the projected length of the DG Tau outflow must be revised downwards to 12′33 (0 5 pc)

Eisloffel & Mundt (1998) determined the velocity of the outermost knot[3] in HH 158 as 197 kms^{-1} I was unable to obtain proper motions for this knot from my images due to the significant amount of nebulosity surrounding this object The results from my proper motion study show that the velocity of HH 702 is comparable to that of HH 158 (both in [SII] emission), despite the 7′7 (0 3 pc) gap between these two objects This point is discussed further in §4 4 2

4.3.3 The DO Tau and HV Tau C region

The 2″ – 4″ long bipolar HH 230 "micro-jet" at a PA of $\sim$ 70° with respect to DO Tau was first observed by Hirth et al (1994) Two newly discovered HH objects, HH 831 and HH 832 (see Chapter 3), to the east of DO Tau appear to be well aligned with HH 230 (see Fig 4 3), suggesting that they are part of this outflow However this proper motion study shows the HH 831 Knots (A and B) to be moving in a completely different direction than that expected if driven by DO Tau

[3]I refer here to Knot C of HH 158 Eisloffel & Mundt (1998) note that there is a slightly more distant Knot (D) in HH 158 however they suggest that this object results from some irregularities in the bow shock (Knot C) structure

			[SII]		Hα	
HH Object	Source	Ang Sep	Velocity /kms^{-1}	Direction /°	Velocity /kms^{-1}	Direction /°
HH 831 A1	[a]		184	331		
HH 831 A2	[a]		166	300		
HH 831 A3	[a]		196	288		
HH 831 A4					141	32
HH 831 A5	[a]		112	284	221	182
HH 831 B1			71	158		
HH 831 B2			79	134		

Table 4 4 Tangential velocity and direction of motion of HH 831 assuming a distance of 140 pc (Elias, 1978, Wichmann et al , 1998) to DO Tau, its previously suggested source

[a] Three IRAS sources are suggested in the text as possible driving sources for HH 831 A1 – A3 and A5

HH 831 A knots A1, A2, A3 and A5 are moving in similar directions between 284° and 331° (Table 4 4) in [SII] emission B1 and B2 (only measured in [SII]) however are moving in different directions at 158° and 134° respectively Only Knots A4 and A5 could be measured in Hα emission however the directions of Knot A4 at 32° is not aligned with any of the directions seen in [SII] and Knot A5 is moving at 182° in Hα, which is not aligned with its [SII] results

From these results it is obvious that HH 831 is not driven by DO Tau, despite the fact that these knots appear to be very well aligned with the known PA of HH 230 (Fig 4 3) These results show a number of different directions of motion within HH 831 – Knots A1, A2, A3 and A5 (in [SII]) are moving westwards, while Knots B1 and B2 are moving to the southeast Knot A4 (in Hα) appears to be separate to all of these and is moving to the northeast There are three IRAS sources to the east and southeast of HH 831 that could be driving the A1, A2, A3 and A5 knots HH 831 A is 6′ at a PA of 292° from IRAS 04365+2605, is 17′ at a PA of 300° from IRAS 04370+2559 and is 14′ at a PA of 320° from IRAS 04368+2557 The HH 831 A1, A2, A3 and A5 knots have an average direction of motion of 301° which is reasonably well aligned with all three of these IRAS sources It is possible that either of the nearby LDN 1527 radio sources could be driving HH 831 B1 and B2 (see Fig 4 3) HH 832, which is seen in [SII] only, is too faint to measure its proper motion

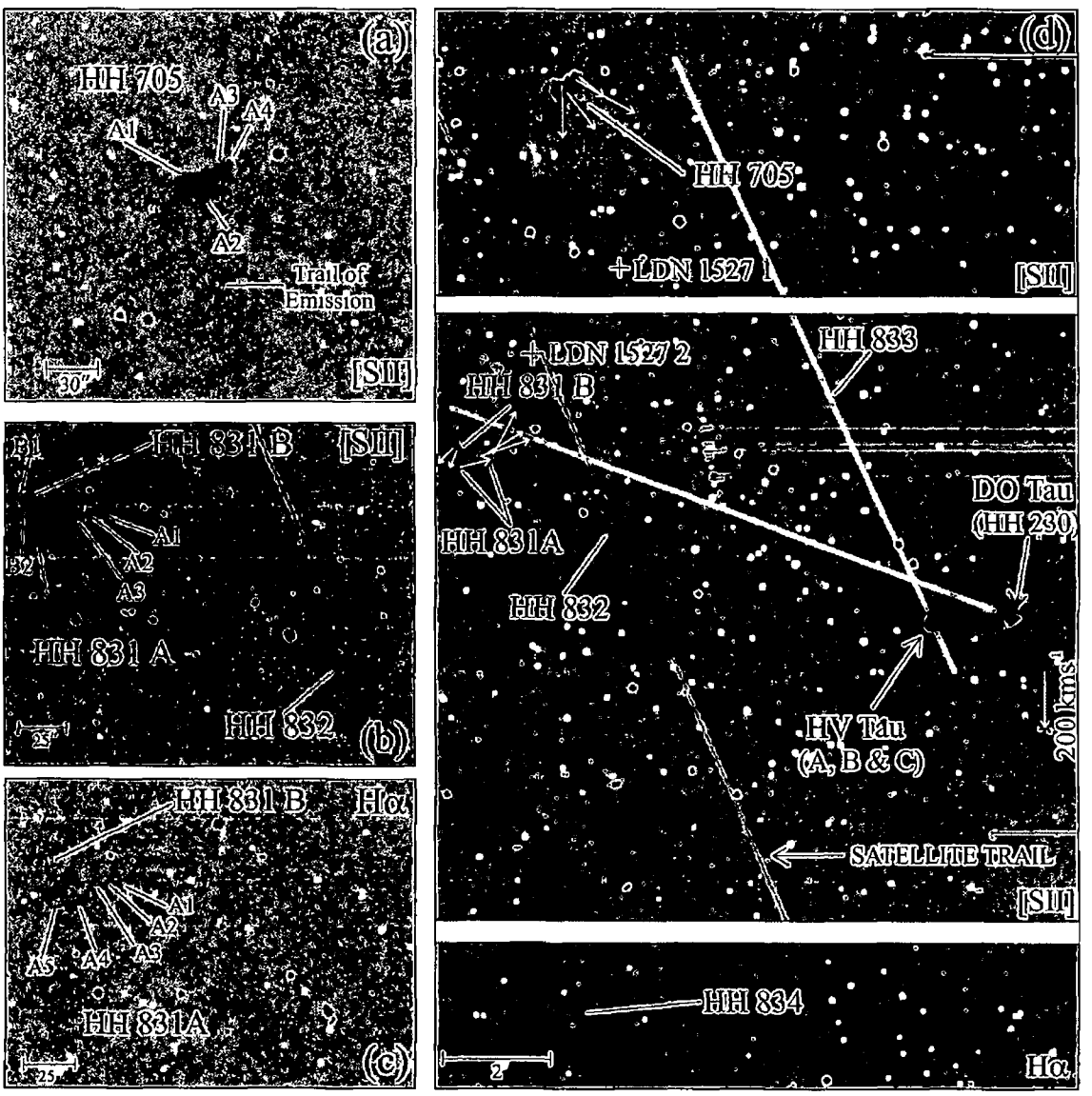

Figure 4 3 The main image (d) shows proper motion vectors for the HH objects in the vicinity of DO Tau and HV Tau C These vectors show, surprisingly, that neither of these sources are driving HH 831 and HH 705 as was suggested in Chapter 3 No proper motions could be detected for the fainter objects HH 832, HH 833 and HH 834, however it is still possible that HH 832 may be driven by DO Tau based on its positional alignment Both HV Tau C and IRAS 04368+2557 (which is outside the field of view of this image) are candidate sources for HH 833 (see text) The smaller images (a – c) show the individual knots in HH 705 and HH 831 for which the proper motion vectors were calculated

			[SII]		Hα	
HH Object	Source	Ang Sep	Velocity /kms^{-1}	Direction /°	Velocity /kms^{-1}	Direction /°
HH 705 A1			187	180	330	186
HH 705 A2			147	218	231	186
HH 705 A3			244	241	194	131
HH 705 A4			99	232	211	227

Table 4 5 Tangential velocity and direction of motion of HH 705 assuming a distance of 140 pc (Elias, 1978, Wichmann et al , 1998) to its previously suggested source, HV Tau C

The velocities of HH 831 A1, A2 and A3 (in [SII]) are comparable and range from 166 kms^{-1} to 196 kms^{-1} with Knot A5 slightly slower at 112 kms^{-1} Knots B1 and B2 have comparable velocities of 71 kms^{-1} and 79 kms^{-1} respectively

A 1″5 long bipolar "micro-jet" was recently discovered from HV Tau C by Stapelfeldt et al (2003), which I estimate to be at a PA of 25° (northern jet) from their images (Chapter 3) HH 833, to the northeast of HV Tau C, is also at a PA of 25° suggesting that it may also be driven by this source (see Fig 4 3) Further out in this direction is HH 705 (independently discovered by Sun et al , 2003) which may also be part of this outflow HH 705 is at a PA of 36° however it is quite likely that the outflow may have precessed over the 7′ 7 distance from HH 833 However HH 705 has a trail of emission towards the south, possibly suggesting a driving source along that direction Two radio sources in this region – LDN 1527 1 and LDN 1527 2 (Anglada et al , 1992) – lie to the south of this HH object and are possible driving sources (Chapter 3, Sun et al , 2003) but it looks unlikely that LDN 1527 1 could generate such a large object so nearby

Proper motion studies of the HH 833 and HH 705 objects did not reveal anything conclusive about their sources HH 833 was too faint to measure, so I still suggest that it is driven by HV Tau C due to its exact alignment with the HV Tau C jet (however see below for an alternative driving source) Fig 4 3 shows the direction of motion of the HH 705 knots which are detailed in Table 4 5 All knots in HH 705 (A1 – A4) are moving to the south/southeast in [SII] emission Similarly the Hα results show a south/southeast direction of motion however A3 is moving in a more

eastern direction The southward motions of HH 705 conclusively rule out HV Tau C, LDN 1527 1 and LDN 1527 2 as its source (see Chapter 3 and Fig 4 3) There is an IRAS source (IRAS 04363+2652) $\sim 37'$ (1 5 pc) to the north of HH 705 at a PA of 7° which remains the only known possible driving source for this object

The proper motions of HH 831 A and relative position of HH 833 may suggest a common source HH 831 A is 14′ at a PA of 320° from the Class 0 (Chini et al , 2001) low-mass source IRAS 04368+2557, as mentioned earlier, and the direction of motion of HH 831 A1, A2, A3 and A5 (in [SII]) is $\sim 301°$, which is therefore well aligned with this source HH 833 is 7′5 from HH 831 at a PA of 280° Allowing for precession over the total distance of 21′5 from IRAS 04368+2557 to HH 833, this is a likely candidate driving source for these two objects, creating a ~ 0 9 pc outflow IRAS 04368+2557 has previously been associated with HH 192 A, B and C (Eiroa et al , 1994, Gomez, Kenyon, & Whitney, 1997) From the images of Gomez, Kenyon, & Whitney (1997) HH 192 A and B are aligned with the blue lobe of a molecular outflow and extend for $\sim 2'$ from the IRAS source at a PA of $\sim 80°$ HH 192 C is aligned with the redshifted lobe of the molecular outflow and is $\sim 4'2$ from IRAS 04368+2557 at a PA of 277° Based on the approximate alignment of HH 831 and HH 833 and the known direction of motion of HH 831 A it is plausible that they are all extensions of the HH 192 outflow

4.3 4 RW Aur

The HH 229 jet from RW Aur was first noted by Hamann (1994) and Hirth et al (1994) The outflow is at a PA of 130° (Dougados et al , 2000, Mundt & Eisloffel, 1998, Hirth, Mundt & Solf, 1997) with respect to RW Aur and is at least 106″ in length while the redshifted outflow is at least 50″ long (Mundt & Eisloffel, 1998) HH 835 is 5′37 from RW Aur at a PA of 310° which is exactly aligned with the redshifted HH 229 jet (see Fig 4 4) This object is much stronger in Hα emission than [SII] and proper motions were only determined for Hα emission In Chapter 3 I suggested that it is a a bow shock with only the northern wing visible here If HH 835 is part of this outflow then the total length of this outflow from the blueshifted HH 229 jet to HH 335 is 0 29 pc (7′)

HH 835 appears to consist of a number of discrete objects which I refer to here

HH Object	Source [a]	Ang Sep	Hα Velocity /kms^{-1}	Hα Direction /°
HH 835 E	RW Aur (R)	4'.5	92	302
HH 835 M	RW Aur (R)	4'.6	208	288
HH 835 W	RW Aur (R)	4'.7	162	216
HH 229 B	RW Aur (B)	0'.4	223	132
HH 229 C	RW Aur (B)	0'.5	307	139
HH 229 D	RW Aur (B)	0'.6	238	127
HH 229 G	RW Aur (B)	1'.6	235	126

Table 4.6 Tangential velocity and direction of motion of HH 835 and HH 229 in the RW Aur outflow assuming a distance of 140 pc (Elias, 1978, Wichmann et al., 1998)

[a] B and R denotes whether the object is aligned with the blue or redshifted jet

as the west (W), middle (M) and east (E) knots in Fig. 4.4 and Table 4.6. The eastern knot appears to be the brightest of these (Fig. 4.4). Proper motion studies show this knot to be moving in a direction of 302° (Table 4.6) which is well aligned with the PA of the redshifted HH 229 jet. The motion of the middle knot is also closely aligned to this at 288°. The western knot however is at 216° and so appears to be moving in a different direction. Overall, these proper motion vectors confirm the suggestion that this object is part of the RW Aur outflow. The velocities of the HH 835 knots vary from 92 kms^{-1} (E) to 162 kms^{-1} (W) to 208 kms^{-1} (M), typical of the variations in velocities seen in HH bow shocks (e.g. Eisloffel & Mundt, 1992).

Proper motions were also obtained for some of the brighter knots in the HH 229 blueshifted outflow. The redshifted outflow was too faint to measure. Knots B, C, D and G (using the nomenclature of Eisloffel & Mundt, 1998) were strong enough in Hα emission to determine their velocity and directions – see Table 4.6. Knots B, D and G can be seen from Fig. 4.4 to be moving along the optically visible jet direction at 132°, 127° and 126° respectively, while Knot C is slightly off this direction at 139°. The velocities of Knots B, D and G are comparable, ranging from 223 kms^{-1} to 238 kms^{-1} while Knot C is $\sim$ 70 kms^{-1} faster at 307 kms^{-1}. A comparison of the HH 229 and HH 835 velocities suggests they are reasonably comparable over the whole length of the outflow.

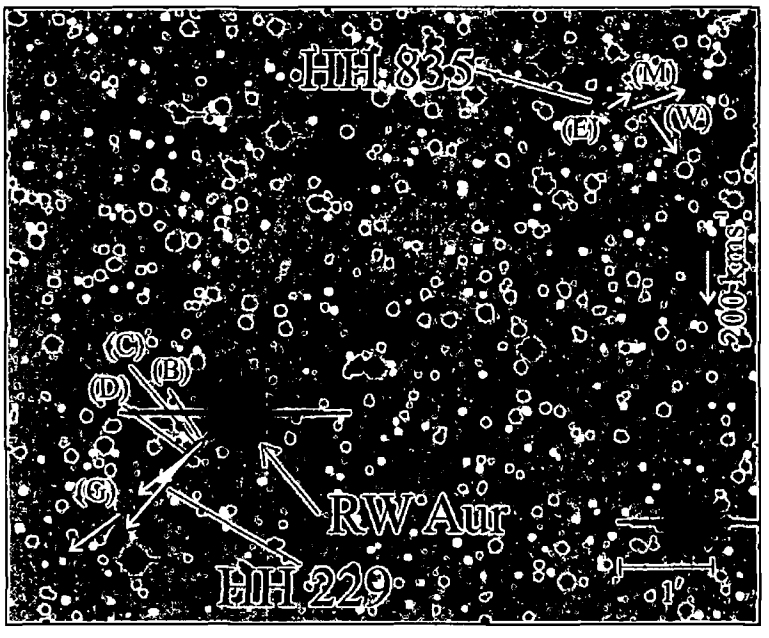

Figure 4 4 Proper motion vectors for HH 835 and HH 229 in the RW Aur outflow in Hα emission The direction of motion of the eastern and middle knots show RW Aur to be driving this object The proper motion directions of some of the knots in the blueshifted HH 229 outflow are well aligned with its optically visible PA

4.4 Discussion

4.4 1 Driving Sources

The proper motion studies undertaken here have confirmed the previously suggested sources for a number of HH objects e g HH 826 and HH 827 (CW Tau), HH 702 (DG Tau) and HH 835 (RW Aur) However they have also refuted the suggested sources for other HH objects – HH 828, HH 829, HH 830, HH 831 and HH 705 This was surprising in some cases as the objects were well aligned with the driving source – this is most noticeable in the DO Tau outflow where HH 831 appeared to be an extension of the HH 230 outflow based on their close alignment In these cases, I have tried to suggest candidate sources based on their direction of motion which is now known

These proper motion studies highlight the need for circumspection in using the apparent alignment of HH objects to derive their driving source Nevertheless, in the *absence* of proper motion studies apparent outflow alignment is *still the best means* of finding potential driving sources Proper motion studies can then conclusively

confirm or refute these sources at a later date

4.4.2 Velocity of Extended Outflows

At the beginning of this chapter I mentioned that the tangential velocity of objects at relatively large distances from their sources is generally not well known In Table 3 6 the dynamical timescales of these outflows were calculated using an assumed tangential velocity of 50 kms^{-1}, comparable to the lowest velocity necessary to collisionally excite the shocks observed However from examining Tables 4 2, 4 3 and 4 6 we see that the velocity of the more extended objects is much faster than this HH 827 (driven by CW Tau) has an average value of 249 kms^{-1} (Knots A and B) in Hα and 199 kms^{-1} (Knot B) in [SII] Knots A, C, D and E of HH 702 (driven by DG Tau) have an average velocity of 188 kms^{-1} in [SII] and of 164 kms^{-1} in Hα Finally HH 835 (driven by RW Aur) has an average velocity of 185 kms^{-1} for the west and middle knots Examination of these values would suggest that *200 kms^{-1}* is a much more accurate velocity to assume for relatively distant objects driven by CTTS outflows The three objects used to obtain this value - HH 827, HH 702 and HH 835 are at $\sim 6'5$, $\sim 11'$ and $4'7$ from their respective sources showing that the velocity remains high over this range of distances

We cannot, of course, conclude that there is little or no deceleration in the outflow over parsec-scale distances as the "events" that give rise to the more distant HH objects could have originated from more violent (FUor) outbursts that those closer to the source Large-scale numerical simulations are required to test whether deceleration might be important particularly in the context of the low density environment surrounding a CTTS

These proper motion studies have determined a faster velocity for the more distant objects than was conservatively used to calculate dynamical timescales in Chapter 3 They have also showed that the lengths of these outflows are shorter than previously suggested (Chapter 3), as some of the HH objects that appeared to be associated with the CTTSs are shown here to be unrelated Re-calculating the timescales to take account of these results reduces them to $1\,4 \times 10^3$ yr for CW Tau, $2\,4 \times 10^3$ yr for DG Tau and $1\,1 \times 10^3$ yr for RW Aur However these are just the *apparent* timescales, the real dynamical timescales are much larger than this

4.4.3 Velocity of "Micro-Jets"

Out of the five "micro-jets" examined here HH 220, HH 158 and HH 229 are optically visible in these images and their proper motions could be measured I find velocities of 323 kms^{-1} for HH 220 (NW) and 251 kms^{-1} for HH 229 (Knots B,C, D and G) and HH 158 (A, B and C) have an average velocity of 241 kms^{-1} (Eisloffel & Mundt, 1998) These velocities are comparable to those found for jets from Class I sources, which are typically 200 – 400 kms^{-1} (cf §1 3 2) This suggests that the velocity of the jets remains high as their sources evolve, despite the fact that the rate of accretion and ejection is about 10 – 100 times smaller for Class II sources than Class I YSOs (Hartigan, Edwards & Ghandour, 1995, Chapter 3)

4 4.4 [SII] verses Hα Velocities

Proper motions were determined in both [SII] and Hα for the majority of HH objects/knots here, the main exception being HH 835 and HH 229 where the individual knots were too weak in [SII] images to measure There are few proper motion studies which calculate proper motions for [SII] and Hα simultaneously, and some find velocity measurements which are very similar e g HH 34 (Reipurth et al , 2002), others find large variations for some knots e g HH 157 driven by FS Tau B (Eisloffel & Mundt, 1998) and some consider these two emission lines together e g HH 111 (Hartigan et al , 2001) The results presented in this chapter show varying degrees of agreement between Hα and [SII], some knots have comparable velocities/directions of motion in these two emission lines, while others are quite different However many of these differences can be compensated for by the associated errors in their measurements Also, Hartigan et al (2001) note that brightness changes between two different epoch images will affect the Hα image more than the [SII] as Hα responds immediately to changes in the preshock density while [SII] averages this variability over the $\sim$ 30 year cooling time The different timescales over which cooling acts may explain some of the discrepancies in the results presented here

Chapter 5

Conclusions

The aims of this thesis are to determine whether parsec-scale outflows occur from intermediate-mass YSOs, and whether they persist into the Class II low-mass phase It is already known that embedded, Class I low-mass YSOs produce such outflows, but neither intermediate-mass or Class II YSOs were previously known to be associated with this phenomenon

This thesis shows that intermediate-mass YSOs can generate outflows of up to $\sim$ *10 pc in length The CTTSs outflows also show evidence for large-scale outflows, albeit smaller in length, typically* $\sim$ *0 5 pc The morphology of both the intermediate-mass YSO- and CTTS- driven outflows are compared to parsec-scale outflows from Class I low-mass sources and many common morphological trends are found The kinematics of the CTTS outflows are also determined and compared to their less evolved counterparts, with comparable velocities found for the jets close to the source Moreover, the velocity of the more distant objects in these outflows, which was poorly known, is determined here and is found to remain high with distance from the source*

The kinematics of the outflows from intermediate-mass sources have not been determined here as the time interval between the earliest and latest epochs in my data is not long enough to measure their motions, especially in the case of the most distant outflows which are at 2 4 kpc

In this Chapter I will summarize the results obtained in both my morphological

(Chapters 2 and 3) and kinematical (Chapter 4) studies Table 5 1 summarizes the parsec - scale outflows (and the HH objects they consist of) from intermediate - mass YSOs and CTTS discovered in the course of this work Future work, arising from and expanding on the work detailed here, is suggested in §5 4

5.1 Parsec - scale outflows from intermediate - mass YSOs

I have investigated the occurrence of parsec - scale outflows from intermediate - mass YSOs As is the case with their lower mass embedded counterparts, such flows appear to be common and I report the discovery of five here (Chapter 2), four of which have well defined sources These include LkHα 198, 1548C27 IRS 1, LkHα 233 and IRAS 19395+2313 All of these YSOs, with the exception of the last for which no outflow activity was known, were previously associated with small - scale outflows

The region surrounding the fifth source, LkHα 234, is cluttered with outflows and candidate sources Eleven new HH objects are reported here, with many of them lying along a preferential axis centred near LkHα 234 and orientated in a northeast-southwest direction Their morphology suggests that at least some are part of a large - scale flow centred on the core of the NGC 7129 cluster, quite possibly driven by LkHα 234

Parsec - scale outflows from intermediate - mass YSOs show a number of similarities to those from their low - mass counterparts In particular
- their lengths and degree of collimation appear comparable,
- they share the same morphological trends such as increasing distance between successive HH objects coupled with increased size and complexity with distance from the source

The lengths of these large - scale outflows are usually comparable to the clump size of their associated clouds This is understandable since any shocks that are generated through interactions with the tenuous ISM/interclump medium will be very faint and may not be observed In fact as the expected outflow lifetimes for intermediate - mass YSOs are much larger than the *apparent* dynamical timescales

suggested by the observations here it seems likely that many have "blown-out" of their cloud complex

Finally, it is evident that the transition from highly collimated jet-like flows to poorly collimated wide-angle outflows such as the "Orion Bullets" *must lie at higher masses and luminosities than the intermediate-mass sources studied here*

5.2 Parsec-scale outflows from CTTSs

I have shown here that a number of (Class II) CTTSs i e DG Tau, CW Tau and RW Aur, which were previously known to drive "micro-jets" or short outflows of $\lesssim$ 1′ ($\lesssim$ 0 04 pc at the distance of the Taurus-Auriga Cloud) in length, are actually capable of driving outflows with lengths of the order of 0 5 pc Morphological studies (Chapter 3) initially suggested that the DG Tau and CW Tau outflows were about twice this length due to the apparent alignment of more distant HH objects with the known jets from these sources, and also suggested that DO Tau and HV Tau C may be driving parsec-scale outflows However proper motion studies (Chapter 4) reveal that *some* of the more distant objects in these apparent outflows were *not* driven by these sources These kinematical studies also determined the velocity of most of the HH objects found in the CTTS survey Currently the velocity of the more distant objects in outflows is poorly known

The morphological trends observed in the parsec-scale CTTSs outflows are comparable to those noted in younger sources (and also those from intermediate-mass sources, as shown here) i e decreasing frequency, increasing dimension and increasing complexity of HH emission with distance from the source In a few cases, small variations in the direction of propagation of the outflow have been found The high degree of collimation of the extended outflows from CTTSs compares well with that observed in the case of similar outflows from less evolved sources, *suggesting that outflows remain focused even as the source evolves from the Class I to the Class II stage* It is clear that the observed parsec-scale lengths of the CTTS outflows are minimum values and in reality they are *much* larger These outflows all show evidence for having blown out of the parent cloud

The tangential velocities obtained from these studies yield valuable information about the velocities of both "micro-jets" close to their source and also more distant HH objects Examination of the "micro-jets" HH 220, HH 158 and HH 229 associated with CW Tau, DG Tau and RW Aur respectively shows them to have velocities of $\sim 240 - 320$ kms^{-1} This is in good agreement with the value expected for jets from more embedded Class I YSOs of typically $200 - 400$ kms^{-1} (Mundt, Brugel & Buhrke, 1987), showing that the velocity of these jets appears to remain high even as the source evolves For the more extended objects in the outflows velocities of $\sim$ *200 kms*$^{-1}$ are indicated Overall the velocities of the HH objects show little or no change over the total length of the outflow This may be because deceleration, due to interactions with the ambient medium, is not important in the tenuous environment surrounding CTTSs The requires, however, further numerical simulations to investigate more fully

The *apparent* dynamical timescale of these extended outflows is typically a few times 10^3 years (revised values taken from Chapter 4) This suggests a linkage between the major accretion events that give rise to the largest HH complexes and the FUor phenomenon Although the timescale for FUor events is estimated to be of the order of 10^4 years (Herbig, 1977, Herbig, Petrov, & Duemmler, 2003, see Chapter 3) the morphology of these outflows suggests long periods of quiescence interrupted by violent mass eruptions As FUor stars are CTTSs in quiescence, the extended outflows of the latter provide the best "fossil record" to test this link

Finally, I suggest that the exponential increase in separation of HH complexes with distance from their source, coupled with their statistically estimated outflow timescales, suggests further HH complexes on scales of tens of parsecs may exist These structures however may be very faint

Proper motion studies highlight the inherent danger in using morphological alignment as a method of source determination for more distant HH objects *However, in the absence of such studies alignment is still the best method for determining candidate sources* The proper motion studies confirmed a number of sources that were suggested in Chapter 3 for the HH objects found there, however they also refuted others In those cases, I have tried to suggest other possible sources, based on the direction of motion of these HH objects which is now known

5.3 Summary of Parsec-Scale Optical Outflows

The parsec-scale outflows described in Chapters 2, 3 and 4 are summarized in Table 5.1. Some previously known outflows from low-mass Class I sources, the typical drivers of such parsec-scale outflows, are included here for comparison purposes. Their values have been taken from the literature.

The outflows are divided into those from CTTSs (Chapters 3 and 4), from intermediate-mass YSOs (Chapter 2) and previously known outflows from Class I low-mass sources. The columns in Table 5.1 represent:

(1) The source of the outflow. For the CTTS outflows this has been confirmed from proper motion studies and for the intermediate-mass outflows it is suggested from morphological alignment. The Class I sources are suggested from proper motion studies and/or alignment – see Reipurth, Bally, & Devine (1997), Ogura (1995) and Bally & Devine (1994) respectively for more information on these outflows.

(2) The distance to the source, taken from the literature.

(3) The luminosity of the source, taken from the literature and estimated in Chapter 2 in the case of IRAS 19395+2313.

(4) The total projected length of the outflow, based on the distance in column 2.

(5) The apparent dynamical timescale of the outflow. This is based on the longest angular length of the bipolar outflow and a velocity of 200 kms^{-1} for the more distant objects in the outflow. The proper motion studies in Chapter 4 show that this is a reasonable velocity for the CTTS outflows, while it is an assumed upper limit for the velocity of the more distant objects in the intermediate-mass and Class I outflows.

(6) The degree of collimation (θ_{flow}) for the outflow. This is calculated by taking the width of the most distant shock in both the outflow and counterflow and dividing by its projected distance from the source. The mean value of θ_{flow} for the outflow and counterflow is given here.

(7) The HH objects on either side of the bipolar outflow are given here. The letter in brackets denotes whether the flow is redshifted (R) or blueshifted (B) if this is known, or if not the direction of the flow is given.

(8) The PA for each side of the outflow. Based on the PA with respect to the (suggested) source and directions derived from proper motions (where available).

(9) The angular extent (in arcseconds/arcminutes) of each side of the outflow.

Source	Distance /pc	L_{bol} /$L_\odot$	Length /pc	τ_{dyn} /10^4 yr	$\theta_{flow}{}^c$ /°	HH Objects	PA / °	Angular Extent
CTTSs								
CW Tau	140	2 6	0 32	0 14	2	HH 220 NW, HH 826 C (R)	315	0′8
						HH 826 A, B, HH 827 (B)	184	7′1
DG Tau	140	8	0 5	0 24	1 4	HH 158 (R)	43	1″5
						HH 158, HH 702 (B)	205	12′3
RW Aur	140	1 1	0 29	0 11	4	HH 229, HH 835 (R)	295	5′4
						HH 229 (B)	131	1′8
Intermediate - mass YSOs								
LkHα 198	600	$\geq$ 160	2 3	1 12	2 8	HH 164 F, HH 801 (NW)	340	5′
						HH 164, HH 461, HH 802 (SE)	160	8′1
1548C27 IRS 1	2400	580	7 5	2 79	11 6	HH 165, HH 365 (NE)	46	8′1
						HH 803 (SW)	223	2′6
IRAS 19395+2313	2400	320	5	2 15	30 2	HH 804 (E)	80	6′3
						HH 805 (W)	260	0′8
LkHα 233	880	$\geq$ 121	3 1	0 88	6 3	HH 398, HH 808 – HH 813(B)	242	7′
						HH 398, HH 814 (R)	47	5′2
LkHα 234	1250	1200	8	1 96	6 2	HH 815 – HH 821 (NE)	59	11′
						HH 822 (SW)	238	10′7
Low - Mass, Class I YSOs								
IRAS 05491+0247*	460	25	7 7	2 15	7 4	HH 111, HH 113 (R)	101	26′
						HH 111, HH 311 (B)	280	31′
HH 1/2 VLA 1*	460	50	5 9	1 56	10 3	HH 1, HH 401 (NW)	319	24′
						HH 2, HH 402 (SE)	139	20′
HH 34 IRS*	460	28	3	0 73	1 5	HH 34N, 126, 85, 40, 33 (R)	351	9′8
						HH 34, 34X, 173, 86, 87, 88 (B)	161	11′5

Table 5 1 Parameters of newly discovered, and some previously known (marked with an asterisk*), parsec - scale outflows from low (Classes I and II) - and intermediate - mass YSOs Explanations of the columns given in the text

Some notes on the sources
– DO Tau and HV Tau C have been excluded here as Chapter 4 shows that they do not drive parsec-scale outflows
– The luminosity given for RW Aur is actually that of the RW Aur A binary and so is an upper limit for the binary component driving this outflow
– IRAS 05491+0247 is the source of HH 111 The three low-mass Class I sources were *not* studied in this thesis and are included here for comparison purposes only

It can be seen from this that, although the CTTS outflows are much shorter, the intermediate-mass outflows are comparable in length to those from the typical Class I (low-mass) YSOs The apparent dynamical timescale for all of these outflows is of the order of 10^{3-4} years, although it has been stressed throughout this thesis that the apparent length is much less than one expects the actual length of these outflows to be The degree of collimation of both the CTTS outflows and those from intermediate-mass sources is quite similar to those from Class I YSOs, with the CTTS outflows actually having slightly higher colhmation

5.4 Future Work

The results presented here show that both intermediate-mass YSOs and CTTSs are important sources of parsec-scale outflows This work can be expanded upon both through observational surveys and numerical simulations as detailed below

• The length of the outflow timescale for a typical CTTS ($\sim 10^6$ yr), and the exponentially increasing separation of HH complexes with distance from their source, suggest that even larger, more chaotic, complexes may exist on scales of tens of parsecs Finding such complexes would be challenging even with existing large format CCDs and "fast optics" i e low f ratios Nevertheless, finding such complexes may give us clues as to how outflows over time contribute to the dynamics and evolution of the ISM

• It is not known whether the large-scale HH complexes undergo deceleration as

they move away from their source, only that their *current* velocities are comparable to those for much closer knots It is possible, for example, that the major accretion events that gave rise to them produced much faster flows, at least initially Numerical simulations are urgently required to test these ideas in the well characterised environment of CTTSs

• The proper motion study of the CTTS-driven outflows emphasise the importance of such studies Although I have data from a number of different epochs for the intermediate-mass star regions presented in Chapter 2, the time difference is not long enough to measure proper motions especially for the more distant outflows However the value of such a study should not be underestimated and should be undertaken when data from a later epoch can be obtained The velocity of the more distant objects in such outflows are currently not well known

• The electron density, excitation and radial velocity of the more distant HH objects needs to be determined through spectroscopic observations Once the basic physical parameters of these complexes are found it is possible, in conjunction with the previously determined tangential velocities, to estimate mass loss rates, momentum fluxes and power of these outflows In turn, we can then gauge their contribution to cloud turbulence and support This goal however will no doubt also require suitable numerical simulations to estimate the degree of coupling of the outflow with its surroundings

Bibliography

Adams, F C , Lada, C J , & Shu, F H 1987, ApJ, 312, 788

Alcalá, J M , Covino, E , Franchini, M , Krautter, J , Terranegra, L , & Wichmann, R 1993, A&A, 272, 225

Allen, D A & Burton, M G 1993, Nature, 363, 54

Alten, V P , Bally, J , Devine, D , & Miller, G J 1997, IAU Symp 182 Herbig-Haro Flows and the Birth of Stars, 182, 51P

Ambartsumian, V A 1957, IAU Symp 3 Non-stable stars, 3, 177

Andre, P 1994, The Cold Universe, Proceedings of the 28th Rencontre de Moriond, Les Arcs, France, 179

Andre, P & Montmerle, T 1994, ApJ, 420, 837

André, P , Ward-Thompson, D , & Barsony, M 1993, ApJ, 406, 122

André, P , Ward-Thompson, D , & Barsony, M 2000, Protostars and Planets IV, 59

Anglada, G , Rodríguez, L F , Canto, J , Estalella, R , & Torrelles, J M 1992, ApJ, 395, 494

Arce, H G & Goodman, A A 2002, ApJ, 575, 911

Arce, H G & Goodman, A A 2001, ApJ, 554, 132

Armstrong, J T & Winnewisser, G 1989, A&A, 210, 373

Aspin, C , McCaughrean, M J , & McLean, I S 1985, A&A, 144, 220

Aspm, C & Reipurth, B 2000, MNRAS, 311, 522

Bacciotti, F , Mundt, R , Ray, T P , Eisloffel, J , Solf, J , & Camezind, M 2000, ApJ (Letters), 537, L49

Bacciotti, F , Ray, T P , Mundt, R , Eisloffel, J , & Solf, J 2002, ApJ, 576, 222

Bachiller, R 1996, ARA&A, 34, 111

Bally, J & Devine, D 1994, ApJ (Letters), 428, L65

Bally, J & Devine, D 1997, IAU Symp 182 Herbig-Haro Flows and the Birth of Stars, 182, 29

Bally, J , Devine, D , & Alten, V 1996, ApJ, 473, 921

Barral, J F & Canto, J 1981, Revista Mexicana de Astronomia y Astrofisica, 5, 101

Barsony, M & Kenyon, S J 1992, ApJ (Letters), 384, L53

Beckwith, S V W , Sargent, A I , Chini, R S , & Guesten, R 1990, AJ, 99, 924

Bechis, K P , Harvey, P M , Campbell, M F , & Hoffmann, W F 1978, ApJ, 226, 439

Bertin, E & Arnouts, S 1996, A&AS, 117, 393

Bertout, C 1987, IAU Symp 122 Circumstellar Matter, 122, 23

Blandford, R D & Payne, D G 1982, MNRAS, 199, 883

Blitz, L 1993, Protostars and Planets III, 125

Blondin, J M , Konigl, A , & Fryxell, B A 1989, ApJ (Letters), 337, L37

Bonnell, I A , Bate, M R , & Zinnecker, H 1998, MNRAS, 298, 93

Bontemps, S , André, P , Terebey, S , & Cabrit, S 1996, A&A, 311, 858

Bouvier, J , Bertout, C , Benz, W , & Mayor, M 1986, A&A, 165, 110

Buhrke, T , Mundt, R , & Ray, T P 1988, A&A, 200, 99

Burton, M G & Allen, D A 1994, ASSL Vol 190 Astronomy with Arrays, The Next Generation, 61

Cabrit, S & André, P 1991, ApJ (Letters), 379, L25

Cabrit, S , Edwards, S , Strom, S E , & Strom, K M 1990, ApJ, 354, 687

Cabrit, S , Lagage, P O , McCaughrean, M , & Olofsson, G 1997, A&A, 321, 523

Cabrit, S & Raga, A 2000, A&A, 354, 667

Calvet, N & Cohen, M 1978, MNRAS, 182, 687

Camenzind, M 1990, Reviews of Modern Astronomy, 3, 234

Canto, J & Raga, A C 1995, MNRAS, 277, 1120

Canto, J , Rodríguez, L F , Calvet, N , & Levreault, R M 1984, ApJ, 282, 631

Chavarria-K , C 1985, A&A, 148, 317

Chernin, L , Masson, C , Gouveia dal Pino, E M , & Benz, W 1994, ApJ, 426, 204

Chini, R , Hoffmeister, V , Kimeswenger, S , Nielbock, M , Nurnberger, D , Schmidtobreick, L , & Sterzik, M 2004, Nature, 429, 155

Chini, R , Ward-Thompson, D , Kirk, J M , Nielbock, M , Reipurth, B , & Sievers, A 2001, A&A, 369, 155

Coffey, D , Bacciotti, F , Woitas, J , Ray, T P , & Eisloffel, J 2004, ApJ, 604, 758

Cohen, M & Kuhi, L V 1979, ApJS, 41, 743

Cohen, M , Kuhi, L V , Spinrad, H , & Harlan, E A 1981, ApJ, 245, 920

Cohen, M & Schwartz, R D 1983, ApJ, 265, 877

Corcoran, D & Ray, T P 1995, A&A, 301, 729

Corcoran, D , Ray, T P , & Bastien, P 1995, A&A, 293, 550 (CRB)

Corcoran, M F , Ishibashi, K , Swank, J H , & Petre, R 2001, ApJ, 547, 1034

Corcoran, M & Ray, T P 1997, A&A, 321, 189

Corcoran, M & Ray, T P 1998, A&A, 336, 535

Craine, E R , Byard, P L , & Boeshaar, G O 1981, AJ, 86, 751

Currie, D G 2003, Revista Mexicana de Astronomia y Astrofisica Conference Series, 15, 59

Davis, C J , Eisloeffel, J , Ray, T P , & Jenness, T 1997, A&A, 324, 1013

DeCampli, W M 1981, ApJ, 244, 124

Dent, W R F & Aspin, C 1992, MNRAS, 259, 401

Devine, D , Bally, J , Reipurth, B , & Heathcote, S 1997, AJ, 114, 2095

De Young, D S 1986, ApJ, 307, 62

Dopita, A 1978, A&A, 63, 237

Dougados, C , Cabrit, S , Lavalley, C , & Ménard, F 2000, A&A, 357, L61

Downes, T P & Cabrit, S 2003, A&A, 403, 135

Duchêne, G , Monin, J -L , Bouvier, J , & Ménard, F 1999, A&A, 351, 954

Dutrey, A , Guilloteau, S , & Bachiller, R 1997, A&A, 325, 758

Duvert, G , Guilloteau, S , Menard, F , Simon, M , & Dutrey, A 2000, A&A, 355, 165

Edge, A C & Rottgering, H 1995, MNRAS, 277, 1580

Edwards, S , Ray, T , & Mundt, R 1993, Protostars and Planets III, 567

Edwards, S & Snell, R L 1983, ApJ, 270, 605

Eiroa, C , Gómez de Castro, A I , & Miranda, L F 1992, A&AS, 92, 721

Eiroa, C , Miranda, L F , Anglada, G , Estalella, R , & Torrelles, J M 1994, A&A, 283, 973

Eisloffel, J 2000, A&A, 354, 236

Eisloffel, J & Mundt, R 1992, A&A, 263, 292

Eisloffel, J & Mundt, R 1994, A&A, 284, 530

Eisloffel, J & Mundt, R 1997, AJ, 114, 280

Eisloffel, J & Mundt, R 1998, AJ, 115, 1554

Elias, J H 1978, ApJ, 224, 857

Elmegreen, B G 1993, Protostars and Planets III, 97

Falgarone, E & Phillips, T G 1990, ApJ, 359, 344

Falle, S A E G & Raga, A C 1995, MNRAS, 272, 785

Fuente, A , Martín-Pintado, J , Bachiller, R , Neri, R , & Palla, F 1998, A&A, 334, 253

Fuente, A , Neri, R , Martín-Pintado, J , Bachiller, R , Rodriguez-Franco, A , & Palla, F 2001, A&A, 366, 873

Gahm, G F , Petrov, P P , Duemmler, R , Gameiro, J F , & Lago, M T V T 1999, A&A, 352, L95

Garmany, C D , Conti, P S , & Massey, P 1980, ApJ, 242, 1063

Ghez, A M , Neugebauer, G , & Matthews, K 1993, AJ, 106, 2005

Gomez, M , Kenyon, S J , & Whitney, B A 1997, AJ, 114, 265

Gómez de Castro, A I 1993, ApJ (Letters), 412, L43

Goodrich, R W 1986, AJ, 92, 885

Goodrich, R W 1993, ApJS, 88, 609

Gómez de Castro, A I & Robles, A 1999, A&A, 344, 632

Gras-Velázquez, À , Ray, T P 2004 (in preparation)

Gregorio-Hetem, J & Hetem, A 2002, MNRAS, 336, 197

Hamann, F 1994, ApJS, 93, 485

Haro, G 1952, ApJ, 115, 572

Haro, G & Mınkowskı, R 1960, AJ, 65, 490

Hartıgan, P , Bally, J , Reıpurth, B , & Morse, J A 2000, Protostars and Planets IV, 841

Hartıgan, P , Edwards, S , & Ghandour, L 1995, ApJ, 452, 736

Hartıgan, P , Morse, J , & Bally, J 2000, AJ, 120, 1436

Hartıgan, P , Morse, J A , Reıpurth, B , Heathcote, S , & Bally, J 2001, ApJ (Letters), 559, L157

Hartmann, L , Avrett, E , & Edwards, S 1982, ApJ, 261, 279

Hartmann, L , Hewett, R , Stahler, S , & Mathıeu, R D 1986, ApJ, 309, 275

Hartmann, L & Kenyon, S J 1996, ARA&A, 34, 207

Hartmann, L & Stauffer, J R 1989, AJ, 97, 873

Harvey, P M , Wılkıng, B A , & Joy, M 1984, ApJ, 278, 156

Harvey, P M , Joy, M , Lester, D F , & Wılkıng, B A 1986, ApJ, 301, 346

Heathcote, S , Morse, J A , Hartıgan, P , Reıpurth, B , Schwartz, R D , Bally, J , & Stone, J M 1996, AJ, 112, 1141

Herbıg, G H 1951, ApJ, 113, 697

Herbıg, G H 1960, ApJS, 4, 337

Herbıg, G H 1977, ApJ, 217, 693

Herbıg, G H & Bell, K R 1988, Lıck Observatory Bulletın, Santa Cruz Lıck Observatory, —c1988,

Herbıg, G H , Petrov, P P , & Duemmler, R 2003, ApJ, 595, 384

Hester, J J , Stapelfeldt, K R , & Scowen, P A 1998, AJ, 116, 372

Hıllenbrand, L A , Strom, S E , Vrba, F J , & Keene, J 1992, ApJ, 397, 613

Hırth, G A , Mundt, R , & Solf, J 1994, A&A, 285, 929

Hirth, G A , Mundt, R , & Solf, J 1997, A&AS, 126, 437

Hirth, G A , Mundt, R , Solf, J , & Ray, T P 1994, ApJ (Letters), 427, L99

Hunter, T R , Phillips, T G , & Menten, K M 1997, ApJ, 478, 283

Jones, B F & Cohen, M 1986, ApJ (Letters), 311, L23

Joy, A H 1945, ApJ, 102, 168

Lada, C J 1987, IAU Symp 115 Star Forming Regions, 115, 1

Lada, C J & Wilking, B A 1984, ApJ, 287, 610

Lagage, P O , Olofsson, G , Cabrit, S , Cesarsky, C J , Nordh, L , & Rodriguez Espinosa, J M 1993, ApJ (Letters), 417, L79

Lavalley, C , Cabrit, S , Dougados, C , Ferruit, P , & Bacon, R 1997, A&A, 327, 671

Leinert, C , Haas, M , & Weitzel, N 1993, A&A, 271, 535

Lim, A J & Raga, A C 1998, MNRAS, 298, 871

Kim, W , Ostriker, E C , & Stone, J M 2003, ApJ, 599, 1157

Konigl, A 1982, ApJ, 261, 115

Konigl, A & Pudritz, R E 2000, Protostars and Planets IV, 759

Kwan, J & Tademaru, E 1995, ApJ, 454, 382

Larson, R B 1999, Star Formation 1999, Proceedings of Star Formation 1999, held in Nagoya, Japan, June 21 - 25, 1999, Editor T Nakamoto, Nobeyama Radio Observatory, p 336-340, 336

Larson, R B 2003, Reports of Progress in Physics, 66, 1651

Lee, J -K & Burton, M G 2000, MNRAS, 315, 11

Mac Low, M , Klessen, R S , Burkert, A , & Smith, M D 1998, Physical Review Letters, 80, 2754

Martí, J , Rodríguez, L F , & Reipurth, B 1993, ApJ, 416, 208

Masciadri, E & Raga, A C 2002, ApJ, 568, 733

Masson, C R & Chernin, L M 1993, ApJ, 414, 230

Matzner, C D & McKee, C F 1999, ApJ (Letters), 526, L109

McCray, R & Kafatos, M 1987, ApJ, 317, 190

McKee, C F , Zweibel, E G , Goodman, A A , & Heiles, C 1993, Protostars and Planets III, 327

Meyer, M R , Adams, F C , Hillenbrand, L A , Carpenter, J M , & Larson, R B 2000, Protostars and Planets IV, 121

Miranda, L F , Eiroa, C , & Gómez de Castro, A I 1993, A&A, 271, 564

Mitchell, G F , Hasegawa, T I , Dent, W R F , & Matthews, H E 1994, ApJ (Letters), 436, L177

Mitchell, G F & Matthews, H E 1994, ApJ (Letters), 423, L55

Mitchell, G F , Sargent, A I , & Mannings, V 1997, ApJ (Letters), 483, L127

Motte, F , André, P , & Neri, R 1998, A&A, 336, 150

Mundt, R , Brugel, E W , & Buhrke, T 1987, ApJ, 319, 275

Mundt, R , Buhrke, T , Fried, J W , Neckel, T , Sarcander, M , & Stocke, J 1984, A&A, 140, 17

Mundt, R & Eisloffel, J 1998, AJ, 116, 860

Mundt, R & Fried, J W 1983, ApJ (Letters), 274, L83

Mundt, R & Ray, T P 1994, ASP Conf Ser 62 The Nature and Evolutionary Status of Herbig Ae/Be Stars, 237

Mundt, R , Ray, T P , & Raga, A C 1991, A&A, 252, 740

Najita, J 1995, Revista Mexicana de Astronomia y Astrofisica Conference Series, 1, 293

Natta, A , Grinin, V P , Mannings, V , & Ungerechts, H 1997, ApJ, 491, 885

Natta, A , Grının, V , & Mannıngs, V 2000, Protostars and Planets IV, 559

Natta, A , Palla, F , Butner, H M , Evans, N J , & Harvey, P M 1993, ApJ, 406, 674

Norman, C A & Ferrara, A 1996, ApJ, 467, 280

O'Dell, C R , Hartıgan, P , Lane, W M , Wong, S K , Burton, M G , Raymond, J , & Axon, D J 1997, AJ, 114, 730

Ogura, K 1995, ApJ (Letters), 450, L23

Osterbrock, D E 1958, PASP, 70, 399

Padgett, D L , Brandner, W , Stapelfeldt, K R , Strom, S E , Terebey, S , & Koerner, D 1999, AJ, 117, 1490

Palla, F & Stahler, S W 1990, ApJ (Letters), 360, L47

Palla, F & Stahler, S W 1993, ApJ, 418, 414

Parthasarathy, M , Vıjapurkar, J , & Drılling, J S 2000, A&AS, 145, 269

Petrov, P P , Gahm, G F , Gameıro, J F , Duemmler, R , Ilyın, I V , Laakkonen, T , Lago, M T V T , & Tuomınen, I 2001, A&A, 369, 993

Phıllıps, J P & Mampaso, A 1996, A&A, 316, 182

Pratap, P , Dıckens, J E , Snell, R L , Mıralles, M P , Bergın, E A , Irvıne, W M , & Schloerb, F P 1997, ApJ, 486, 862

Raga, A C , Bınette, L , Canto, J , & Calvet, N 1990, ApJ, 364, 601

Raga, A & Cabrıt, S 1993, A&A, 278, 267

Raga, A C , Cabrıt, S , & Canto, J 1995, MNRAS, 273, 422

Raga, A , Cabrıt, S , Dougados, C , & Lavalley, C 2001, A&A, 367, 959

Ray, T P 1987, A&A, 171, 145

Ray, T P , Poetzel, R , Solf, J , & Mundt, R 1990, ApJ (Letters), 357, L45

Reıpurth, B 1985, A&A, 143, 435

Reipurth, B 1989, Nature, 340, 42

Reipurth, B & Aspin, C 1997, AJ, 114, 2700

Reipurth, B & Bally, J 2001, ARA&A, 39, 403

Reipurth, B , Bally, J , & Devine, D 1997, AJ, 114, 2708

Reipurth, B , Chini, R , Krugel, E , Kreysa, E , & Sievers, A 1993, A&A, 273, 221

Reipurth, B & Heathcote, S 1997, IAU Symp 182 Herbig-Haro Flows and the Birth of Stars, 182, 3

Reipurth, B , Heathcote, S , Morse, J , Hartigan, P , & Bally, J 2002, AJ, 123, 362

Richer, J S , Shepherd, D S , Cabrit, S , Bachiller, R , & Churchwell, E 2000, Protostars and Planets IV, 867

Rodríguez, L F , Moran, J M , & Ho, P T P 1980, ApJ (Letters), 240, L149

Scalo, J 1998, ASP Conf Ser 142 The Stellar Initial Mass Function (38th Herstmonceux Conference), 201

Scarrott, S M , Rolph, C D , & Tadhunter, C N 1991, MNRAS, 249, 310

Schwartz, R D 1975, ApJ, 195, 631

Schwartz, R D , Wilking, B A , & Giulbudagian, A L 1991, ApJ, 370, 263

Shang, H , Shu, F H , & Glassgold, A E 1998, ApJ (Letters), 493, L91

Shepherd, D S , Churchwell, E , & Wilner, D J 1997, ApJ, 482, 355

Shepherd, D S , Watson, A M , Sargent, A I , & Churchwell, E 1998, ApJ, 507, 861

Shevchenko, V S & Yakubov, S D 1989, Soviet Astronomy, 33, 370

Shu, F H , Adams, F C , & Lizano, S 1987, ARA&A, 25, 23

Shu, F , Najita, J , Ostriker, E , Wilkin, F , Ruden, S , & Lizano, S 1994, ApJ, 429, 781

Shu, F H , Najıta, J R , Shang, H , & Lı, Z -Y 2000, Protostars and Planets IV, 789

Shu, F H , Ruden, S P , Lada, C J , & Lızano, S 1991, ApJ (Letters), 370, L31

Sımon, M , Holfeltz, S T , & Taff, L G 1996, ApJ, 469, 890

Smıth, M D , Suttner, G , & Yorke, H W 1997, A&A, 323, 223

Solf, J 1997, IAU Symp 182 Herbıg-Haro Flows and the Bırth of Stars, 182, 63

Snell, R L , Loren, R B , & Plambeck, R L 1980, ApJ (Letters), 239, L17

Stahler, S W 1994, ApJ, 422, 616

Stahler, S W , Palla, F , & Ho, P T P 2000, Protostars and Planets IV, 327

Stapelfeldt, K , Burrows, C J , Krıst, J E , & WFPC2 Scıence Team 1997, IAU Symp 182 Herbıg-Haro Flows and the Bırth of Stars, 182, 355

Stapelfeldt, K R , Ménard, F , Watson, A M , Krıst, J E , Dougados, C , Padgett, D L , & Brandner, W 2003, ApJ, 589, 410

Staude, H J & Elsasser, H 1993, A&A Rev , 5, 165

Stone, J M & Norman, M L 1994, ApJ, 420, 237

Stone, J M , Ostrıker, E C , & Gammıe, C F 1998, ApJ (Letters), 508, L99

Strom, K M , Strom, S E , Wenz, M , Wolff, S C , & Morgan, J 1986, ApJS, 62, 39

Suttner, G , Smıth, M D , Yorke, H W , & Zınnecker, H 1997, A&A, 318, 595

Sun, K , Yang, J , Luo, S , Wang, M , Deng, L , Zhou, X , & Chen, J 2003, Chınese Journal of Astronony and Astrophysıcs, 3, 458

Taylor, S D & Raga, A C 1995, A&A, 296, 823

Valentıjn, E A 1981, A&A, 102, 53

Vılchez, J M , Mampaso, A , Rıera, A , & Phıllıps, J P 1989, A&A, 213, 303

Volker, R , Smıth, M D , Suttner, G , & Yorke, H W 1999, A&A, 343, 953

Walter, F M 1986, ApJ, 306, 573

Walter, F M , Brown, A , Mathieu, R D , Myers, P C , & Vrba, F J 1988, AJ, 96, 297

Wardle, M & Konigl, A 1993, ApJ, 410, 218

Ward-Thompson, D 2002, Science, 295, 76

Weintraub, D A , Kastner, J H , & Mahesh, A 1994, ApJ (Letters), 420, L87

Wichmann, R , Bastian, U , Krautter, J , Jankovics, I , & Rucinski, S M 1998, MNRAS, 301, L39

Williams, J P , Blitz, L , & McKee, C F 2000, Protostars and Planets IV, 97

Williams, J P , Blitz, L , & Stark, A A 1995, ApJ, 451, 252

Woitas, J & Leinert, C 1998, A&A, 338, 122

Woitas, J , Ray, T P , Bacciotti, F , Davis, C J , & Eislöffel, J 2002, ApJ, 580, 336